



HAL
open science

The role of PLA2 enzymes in host cell cytosol uptake and blood stage growth of *Plasmodium falciparum*

Matthias Paulus Wagner

► **To cite this version:**

Matthias Paulus Wagner. The role of PLA2 enzymes in host cell cytosol uptake and blood stage growth of *Plasmodium falciparum*. Parasitology. Université Paris Cité, 2021. English. NNT : 2021UNIP7239 . tel-04009909

HAL Id: tel-04009909

<https://theses.hal.science/tel-04009909v1>

Submitted on 1 Mar 2023

HAL is a multi-disciplinary open access archive for the deposit and dissemination of scientific research documents, whether they are published or not. The documents may come from teaching and research institutions in France or abroad, or from public or private research centers.

L'archive ouverte pluridisciplinaire **HAL**, est destinée au dépôt et à la diffusion de documents scientifiques de niveau recherche, publiés ou non, émanant des établissements d'enseignement et de recherche français ou étrangers, des laboratoires publics ou privés.



Université de Paris

ED 562 – Bio Sorbonne Paris Cité

Biologie de Plasmodium et Vaccins, Institut Pasteur Paris

THE ROLE OF PLA₂ ENZYMES IN HOST CELL CYTOSOL UPTAKE AND BLOOD STAGE GROWTH OF *PLASMODIUM FALCIPARUM*

présentée par
Matthias Paulus Wagner

Thèse de doctorat d'infectiologie et parasitologie

dirigée par
Chetan E. Chitnis

Présentée et soutenue publiquement le 07.06.2021

Devant un jury composé de

Dr. Yves Colin-Aronovicz, *INTS Paris*

Dr. Isabelle Tardieux, *Université Grenoble Alpes*

Dr. Tim-Wolf Gilberger, *Universität Hamburg*

Dr. Caroline Demangel, *CNRS, Institut Pasteur*

Dr. Kai Wengelnik, *Université Montpellier*

Dr. Chetan Chitnis, *Institut Pasteur*

Président

Rapporteuse

Rapporteur

Examinatrice

Examineur

Directeur de thèse

*“Here’s a smile for your baby soul
That you’ve forgotten.”*

– **Abhishek Joshi**

Caramel Sons – Let You Rollin

Contents

1	Abstract	8
2	Résumé	10
3	Introduction	12
3.1	Introduction to malaria	13
3.2	The life cycle of <i>Plasmodium falciparum</i>	13
3.3	Host cell cytosol uptake and hemoglobin digestion	15
3.3.1	Mechanistic models of host cell cytosol uptake	16
3.3.2	Elevated oxidative stress in the parasite causes lipid oxidation	18
3.3.3	Physiological basis of Artemisinin activity and resistance	19
3.4	Lipid oxidation	21
3.4.1	Molecular basis and physiological effects of lipid oxidation	21
3.4.2	Measurement of lipid oxidation	23
3.4.3	Lipid oxidation in RBCs and <i>P. falciparum</i> infected RBCs	23
3.5	Lipid oxidation control and detoxification	24
3.5.1	Enzymatic ROS detoxification	24
3.5.2	Prevention and termination of lipid oxidation by antioxidants	24
3.5.3	Reduction of lipid peroxides by peroxidases	25
3.5.4	Repair of OxPLs by phospholipases A ₂ and acyltransferases	25
3.5.4.1	Platelet-activating factor acetylhydrolases (PAF-AH)	27
3.5.4.2	Cytosolic PLA ₂ (cPLA ₂)	28
3.5.4.3	Ca ²⁺ -independent PLA ₂ (iPLA ₂)	28
3.5.4.4	Secreted PLA ₂ (sPLA ₂)	29
3.5.4.5	Lysosomal PLA ₂ (LPLA ₂)	29
3.5.4.6	Lecithin:cholesterol acyltransferase (LCAT)	29
3.6	Peroxiredoxin 6 – a trifunctional lipid oxidation repair enzyme	29
3.6.1	PLA ₂ activity of PRDX6	30
3.6.2	Peroxidase activity of PRDX6	31
3.6.3	Lysophosphatidylcholine acyl transferase (LPCAT) activity of PRDX6	31
3.6.4	Physiological roles of PRDX6	32
3.6.5	PRDX6 knockout models and natural PRDX6 mutants	33

3.7	Protective mechanisms against lipid oxidation and membrane repair in RBCs and <i>Plasmodium</i>	33
3.7.1	Antioxidant Protective Enzymes in RBCs and <i>Plasmodium</i>	33
3.7.2	Non-enzymatic antioxidants in RBCs and <i>Plasmodium</i>	33
3.7.2.1	Glutathione and thioredoxin peroxidases of RBCs and <i>Plasmodium</i>	34
3.7.2.2	PLA ₂ enzymes in RBCs and <i>Plasmodium</i>	35
3.7.2.3	PLA ₂ enzymes in other apicomplexans and related parasites	35
3.7.3	The antioxidant host-parasite relationship and uptake of host RBC antioxidant enzymes	36
3.8	Summary and thesis aim	36
4	Material and Methods	38
4.1	Media and buffers	39
4.2	<i>Plasmodium falciparum</i> strains	39
4.3	Mice	40
4.4	Antibodies	40
4.5	Drugs and Inhibitors	40
4.6	Enzymes	41
4.7	Fluorescent Probes	41
4.8	Lipids	41
4.9	<i>In vitro</i> culture of <i>P. falciparum</i>	41
4.9.1	Giemsa staining of thin blood smears	42
4.10	Synchronisation and purification of parasites	42
4.10.1	Synchronisation of parasite culture with sorbitol	42
4.10.2	Purification of schizonts with Percoll	42
4.11	Flow cytometric measurement of <i>P. falciparum</i>	43
4.11.1	Screening of different fluorescent nucleic acid dyes	43
4.11.2	Final flow cytometry protocol for life stage determination	43
4.11.3	Progression and growth assay	44
4.11.4	Re-Invasion Assay with pretreated RBCs	45
4.11.5	Artemisinin ring stage survival assay	45
4.12	Measurement of lipid oxidation	46
4.12.1	Parasite labelling with BODIPY ^{581/591} C11 lipid oxidation sensor	46
4.12.2	TBARS assay	46
4.13	Recombinant expression of human PRDX6 in <i>E. Coli</i>	47
4.14	Bioinformatic analysis of <i>P. falciparum</i> protein sequences	47

4.15	Enzyme activity assays	48
4.15.1	Lp-PLA ₂ activity assay	48
4.15.2	LDH activity assay	48
4.15.3	PRDX6 activity assays	48
4.15.3.1	Phosphorylation of PRDX6	48
4.15.3.2	PRDX6 PLA ₂ activity assay	48
4.16	Inhibitor binding studies	49
4.16.1	PRDX6 binding assays with activity-based protein profiling	49
4.16.2	<i>In silico</i> PRDX6 docking studies	49
4.17	Infection of PRDX6 KO mice with rodent malaria	50
4.17.1	Infection and <i>in vivo</i> growth assay	50
4.17.2	<i>Ex vivo</i> <i>P. yoelii</i> YM progression assay	50
4.18	Immunoblotting of parasite lysate	50
4.18.1	Selective lysis with Saponin and sample preparation	50
4.18.2	SDS-PAGE and Immunoblotting	51
4.19	Microscopy	51
4.19.1	Fluorescence microscopy	51
4.19.1.1	Immuno-fluorescence microscopy	51
4.19.1.2	Preloading of RBCs with LysoSensor Blue/Yellow Dextran, infection with parasites and host cell cytosol-uptake assay	52
4.19.2	Transmission electron microscopy	53
4.19.2.1	Treatment of parasites for host cell cytosol uptake assay	53
4.19.2.2	Fixation of parasites	53
4.19.2.3	Immuno-TEM	53
4.19.2.4	EPON resin embedding	54
5	Results	55
5.1	Establishment of a flow cytometry-based assay to score <i>P. falciparum</i> blood stages by nucleic acid staining	56
5.1.1	Selection of a fluorescent nucleic acid dye	56
5.1.2	Establishment of the optimal SYBR Green concentration	57
5.1.3	Validation of the gating strategy and separation of <i>P. falciparum</i> blood stages	57
5.2	Phospholipase A ₂ (PLA ₂) inhibitors Darapladiib, MAFP and ATK block <i>P. falciparum</i> blood stage progression and growth	59
5.3	Darapladiib raises oxidative stress levels in <i>P. falciparum</i> blood stages	60
5.3.1	Lipid oxidation sensor BODIPY ^{581/591} C11	60
5.3.2	Measurement of MDA levels by TBARS assay	61

5.4	Progression and growth of <i>P. falciparum</i> blood stages inhibited by Darapladib can be restored by addition of α -tocopherol and dioleoyl-PC	62
5.5	Known targets of the PLA ₂ -inhibitors Darapladib, MAFP and ATK are absent in RBCs and <i>P. falciparum</i>	63
5.5.1	Lp-PLA ₂ -mediated platelet-activating factor signalling	65
5.6	Pre-treatment of RBCs with MAFP inhibits <i>P. falciparum</i> blood stage progression, but not invasion	65
5.7	Target identification of Darapladib and MAFP	66
5.7.1	Production and validation of recombinant human PRDX6	66
5.7.2	Human PRDX6 is a target for Darapladib, MAFP and ATK, but not Varespladib	67
5.7.3	Darapladib inhibits the PLA ₂ activity of PRDX6	69
5.7.4	<i>In silico</i> docking of Darapladib to PRDX6	69
5.8	Role of PRDX6 in a malaria mouse model using PRDX6 ^{-/-} mice	70
5.8.1	<i>In vivo</i> growth assay	71
5.8.2	<i>Ex vivo</i> progression assay with Darapladib	72
5.9	Internalisation and localisation of host RBC PRDX6	72
5.9.1	Human PRDX6 is localised within the PVM of <i>P. falciparum</i> schizonts	72
5.9.2	Vesicular hPRDX6 co-localises with the parasite in IFA	73
5.9.3	Immuno-EM shows human PRDX6 co-localises with host cell cytosol-containing vesicles	74
5.10	Darapladib treatment disrupts HcV transport to the FV	76
5.10.1	Co-treatment of parasites with E64 and Darapladib	76
5.10.2	Darapladib inhibits delivery of host cell cytosol to the FV	77
5.10.3	Hemozoin crystal size is reduced upon Darapladib treatment	79
5.11	Co-treatment of Artemisinin with Darapladib shows synergism	79
6	Discussion	82
6.1	Context of this study	83
6.2	Establishment of flow cytometric scoring of life stages by nucleic acid staining	83
6.3	PLA ₂ inhibitors block <i>P. falciparum</i> ring to schizont progression and blood stage growth	84
6.4	Darapladib treatment raises oxidative stress levels in <i>P. falciparum</i>	84
6.5	Inhibition of progression and growth of <i>P. falciparum</i> blood stages by Darapladib can be restored by α -tocopherol and dioleoyl-PC	85
6.6	Established targets of PLA ₂ inhibitors are not present in <i>Plasmodium spp.</i> and RBCs	86

6.7	Pre-treatment of RBCs with MAFP suggests that a host RBC PLA ₂ is essential for <i>P. falciparum</i> blood stage progression, but not invasion	88
6.8	Darapladib, MAFP and ATK target human PRDX6	89
6.9	Role of host PRDX6 in a rodent malaria model using PRDX6 ^{-/-} mice	91
6.9.1	Available approaches for genetic studies in RBCs	91
6.9.2	<i>In vivo</i> growth and <i>ex vivo</i> progression in rodent malaria models	93
6.10	PRDX6 is internalised by <i>P. falciparum</i> and co-localises with host cell cytosol-containing vesicles	95
6.11	Darapladib blocks HcV transport and delivery of hemoglobin to the FV	96
6.12	Reversal of Artemisinin resistance by co-treatment with Darapladib	98
6.13	Summary	100
6.14	Outlook and outstanding questions	100
7	Acknowledgements	103
8	Bibliography	106
9	Appendix	134
I	List of figures	i
II	List of tables	ii
III	Abbreviations	iii
IV	Gen sequences	vi
IV.i	Human PRDX6 6x-His tagged	vi
IV.ii	hPRDX6-His in pET28a	vi

1 Abstract

Abstract

Plasmodium falciparum internalises host red blood cell (RBC) cytosol during its intraerythrocytic development in an endocytic process called host cell cytosol uptake (HCCU). Internalised host cell cytosol is transported to the parasite's food vacuole (FV), where proteins such as hemoglobin are digested to provide nutrients for parasite growth. In addition to hemoglobin, the host RBC cytosol contains antioxidant protective enzymes which have been shown to detoxify reactive oxygen species (ROS) and repair membrane lipid oxidation damage.

Here, we demonstrate that the host RBC enzyme peroxiredoxin 6 (PRDX6), which has both peroxiredoxin and phospholipase A₂ (PLA₂) activity, is taken up by the parasite during HCCU and plays an essential role in blood stage progression. Treatment of parasites with PLA₂ inhibitors blocked parasite growth and ring to schizont progression. Notably, the PLA₂ inhibitor Darapladib increased overall lipid oxidation, disrupted vesicular transport of host cell cytosol-containing vesicles (HcV) to the FV and led to accumulation of HcVs inside the parasite cytosol. Darapladib was found to target human PRDX6 and inhibited its PLA₂ activity. hPRDX6 was localised in HcVs by electron microscopy. Pre-treatment of RBCs with the covalently binding PLA₂ inhibitor methoxy arachidonyl fluorophosphonate (MAFP) allowed successful invasion of rings, but precluded progression of invaded parasites to schizont stage underlining the importance of host RBC PLA₂ for intraerythrocytic parasite growth. Resistance against the state-of-the-art antimalarial drug Artemisinin (ART) is linked to reduced HCCU in early ring stages. Co-treatment of ART-resistant parasites with Dihydroartemisinin and Darapladib showed a synergistic effect and reduced parasite survival significantly, presumably by raising oxidative stress levels.

Taken together, PRDX6 is a completely novel host-based antimalarial drug target candidate which is not essential for the host. Identification of a pharmacologically improved PRDX6 inhibitor could open up a new approach to develop antimalarial drugs that target host enzymes, which may preclude development of drug resistance. Furthermore, selective inhibition of host PRDX6 could help overcome emerging parasite resistance against Artemisinin-based therapies.

Keywords: *Plasmodium falciparum*; Malaria; Host cell cytosol uptake; Hemoglobin; Lipid oxidation; Reactive oxygen species; Artemisinin resistance

2 Résumé

Résumé

Le rôle des enzymes PLA₂ dans l'absorption du cytosol par les cellules hôtes et la croissance au stade sanguin de *Plasmodium falciparum*

Plasmodium falciparum intériorise le cytosol des globules rouges (GR) au cours de son développement intraérythrocytaire dans un processus endocytaire appelé absorption du cytosol dans la cellule hôte (*host cell cytosol uptake*, HCCU). Le cytosol internalisé de la cellule hôte est transporté vers la vacuole alimentaire du parasite (*food vacuole*, FV), où des protéines telles que l'hémoglobine sont digérées pour fournir des nutriments à la croissance du parasite. En plus de l'hémoglobine, le cytosol des GRs contient des enzymes protectrices antioxydantes dont il a été démontré qu'elles détoxifient les dérivés réactifs de l'oxygène (*reactive oxygen species*, ROS) et réparent les dommages causés par l'oxydation des lipides membranaires.

Ici, nous démontrons que l'enzyme RBC hôte peroxiredoxin 6 (PRDX6), qui a une activité peroxiredoxine et aussi phospholipase A₂ (PLA₂), est absorbée par le parasite pendant le HCCU et joue un rôle essentiel dans la progression du stade sanguin. Le traitement des parasites avec des inhibiteurs de PLA₂ bloque la croissance du parasite et la progression du parasite de stade anneau à schizonte. Notamment, l'inhibiteur Darapladib augmente l'oxydation globale des lipides, perturbe le transport vésiculaire des vésicules contenant le cytosol de la cellule hôte (*host cell cytosol-containing vesicles*, HcV) vers le FV et conduit à l'accumulation de HcVs à l'intérieur du cytosol du parasite. Le Darapladib cible le PRDX6 humain et inhibe son activité PLA₂. *hPRDX6* a été localisé dans les HcVs par microscopie électronique. Le prétraitement des GRs avec l'inhibiteur covalente PLA₂ méthoxy arachidonyle fluorophosphonate (MAFP) a permis l'invasion réussie des mérozoïtes, mais a empêché la progression des parasites au stade schizonte, soulignant l'importance des enzymes PLA₂ de l'hôte GR pour la croissance parasitaire intraérythrocytaire. La résistance à l'artémisinine (ART), un antipaludique de pointe, est liée à une réduction du HCCU aux premiers stades de l'anneau. Le co-traitement des parasites résistants au ART avec la dihydroartémisinine et le Darapladib a montré un effet synergique et réduit de manière significative la survie des parasites, vraisemblablement en augmentant les niveaux de stress oxydatif.

Du fait, PRDX6 est un cible entièrement nouvelle pour un médicament antipaludique basé sur un enzyme de l'hôte, qui n'est pas essentiel pour l'hôte. L'identification d'un inhibiteur du PRDX6 pharmacologiquement amélioré pourrait ouvrir une nouvelle approche pour développer des médicaments antipaludiques qui ciblent les enzymes de l'hôte. Cela pourrait empêcher le développement d'une résistance du parasite aux médicaments. En outre, l'inhibition sélective de l'hôte PRDX6 pourrait aider à surmonter la résistance émergente des parasites contre les thérapies à base d'artémisinine.

Mots clefs: *Plasmodium falciparum*; Malaria; Paludisme; Absorption du cytosol des cellules hôtes; Hémoglobine; Oxydation lipidique; Espèces réactives de l'oxygène; Résistance à l'artémisinine

3 Introduction

3.1 Introduction to malaria

Malaria is a mosquito-borne parasitic disease that continues to cause significant morbidity and mortality in the tropical world [1]. According to the World Malaria Report 2020, about 229 million cases of malaria and an estimated 409 000 deaths from malaria occurred worldwide in 2019 [2]. About 94% of all these malaria cases occurred in sub-Saharan Africa. Malaria not only poses a threat to public health, but has severe effects on productivity and economic growth of endemic countries [3]. Despite the general availability of drugs against malaria, the mortality in poverty-stricken countries remains high because of the limited access to treatment in poor rural regions and the fact that no vaccine is available, yet [4]. Furthermore, increased resistance against nearly all anti-malaria drugs has been reported [5]. Thus, there is a great need for research on novel drugs and effective vaccines [1].

Malaria is caused by protozoan parasites that belong to the genus *Plasmodium* and that are transmitted by female *Anopheles* mosquitoes. Reducing the numbers of mosquitoes in endemic areas and limiting contact with humans is known as vector control and is an important strategy in the fight against malaria [2]. *Plasmodium* belongs to the phylum *Apicomplexa*. Similar apicomplexan parasites are *Toxoplasma gondii*, *Babesia spp.* and *Cryptosporidium parvum* [6]. From these parasites, *Toxoplasma gondii* is the most studied and closely related apicomplexan parasite and despite distinct differences in their respective biology, both *Plasmodium* and *Toxoplasma* share fundamental characteristics in key biological processes such as host cell invasion and molecular signaling pathways [6,7]. In the genus *Plasmodium* itself, there are five different species known to infect humans: *P. falciparum*, *P. vivax*, *P. ovale*, *P. malariae* and *P. knowlesi*. The severest form of malaria is caused by *P. falciparum*. Rodent malaria is used as a model for human malaria. Four rodent-infecting *Plasmodium* species are known: *P. berghei*, *P. yoelii*, *P. chabaudi* and *P. vinckei*.

3.2 The life cycle of *Plasmodium falciparum*

The life cycle of *P. falciparum* can be roughly divided into four stages as shown in Figure 3.1: The liver stage (A), the asexual erythrocytic stage (B), the sexual erythrocytic stage (C) and the sporogonic cycle in the mosquito (D). The life cycle inside the human host starts with the injection of sporozoites into the dermis by an infected female *Anopheles* mosquito during a blood meal. From there, the sporozoites move through the dermis until they come into contact with a blood vessel and travel to the liver via the circulatory system [12]. Having reached the liver, the sporozoite invades a hepatocyte by crossing the liver sinusoidal layer through Kupffer cells and further migrates through several hepatocytes [13]. Following multiple rounds of entry and exit through hepatocytes, the sporozoite invades a hepatocyte and forms a parasitophorous vacuole (PV) [14]. The sporozoite multiplies inside this PV and develops into a liver stage schizont containing tens of thousands of merozoites (Figure 3.1 A).

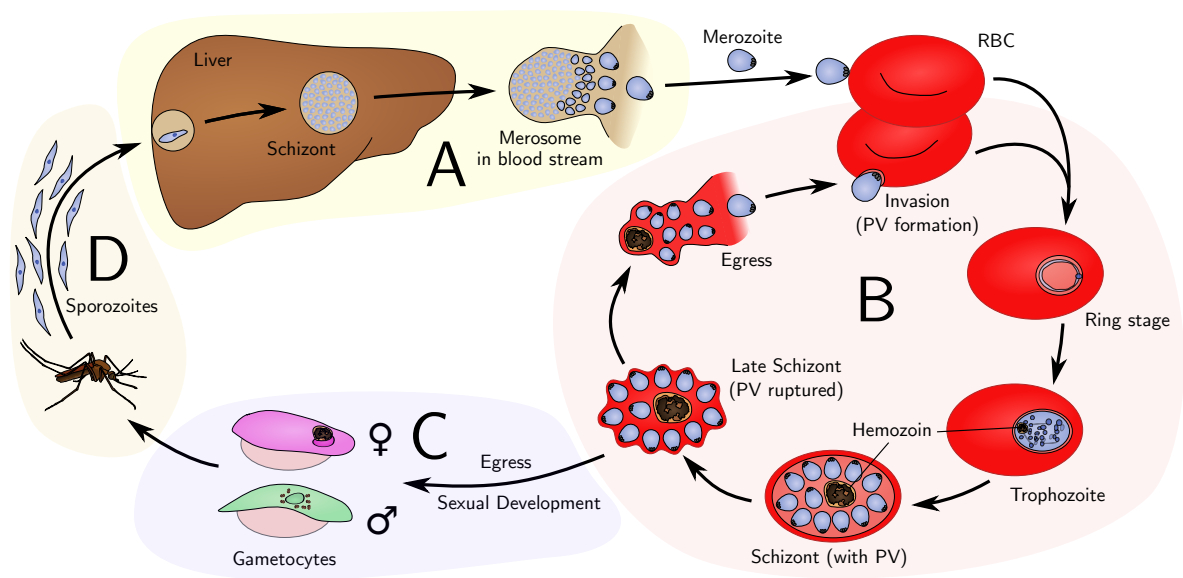


Figure 3.1: The life cycle of *Plasmodium falciparum*. (A) Sporozoites are injected under the skin of the host during the blood meal of an infected female *Anopheles* mosquito and travel to the liver sinusoid using the blood circulatory system. Having crossed the liver sinusoid, each sporozoite invades a hepatocyte, multiplies and forms a liver stage schizont with thousands of merozoites. This schizont then buds off merozoite-filled vesicles, called merosomes, into the bloodstream. (B) The blood stage of the life cycle starts with the invasion of red blood cells (RBCs) by merozoites. During the invasion of the RBC, the merozoite forms the parasitophorous vacuole (PV) in which it develops into a trophozoite. During its development, the parasite feeds on host cell proteins, most notably hemoglobin [8]. The digestion of hemoglobin releases toxic oxidative free heme which is detoxified by the parasite by the formation of hemozoin crystals [9,10]. In the schizont stage, the parasite multiplies by nuclear division and forms 8–32 new merozoites. After rupture of the PV membrane, the RBC membrane and degradation of the RBC cytoskeleton, the merozoites egress from the schizont and re-invade other RBCs. (C) A small proportion of parasites develops into sexual forms: male and female gametocytes. (D) Gametocytes are taken up by a female *Anopheles* mosquito during a blood meal. They mature into male and female gametes inside the mosquito midgut in response to environmental signals. The gametes egress and fertilise to form zygotes, which then transform into ookinets that traverse the midgut wall to form an oocyst [11]. Each oocyst releases thousands of sporozoites which migrate to and invade salivary glands and can be transmitted to humans again during the next blood meal. **Abb.:** PV, parasitophorous vacuole; RBC, red blood cell.

These merozoites are released in parasite-filled vesicles called merosomes, which then release single merozoites into the bloodstream [15]. This marks the start of the blood stage of the parasite life cycle (Figure 3.1 B). All clinical symptoms of malaria are caused by this blood stage. The free merozoites invade red blood cells (RBCs) by a complex multi-step process involving interaction between surface receptors on the RBC membrane and parasite ligands on the merozoite. This process, called invasion, can roughly be divided into four steps: attachment, reorientation, junction formation and invasion [16,17]. The junction formation between merozoite and RBC enables entry by creation of a parasitophorous vacuole (PV) surrounded by a vacuolar membrane (PVM) [18]. Following invasion, the merozoite develops into a ring

form and about 24 hours later into a trophozoite. The trophozoite feeds on proteins such as hemoglobin, lipids and other nutrients of the host RBC (detailed introduction in Section 3.3). The salvage of host cell hemoglobin releases the toxic prosthetic heme group which is rendered harmless by converting free heme into non-toxic hemozoin crystals [9, 10]. During the trophozoite stage, DNA multiplication marks the first step of parasite multiplication by the process of schizogony [19]. Subsequent successive rounds of nuclear division in the early schizont stage lead to the formation of 8–32 new merozoites [15, 20]. These merozoites, which develop and mature inside the schizont are trapped within two membranes, the PVM and RBCM. The rupture of both membranes and the cleavage of the RBC cytoskeleton allows merozoites to egress from mature schizonts [21]. Having egressed, the merozoites invade other RBCs to start a new infectious cycle [22, 23].

During the blood stage life cycle, a small subpopulation of intraerythrocytic parasites commit to sexual development and form male and female gametocytes (Figure 3.1 C) [24, 25]. Only these gametocytes can infect and develop further in the mosquito vector. They are taken up during a blood meal from an infected human (Figure 3.1 D). The gametocytes differentiate inside the mosquito gut into male and female gametes that fuse to fertilize and form a diploid zygote, which undergoes meiosis and develops into a tetraploid ookinete which then translocates to the outer wall of the mid-gut and forms the oocyst [11, 26]. In the oocyst, thousands of haploid sporozoites are produced by endomitotic multiplication (also called sporogony). The oocyst then ruptures and releases sporozoites which migrate to and invade the salivary glands of the mosquito. During the next blood meal, the sporozoites will be transmitted to humans to start the host life cycle again.

The life cycles of the five aforementioned *Plasmodium* species which infect humans are similar to each other [27]. A notable difference is the formation of a dormant hypnozoite form in the liver by *P. vivax* and *P. ovale*. These hypnozoites are not eradicated by standard antimalarial drugs [28, 29]. Furthermore, the number of merozoites formed during schizogony differs between the species.

3.3 Host cell cytosol uptake and hemoglobin digestion

Plasmodium spp. internalise and digest about 75% of the host red blood cell's hemoglobin to provide single amino acids for synthesis of parasite proteins during each cycle of intraerythrocytic replication [30, 31]. Furthermore, the uptake and digestion of host cell cytosol creates space for the intracellular development of the parasite and generates osmolytes which prevent the premature hemolysis of the highly permeabilised infected RBC [31–34]. The process in which *Plasmodium spp.* take up proteins and lipids from the host red blood cell's cytoplasm is known as host cell cytosol uptake (HCCU) (Figure 3.2) [8, 35]. Internalised host cell cytosol is transported in host cell cytosol-containing vesicles (HcV) and salvaged

by the parasite in a specialised, acidic organelle called food vacuole (FV) located in the parasite's cytosol [36]. To reach the FV, the host cell cytosol has to be transported across three membranes: the parasitophorous vacuole membrane (PVM), the parasite plasma membrane (PM) and the FV membrane. Inside the FV, the salvage of hemoglobin yields single amino acids, which are used by the parasite for protein synthesis, and free heme (ferriprotoporphyrin IX). This free heme is toxic and causes oxidative stress due to the Fe(II)-ion bound inside the protoporphyrin structure (detailed introduction in sec. 3.3.2) [36]. To detoxify the free heme, it is crystallised into chemically inert hemozoin crystals which accumulate inside the FV [9, 10].

3.3.1 Mechanistic models of host cell cytosol uptake

The earliest models of HCCU were published in 1966 and are based on electron microscopy studies of avian malaria and *P. falciparum* trophozoites by AIKAWA ET AL. and LADDA ET AL., respectively [37, 38]. Both teams published electron microscopy images showing distinctly dark-coloured endocytic vesicles called cytotomes in the cytoplasm of trophozoites. The dark appearance of the cytotomes suggested that they are densely loaded with hemoglobin, as the large iron atom inside the prosthetic heme group has low transmission for the electron beam causing the structure to appear dark (atomic number -, or Z contrast) [39, 40]. Cytotomes are surrounded by a double membrane structure, resulting from the invagination at both the parasite membrane (PM) and the parasitophorous vacuole membrane (PVM) [41].

The mechanistic details of HCCU in *Plasmodium spp.* are still debated in the literature. In the most widely accepted model, host cell cytosol is taken up through an endocytosis-like process (Figure 3.2) [35, 42]. Through an invagination at the PM/PVM interface, the parasite forms so-called cytotomes containing host cell cytosol. Multiple parasite proteins have been shown to be involved in the formation of cytotomes: Kelch13 (K13), the endocytosis-related adaptor protein 2 (AP2) complex, especially the AP2 μ subunit, a *P. falciparum* homologue of human epidermal growth factor receptor substrate 15 (EPS15), ubiquitin carboxyl-terminal hydrolase 1 (UBP1) and nine unidentified proteins called Kelch13 interaction candidates (KIC1-9) [42–44]. Mutations in these proteins confer reduced susceptibility to the current anti-malaria drug Artemisinin and its derivatives (ART) as they reduce the HCCU in early parasite stages (detailed introduction in Section 3.3.3) [43, 45]. The endocytic mechanisms in *Plasmodium spp.* differ substantially from other eukaryotes. In humans and most other eukaryotes, endocytosis is initiated by formation of the AP2 complex, which recruits clathrin monomers to form clathrin-coated vesicles [46–48]. In contrast, recent findings in *P. falciparum* suggest that the parasite AP-2 complex initiates vesicle formation without involvement of clathrin [44]. Two models are described for the release of host cell cytosol-containing vesicles (HcV) from the mature cytotomes: The “cytotome maturation model” suggests that

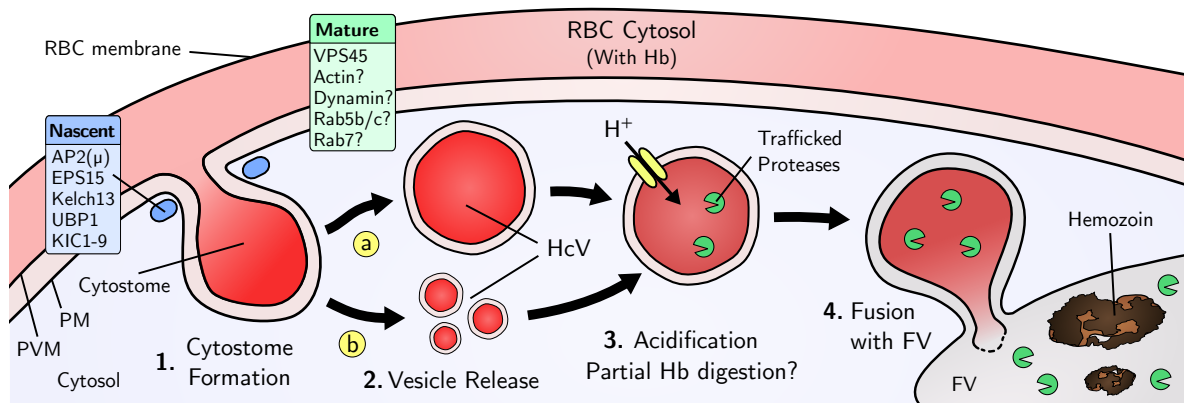


Figure 3.2: Current model for host cell cytosol uptake in *P. falciparum*. 1. Early cytostomes form at the surface of the parasite membrane through invagination of host cell cytosol. The neck of the cytostome is formed and stabilised by a collar consisting of a protein complex with various endocytosis adapter proteins such as AP2 μ and Kelch13. 2. Two models are described for the release of host cell cytosol-containing vesicles (HcV) from cytostomes: (a) The “cytostome maturation model” suggesting that the whole cytostome is formed *de Novo* and released in its entirety and (b) the “cytostome hub model” where small HcVs pinch off a persistent parent cytostome. VPS45 is essential for the transport of released vesicles. Actin and Dynamin potentially play a role in transport, Rab5b/c could be involved in the endolysosomal system and Rab7 might play a role in retrograde transport for recycling. 3. Several studies suggest released mature vesicles acidify and proteases such as Plasmepsin II are trafficked to HcVs from the ER or Golgi. No hemozoin is detected in HcVs suggesting limited or absent Hb digestion. 4. The HcV fuses with the FV and releases its content. Free heme from the digestion of Hb is detoxified by crystallisation into hemozoin crystals. **Abb.:** FV, food vacuole; Hb, Hemoglobin; HcV, host cell cytosol-containing vesicle; PM, parasite membrane; PVM, parasitophorous vacuole membrane; RBC, red blood cell.

the whole cytostome is formed *de novo* and released in its entirety (Figure 3.2 2a) [49, 50], whereas the “cytostome hub model” suggests that small HcVs pinch off a persistent parent cytostome (Figure 3.2 2b) [42].

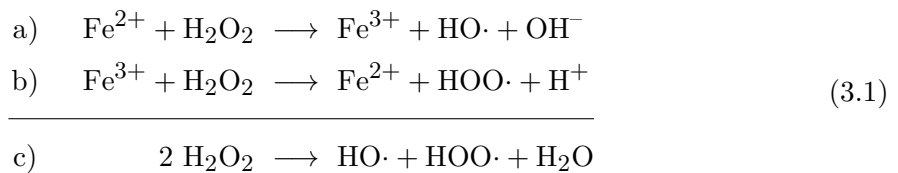
Once released, HcVs have to be actively transported towards the FV. Recently, the *P. falciparum* orthologue of the vacuolar protein sorting-associated protein 45 (VPS45) was identified to be essential for transport of HcVs in *P. falciparum* [50]. The authors demonstrated that HcV accumulated in the parasite’s cytosol and did not get delivered to the FV upon conditional inactivation of *PfVPS45*. Inhibitor studies suggested the further involvement of actin, dynamin, phosphatidylinositol 3-kinases (PI3K) and SNARE proteins in the transport and maturation of HcVs [51–54]. In humans, Ras-associated binding (Rab) proteins are known to localise to early endosomes and play an essential part in the maturation of endosomes [55]. *P. falciparum* expresses Rab orthologues, but their role in cytostomes and HCCU remains unclear [42]. A conditional inactivation of *PfRab5a* leads to growth arrest only in late schizont stage, suggesting that it is not essential during the main HCCU in ring or trophozoite stages [56]. Based on the function of their orthologues in humans and other eukaryotes, Rab5b and Rab5c could be involved in the endolysosomal system and Rab7 might play a role

in retrograde transport for recycling, but neither has yet been directly assessed [42,57–59]. It remains unclear, whether hemoglobin and other host cell cytosol proteins are digested within HcVs before fusion with the FV [35,42,60,61]. No hemozoin was detected in arrested HcVs upon inactivation of *PfVPS45* suggesting limited or absent Hb digestion before the fusion with the FV [50]. However, there is evidence that Hb-proteases such as plasmepsin II are trafficked to HcVs from the parasite ER and Golgi [62]. During their maturation and before the fusion with the FV, HcVs acidify and thus effectively allow HcV-located proteases to work in their pH optima [63,64]. Finally, HcVs fuse with the FV and release their content into the FV lumen where it is proteolytically digested [36].

Between the years 2008 and 2010, several studies claimed various additional models of HCCU. The group of ELLIOTT ET AL. proposed in 2008 that early ring stages take up hemoglobin by folding around a “big gulp” of RBC cytoplasm in a process related to macropinocytosis [65]. They report a cytotome- and actin-independent HCCU pathway in mature parasites called phagotrophy [65]. Conversely, LAZARUS ET AL. suggested in 2008 that cytotomes are mutually connected both to the FV lumen and the RBC cytosol, thus allowing a non-vesicular transport of host cell cytosol [51]. Both the “big gulp” model by ELLIOTT ET AL. and the non-vesicular model by LAZARUS ET AL. are repudiated in more recent publications [42,49,50,63]. ABU BAKAR ET AL. confirmed that parasites form an invaginated cup shape at ring stage, but showed that this invagination pocket stays connected to the RBC cytosol and does not form a separated vesicular structure [63].

3.3.2 Elevated oxidative stress in the parasite causes lipid oxidation

The main source of nearly all amino acids needed by *Plasmodium spp.* for their growth stems from digestion of host RBC hemoglobin [31]. The proteolytic cleavage of hemoglobin inside the parasite FV releases free heme (ferriprotoporphyrin IX or α -hematin) which contains a Fe(II)-ion bound inside a protoporphyrin structure. This heme-bound Fe(II)-ion causes the production of reactive oxygen species (ROS) via the Fenton reaction (Equation 3.1) [66,67]. Briefly, oxidation of Fe(II) with H_2O_2 yields a hydroxyl radical, a hydroxide ion and Fe(III) (eq. 3.1a). The Fe(III) is then reduced again with another molecule of H_2O_2 to form a hydroperoxyl radical, a proton and Fe(II) (eq. 3.1b). As the net reaction product, hydrogen peroxide is disproportionated into a hydroxyl radical, a hydroperoxyl radical and water (eq. 3.1c).



Furthermore, the liberated electron from the oxidation of Fe(II) to Fe(III) can react with molecular oxygen to form superoxide anions ($O_2 + e^- \rightarrow \cdot O_2^-$) [31]. To inhibit the production of ROS, the parasite crystallises reactive free α -hematin monomers into chemically inert β -hematin crystals, which are also called hemozoin [68, 69]. This process is unique to hemaphysal parasites and substantially different from humans, which degrade hemoglobin to bilirubin, free Fe^{2+} and carbon monoxide [70]. Next to hemozoin crystallisation, the malaria parasite may possess alternative ways to detoxify free heme, such as direct enzymatic heme degradation [71, 72]. Despite the detoxifying crystallisation processes in the FV, a small proportion of free heme can escape the FV and locates to the parasite and RBC cytosol, causing oxidative damage [73, 74]. Free heme has also been shown to directly bind to membranes causing lysis [75]. Next to heme-induced oxidative stress, oxidative bursts from host immune cells such as macrophages and T-cells could further increase oxidative stress levels in the parasite [76]. Elevation of oxidative stress caused by accumulation of Fe(II) is also observed in ferroptosis, a regulated, non-apoptotic and tightly controlled type of cell death which can be selectively triggered by nearly all cell types [77, 78].

It is widely agreed that iron- and heme-induced elevation of ROS levels causes extensive lipid oxidation damage [31, 73, 78–80]. Lipid oxidation is covered in detail in section 3.4.

3.3.3 Physiological basis of Artemisinin activity and resistance

Recently, hemoglobin digestion in *Plasmodium spp.* and the subsequent elevation of oxidative stress levels shifted back into the research focus, as the current state-of-the-art antimalarial drug Artemisinin (ART) has been shown to be activated by free heme from hemoglobin digestion [81, 82]. Artemisinin was discovered in the 1970s by the group of YOUYOU TU in studies on antimalarial activity of traditional Chinese herbal medicines [83, 84]. Because of the low bioavailability and solubility of Artemisinin, several semisynthetic derivatives with improved

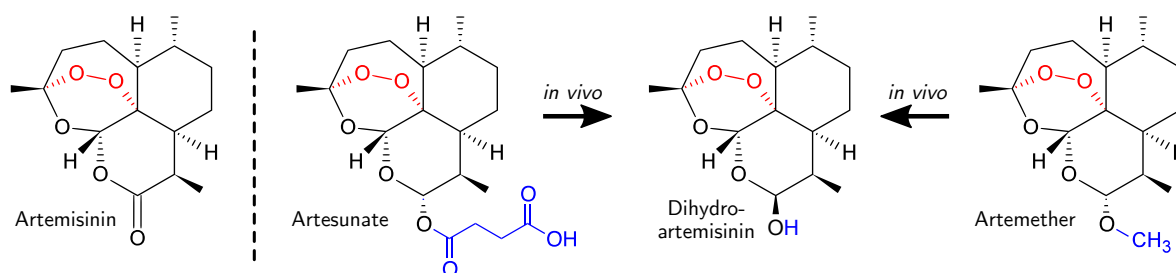


Figure 3.3: Artemisinin and its clinically relevant derivatives. Due to the low bioavailability and solubility of Artemisinin, several improved derivatives have been developed. Of these, Artesunate and Artemether are most widely used. All Artemisinin derivatives are rapidly converted *in vivo* into biologically active Dihydroartemisinin. Inside the infected RBC, Artemisinin is activated by heme-mediated oxidative cleavage of the endoperoxide bridge (shown in red) which then promiscuously binds to multiple targets causing extensive cellular damage.

solubility have been developed (Figure 3.3) [82]. From these, Artesunate and Artemether are the clinically most relevant derivatives [85]. All Artemisinin derivatives are metabolised to the biologically active form Dihydroartemisinin (Figure 3.3) [86]. For better readability, this study refers to all derivatives collectively as “Artemisinin” if not otherwise indicated. Chemically, Artemisinin is classified as a sesquiterpene lactone and contains a reactive 1,2,4-trioxane endoperoxide bridge (Figure 3.3, shown in red) [82]. The cleavage of this endoperoxide bridge is essential for the antimalarial action of Artemisinin and is facilitated by heme-bound Fe(II) [82,87,88]. Chelation of free ferrous Fe(II) ions did not inhibit activation of Artemisinin [88]. This indicates that not free Fe(II) ions, but heme-bound Fe(II) catalyses the cleavage of the endoperoxide [88]. The inhibition of hemoglobin digestion, and thus free heme production, in *P. falciparum* significantly reduced Artemisinin activation [81]. These findings underline the pivotal role of free heme for the activation of Artemisinin. In addition, it has been shown that Artemisinin can be activated by high ROS concentration in yeast mitochondria [89,90]. Taken together, these findings indicate that in a first step, Artemisinin is activated by heme-bound Fe(II) and possibly also high ROS levels through oxidative cleavage of the endoperoxide bridge [82,88].

The downstream mode of action of activated Artemisinin was not understood for a long time [82]. Reports in 2003 suggested that Artemisinin selectively targets the *P. falciparum* sarco/endoplasmic reticulum Ca^{2+} -ATPase 6 (SERCA, *PfATP6*) [91]. The claims of a single specific target have since been refuted in the literature and were replaced by the hypothesis that Artemisinin promiscuously binds to multiple targets [82,88,92,93]. In 2015, alkyne-tagged, heme-activated Artemisinin was shown to covalently bind 124 proteins in *P. falciparum* [88]. An independent complementary study confirmed the promiscuous targeting of Artemisinin a year later [93]. Furthermore, activated Artemisinin was found to inhibit heme crystallisation by alkylation of heme [94]. This makes heme both an activator and a target of Artemisinin. Next to causing extensive cellular damage due to nucleophilic reaction of activated Artemisinin with susceptible groups of proteins and lipids, Artemisinin has been shown to inhibit the parasite’s proteasome leading to a lethal accumulation of unfolded, polyubiquitinated proteins [95].

Due to the promiscuous, unspecific targeting of Artemisinin, drug resistance in *Plasmodium spp.* cannot be attained by simple target mutation. From 2008 on, however, first reports of ART-resistant parasites emerged [96,97]. The first identified molecular marker which caused ART-resistance was a C580Y mutation in the β -propeller domain of the *PfKelch13* (K13) protein [45,98]. K13 has been shown to be involved in the formation of cytosomes during host cell cytosol uptake (HCCU, Figure 3.2) [43]. Further proteins linked with ART-resistance, EPS15 and AP-2 μ , have also been shown to be involved in HCCU [42–44]. Taken together, these findings suggest that mutations in K13, EPS15 and AP-2 μ reduce HCCU and thus hemoglobin digestion in the FV. This in turn lowers the level of free heme being produced

which then inhibits downstream activation of Artemisinin, conferring ART-resistance [43–45]. Notably, these resistance-causing mutations only affect HCCU in ring stage parasites [43].

The most widely used ART derivate Artesunate and its active metabolite Dihydroartemisinin (DHA) have a very short *in vivo* half-life and are completely cleared from patients within about 6 h [99–101]. In these 6 h, the decreased hemoglobin digestion in ART-resistant ring stage parasites effectively impairs the activation of Artemisinin and enables parasite survival [43, 45]. Once Artemisinin is cleared from the system, surviving ART-resistant ring stage parasites can progress and grow normally [45]. So far, no resistance against Artemisinin in trophozoites or schizonts has been observed, most probably because of high levels of free heme in these life stages [45].

The recent identification of the main ART-resistance causing mechanism as reduced HCCU during ring stage allows the specific development of drugs to overcome these resistance mechanisms. One possibility would be to raise general oxidative stress levels in ring stages to allow activation of Artemisinin despite reduced hemoglobin uptake and digestion.

3.4 Lipid oxidation

3.4.1 Molecular basis and physiological effects of lipid oxidation

Lipid oxidation describes the oxidation of mono- or poly-unsaturated fatty acids (MUFA, PUFA) and is initiated non-enzymatically by ROS or enzymatically by lipoxygenases (LOX) [102]. Enzymatic lipid oxidation will not be discussed in detail here, as this study focusses on ROS-initiated non-enzymatic oxidation of phospholipids. Non-enzymatic lipid oxidation is a free radical chain reaction. It is initiated with the abstraction of an unsaturated lipid-bound allylic hydrogen by a free radical yielding a lipid radical (Figure 3.4) [102]. In contrast to saturated FAs, only unsaturated FAs are susceptible to hydrogen abstraction by radicals because their allylic or bis-allylic methylene groups stabilise the carbon-centered secondary

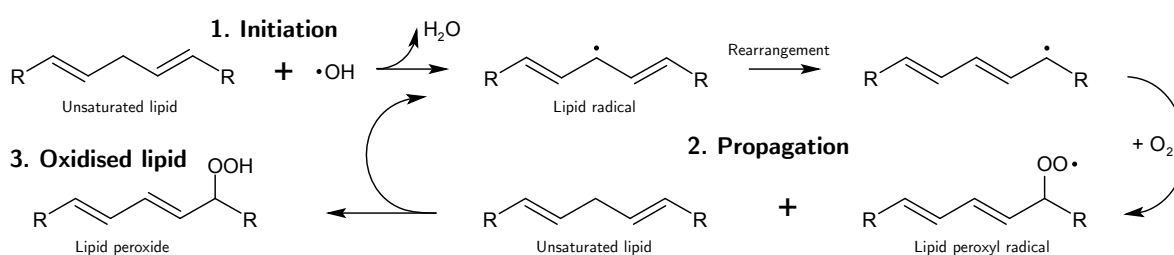


Figure 3.4: Molecular mechanism of the lipid oxidation radical chain reaction. Non-enzymatic lipid oxidation is initiated by the abstraction of an allylic hydrogen of an unsaturated lipid by a free radical. The formed lipid radical rearranges, reacts with molecular O₂ and forms a lipid peroxy radical. This lipid peroxy radical then abstracts the hydrogen of another unsaturated lipid to form a lipid peroxide and causes the propagation of the radical chain reaction.

radical via resonance structures [103]. After a rearrangement, the carbon-centered radical reacts with molecular O₂ and forms a peroxy radical. This lipid peroxy radical then abstracts allylic hydrogens from other unsaturated FAs leading to the production of a lipid peroxide and a new lipid radical, which initiates the further propagation of the radical chain reaction [102, 103]. Peroxidised FAs can undergo further oxidation leading to polyoxygenation, cyclisation or oxidative fragmentation of FAs [102]. Furthermore, oxidised lipids containing an electrophilic aldehyde or carbonyl end group can form adducts with nucleophilic side chains of amino acids, for example the thiol group of cysteine or the amino group of lysine, causing extensive protein damage [102, 104]. Termination of lipid oxidation as well as detoxification and repair of oxidised phospholipids is discussed in detail in Section 3.5.

In vivo, the major targets for lipid oxidation are mono- and poly-unsaturated fatty acids (MUFA, PUFA) bound to a phospholipid (PL) backbone [102]. PLs are the major constituent of cell membranes. Thus, oxidative damage of membrane-bound PLs causes a threat for membrane integrity [102, 105–107]. The oxidation of PLs greatly reduces the hydrophobicity of the FA residue which causes the reorientation of the FAs to the aqueous phase outside of the membrane bilayer [108]. This leads to a drastic decrease in membrane fluidity (lateral diffusion of lipids), significantly changes membrane rigidity and increases the curvature of the lipid bilayer [109–111]. The increased curvature of the lipid bilayer in turn increases the spacing between lipids and enhances the steric accessibility of unoxidised, unsaturated FA side chains [109, 111]. This elevates the risk for further oxidative damage in already oxidised membranes [111]. Furthermore, the oxidatively enlarged intra-lipid spacing has been shown to increase permeability of membranes which can lead to complete membrane disruption [110, 112]. Oxidised phospholipids (OxPL) are a marker of apoptotic and ferroptotic cells and, especially as protein-OxPL adducts, can serve as oxidation-specific epitopes which can be recognised by immune cells and antibodies [102, 113]. Lipid oxidation can also directly trigger apoptosis pathways [114, 115]. Oxidation of cytosolic phosphatidylserine (PS) was shown to trigger the externalisation of unoxidised PS, which is a signal for apoptosis [114].

Cellular signalling and expression of antioxidant proteins is directly controlled by OxPL levels [79, 116]. OxPLs have been shown to modulate the activity of transcription factors such as Nuclear factor erythroid 2-related factor 2 (NRF2) or nuclear factor κ B (NF- κ B) which in turn regulate the expression of antioxidant enzymes and cytokines such as heme oxygenase 1 (HO1) or interleukin 8 (IL-8) [102, 116, 117]. As RBCs do not contain a nucleus, transcription regulation by OxPLs has no implication in uninfected RBCs. However, *P. falciparum* expresses orthologous transcription factors indicating that lipid oxidation could modulate expression of antioxidant parasite proteins [73]. Furthermore, OxPLs can directly bind and activate multiple signalling receptors, such as Toll-like receptor 4 (TLR4), multiple G protein-coupled receptors (GPCR) and the platelet-activating factor receptor (PAFR) inducing various antioxidant responses [79, 102, 116, 118, 119].

3.4.2 Measurement of lipid oxidation

Direct quantification of oxidised lipids is challenging due to the high variety and low abundance of oxidised FAs compared to their unoxidised precursors [102]. Despite the technical difficulties, chromatography-coupled mass spectrometry has been successfully employed to quantify oxidised lipids and has been termed *oxidative lipidomics* [120]. However, complex biological samples contain many molecules with similar mass-to-charge ratios (m/z) as oxidised lipids. This makes oxidative lipidomics impractical for investigation of complex biological processes. In contrast, secondary lipid oxidation products such as malondialdehyde (MDA) and 4-hydroxynonenal (4-HNE) have been studied extensively as biomarkers for lipid oxidation in biological samples since the 1960s [121]. MDA is formed non-enzymatically during the decomposition of oxidised arachidonic acid and larger PUFAs and can be measured conveniently using the thiobarbituric acid reactive substances (TBARS) assay [122]. Even if measurement of TBARS is widely accepted to correlate with lipid oxidative damage in a sample [121], it is known to not be entirely specific for several reasons: Firstly, MDA is not exclusively formed in decomposition of oxidised lipids, secondly not all oxidised lipids decompose into MDA and thirdly thiobarbituric acid can react with substances other than MDA leading to false positive results [123]. Thus, measurement of MDA with the TBARS assay allows the general assessment of the lipid oxidation status in a biological sample, but results should be validated with further investigations using complementary assays [123].

More recently, the lipophilic fluorescent dye BODIPY (4,4-difluoro-3a,4a-diaza-s-indacene) has been employed as a PL- or FA-conjugated probe to measure lipid oxidation directly within membranes [124]. Oxidation of the polyunsaturated lipid bound to the BODIPY dye causes a blue shift of the fluorescence emission peak from red (≈ 590 nm) to green (≈ 510 nm). However, it has been reported that BODIPY lipid oxidation probes are more readily oxidised than endogenous lipids and can act as potent radical scavengers [125]. Thus, BODIPY probes overestimate lipid oxidation damage and do not yield quantitative information on lipid oxidation. Nonetheless, they serve as sensitive indicators for a chemical environment which potentially causes lipid oxidation [125, 126].

3.4.3 Lipid oxidation in RBCs and *P. falciparum* infected RBCs

RBCs are especially prone to lipid oxidation due to the high content of unsaturated PLs in their lipid bilayer, their constant exposure to oxygen and the high concentration of heme-bound Fe(II) within the RBC cytosol [106, 127–129]. As RBCs do not possess either nucleus or a protein expression machinery, they cannot react to changes in oxidative stress [127]. Antioxidant enzymes and mechanisms of RBCs are discussed in detail in Section 3.7.

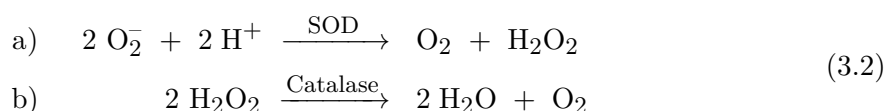
Despite the clear indication that the release of heme during hemoglobin digestion by *P. falciparum* directly causes toxic lipid oxidation damage, direct research of lipid oxidation during

P. falciparum infection has been scarce [73, 126, 130]. Similar to uninfected RBCs, the membranes of *P. falciparum* within the RBC consist largely of unsaturated FAs [131]. During infection, the ratio of unsaturated to saturated FA side chains within the RBC membrane further increases [132]. Initial studies from 1985 and 1992 didn't find direct evidence for lipid oxidation in *P. falciparum* infected RBCs [133, 134]. However, more recent studies successfully demonstrated increased lipid oxidation in *P. falciparum* infected RBCs [126, 130, 135]. Notably the study of *P. falciparum* infected RBCs stained with the fluorescent lipid oxidation sensor BODIPY^{581/591}-PC by FU ET AL. indicated that mostly the parasite membranes, but not host RBC membranes were subjected to lipid oxidation [126]. Treatment of *P. berghei* infected mice with oxidised FAs leads to reduced parasite survival [136]. Recently, it has been shown that host lipid oxidation regulating enzymes are essential during the liver stage of *P. berghei* [137].

3.5 Lipid oxidation control and detoxification

3.5.1 Enzymatic ROS detoxification

Initiation of the radical lipid oxidation chain reaction can be prevented by enzymatic detoxification of small ROS molecules, such as H₂O₂. Superoxide dismutase (SOD) catalyses the dismutation of the superoxide radical O₂⁻ into oxygen and H₂O₂ (Equation 3.2a), and catalase cleaves H₂O₂ into water and oxygen (Equation 3.2b) [77, 127]. Small ROS molecules like H₂O₂ are also reduced and detoxified by glutathione peroxidases (GPx), thioredoxin peroxidases (TPx) and peroxiredoxins (PRDX) through the oxidation of a dithiol-disulfide reductant such as glutathione (GSH) or thioredoxin (Trx) (Figure 3.5B/C) [138]. Oxidised glutathione and thioredoxin are then recycled via the oxidation of NADPH to NADP⁺.



3.5.2 Prevention and termination of lipid oxidation by antioxidants

Antioxidant radical scavengers form stable radicals and are excellent hydrogen donors due to stabilising resonance structures and large delocalised electron systems [139]. Thus, antioxidant radical scavengers can prevent the initiation of the chain reaction by scavenging free radicals (Figure 3.5A) [77, 140]. Furthermore, the lipid oxidation radical chain reaction can be terminated by scavenging of reactive lipid and lipid peroxy radicals by antioxidant compounds such as α -tocopherol (vitamin E), Coenzyme Q₁₀, ascorbic acid (Vitamin C), ferrostatin-1 or lipoxstatin [111, 140–142]. Key antioxidant compounds in RBCs and *Plasmodium spp.* are discussed in detail in Section 3.7.2.

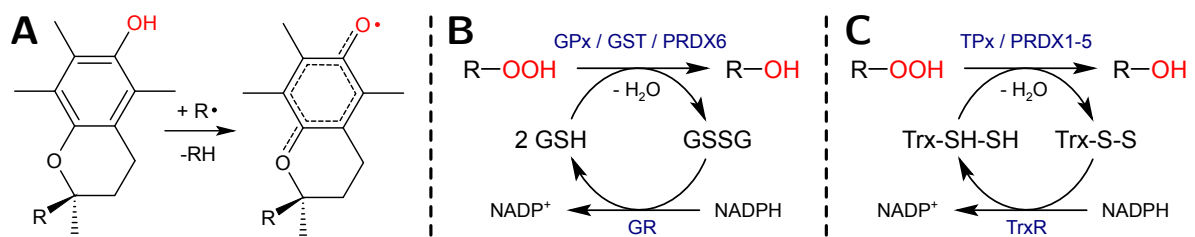


Figure 3.5: Control and repair of lipid oxidation. (A) The lipid oxidation radical chain reaction can be terminated by scavenging of radicals, such as α -tocopherol (shown). The chain reaction is terminated due to the stability of the antioxidant radical. (B) Small ROS molecules such as H_2O_2 and reactive phospholipid peroxides are reduced by glutathione peroxidases (GPx), glutathione S-transferases (GST) and peroxiredoxin 6 (PRDX6) to water or a less reactive lipid hydroxide, respectively, via the oxidation of glutathione (GSH). GPx4 and PRDX6 preferably reduce oxidised phospholipids, whereas other glutathione peroxidase family members reduce small ROS molecules. Oxidised glutathione is recycled by glutathione reductase (GR) under the use of NADPH. (C) Thioredoxin peroxidases (TPx) and PRDX1–5 can reduce reactive peroxides with thioredoxin (Trx), a thioredoxin reductase (TrxR) and NADPH. **Abb.:** GR, glutathione reductase; GPx, glutathione peroxidase; GSH, glutathione; GST, glutathione S-transferases; PRDX, peroxiredoxin; Trx, thioredoxin; TPx, thioredoxin peroxidase; TrxR, thioredoxin reductase.

3.5.3 Reduction of lipid peroxides by peroxidases

Highly reactive lipid peroxides can be reduced to less reactive lipid hydroxides by enzymes such as glutathione peroxidases (GPx), thioredoxin peroxidases (TPx) and peroxiredoxins (PRDX) (Figure 3.5B) [102, 143]. The enzymes GPx4 and PRDX6 show the highest activity for the reduction of membrane-bound oxidised phospholipids, whereas other GPx and PRDX family members are involved in reduction of small ROS molecules such as H_2O_2 as described above [77, 102, 107]. GPx4 and PRDX6 reduce lipid peroxides by oxidation of glutathione (GSH), thereby generating a less reactive lipid hydroxide and oxidised glutathione [102, 107, 144]. Oxidised glutathione is then recycled by glutathione reductase (GR) under the use of NADPH (Figure 3.5B) [144]. In RBCs, NADP^+ is then recycled back to NADPH exclusively by the enzyme glucose-6-phosphate dehydrogenase (G6PD) [73, 145].

In addition to GPxs and PRDXs, lipid peroxides can be reduced by glutathione S-transferases (GST) (Figure 3.5B) [146, 147]. Similarly to GPxs, thioredoxin peroxidases (TPx) can reduce lipid peroxides with thioredoxin (Trx), a respective thioredoxin reductase (TrxR) and NADPH (Figure 3.5C) [144, 148, 149].

3.5.4 Repair of OxPLs by phospholipases A₂ and acyltransferases

Phospholipids (PLs) consist of a glycerol backbone which is esterified with two fatty acid residues and a polar phosphate-containing head group (Figure 3.6A). To precisely name the configuration of PLs, the carbon atoms of the glycerol backbone are numbered. The carbon

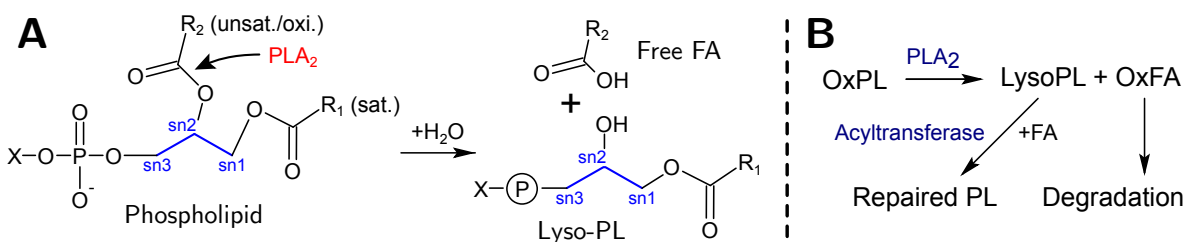


Figure 3.6: Repair of OxPLs by PLA₂. (A) Phospholipase A₂ enzymes selectively cleave the *sn2*-FA of phospholipids by hydrolysis. In phospholipids, the *sn1*-FA (here R₁) is generally unsaturated and thus not oxidised whereas the *sn2*-FA (R₂) has varying degrees of unsaturation and can be oxidised. (B) OxPLs are repaired by selective cleavage of the oxidised *sn2*-FA and replacement with an unoxidised FA via an acyltransferase. The free oxidised FA is subsequently degraded via β -oxidation. **Abb.:** FA, fatty acid; (Ox)PL, (oxidised) phospholipid; X, phospholipid head group, such as choline, ethanolamine, inositol or serine.

atom, which is the farthest from the polar head group is designated as *sn1* (stereospecifically numbered 1), the middle carbon atom as *sn2* and the carbon esterified with the phosphate group as *sn3* [150]. The saturation of FA residues of PLs is asymmetric between the *sn1* and *sn2* position. Generally, the *sn1*-FA is saturated, whereas the *sn2*-FA has varying degrees of unsaturation [151, 152]. The reason for this asymmetry was not understood until recently. MANNI ET AL. provided evidence that membranes with artificially increased abundance of *sn1*- and *sn2*-unsaturated PLs showed drastically elevated permeability and vesiculation frequency [151]. The authors concluded that the saturation asymmetry between *sn1* and *sn2* FAs provided a good trade-off between membrane stability and permeability [151]. The finding that the *sn1*-FA is generally saturated implies that PL oxidation damage is nearly exclusively restricted to unsaturated *sn2*-FA residues.

Phospholipases which selectively and exclusively cleave the *sn1*- or the *sn2*-FA are called phospholipase A₁ (PLA₁) and phospholipase A₂ (PLA₂), respectively. Phospholipases which cleave both *sn1*- and *sn2*-FAs are classified as phospholipase B (PLB). As the majority of lipid oxidation concerns *sn2*-FAs, PLA₂ enzymes play a crucial role for detoxification of OxPLs. Mechanistically, PLA₂ (and similarly PLA₁ and PLB) cleave the ester bond between the glycerol backbone and the FA by hydrolysis (Figure 3.6A and B) [102, 107, 153]. The net reaction product is a lyso-phospholipid (Lyso-PL) and a free FA. A summary of the PLA₂ mediated repair mechanism of OxPLs is shown in Figure 3.6B. After cleavage of the oxidised *sn2*-FA by a PLA₂, the resulting Lyso-PL is complemented with an unoxidised FA by an acyltransferase (AT) [102, 154]. The free oxidised *sn2*-FA is then degraded and detoxified by β -oxidation [102, 107, 153, 155]. Several PLA₂ enzymes have been shown to selectively cleave OxPLs and are discussed in detail in the following sections.

3.5.4.1 Platelet-activating factor acetylhydrolases (PAF-AH)

Several PLA₂ enzymes from the class of platelet-activating factor acetylhydrolases (PAF-AH) have been reported to cleave oxidised lipids: Lipoprotein-associated PLA₂ (Lp-PLA₂), platelet-activating factor acetylhydrolase 2 (PAF-AH2) and the heterotrimeric platelet-activating factor acetylhydrolase 1b (PAF-AH1b). All PAF-AH enzymes contain a Ser-His-Asp catalytic triad in their active site and are Ca²⁺-independent [156]. PAF-AHs are classified in group VII and VIII of the PLA₂ superfamily.

Human lipoprotein-associated PLA₂ (Lp-PLA₂) is the most studied enzyme in PLA₂ group VII [157]. The naming of Lp-PLA₂ has been inconsistent in the literature. Other names for Lp-PLA₂ are PLA2G7, LDL-PLA₂ and platelet-activating factor acetylhydrolase (PAF-AH), which is not used here to avoid confusion with the enzyme class PAF-AH. The primary enzymatic action of Lp-PLA₂ is the cleavage of the phospholipid platelet-activating factor (PAF) into lyso-PAF. PAF is a unique phospholipid as it has an *ether* linked saturated C16 acyl chain at *sn1* and a short C2 acetyl group esterified at *sn2*. PAF has a phosphocholine head group. Lp-PLA₂ exhibits specificity for very short *sn2*-FAs, such as the *sn2* C2 acetyl group of PAF. The cleavage efficiency is significantly decreased with increasing chain length of the *sn2* residue with relative activity of about 2% for cleavage of a C9 *sn2*-FA [157]. However, if the *sn2*-FA is oxidised, Lp-PLA₂ was shown to effectively cleave oxidised *sn2*-FAs up to C9 [105, 157–159]. Lp-PLA₂ is an extracellular plasma protein and exported to the blood stream after production in CD14⁺ inflammatory cells [157]. Because of the involvement of Lp-PLA₂ in the cleavage of oxidised low-density lipoproteins (Ox-LDL), which play a major role in vascular diseases, it was proposed that inhibition of Lp-PLA₂ could confer protection against vascular diseases such as atherosclerosis [157, 159, 160]. For this, the specific Lp-PLA₂ inhibitor Darapladib was developed by GlaxoSmithKline (Figure 3.7A) [160]. Despite exhibiting a very good pharmacological profile with an IC₅₀ for Lp-PLA₂ of 0.25 nM, Darapladib failed as a drug against atherosclerosis in Phase III trials [161]. One major drawback of the lipophilic

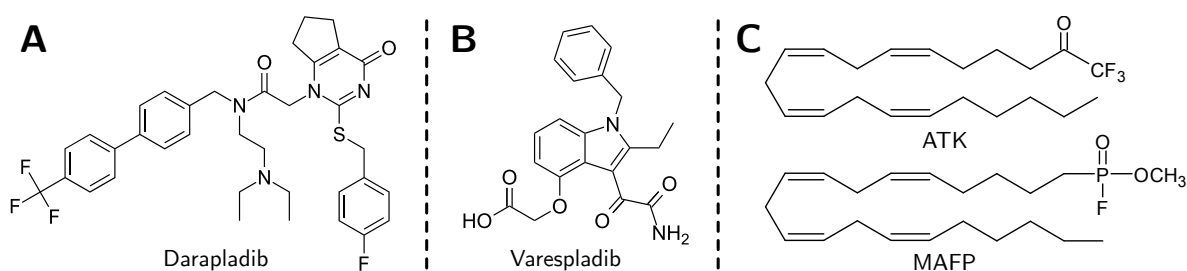


Figure 3.7: Inhibitors of PLA₂. (A) Darapladib inhibits human Lp-PLA₂. (B) Varespladib targets sPLA₂ enzymes of groups IIA, V and X. (C) ATK and MAFF target both cPLA₂ and iPLA₂. MAFF has furthermore been shown to inhibit Lp-PLA₂. **Abb.:** ATK, Arachidonyl trifluoromethyl ketone; cPLA₂, cytosolic PLA₂; Lp-PLA₂, Lipoprotein-associated PLA₂; MAFF, Methoxy arachidonyl fluorophosphate; sPLA₂, secreted PLA₂.

drug Darapladib is its low bioavailability with a maximum plasma concentration of only 20nM after administration of 160 mg intravenously [162]. In addition to Darapladib, the covalent inhibitor methoxy arachidonyl fluorophosphonate (MAFP) has been shown to inhibit Lp-PLA₂ (Figure 3.7C) [163, 164].

Platelet-activating factor acetylhydrolase 2 (PAF-AH2) is the cytoplasmic isoform of extracellular Lp-PLA₂ and shares about 41% identity [165, 166]. PAF-AH2 shows a very similar selective activity against PAF and oxidised lipids shorter than C10 as Lp-PLA₂ [165–167]. No specific inhibitors against PAF-AH2 have been developed so far.

PAF-AH1b, also sometimes called PLA2G8, is another intracellular PAF-AH but substantially different from Lp-PLA₂ and PAF-AH2 [168–170]. PAF-AH1b is a heterotrimeric enzyme consisting of a regulatory subunit (PAF-AH1b1) and two catalytic subunits (PAF-AH1b2/3) [168]. The PAF-AH1b complex shows a similar activity profile as Lp-PLA₂ and PAF-AH2 against PAF and short oxidised lipids [165, 167, 171, 172]. The compound P11 selectively inhibits the catalytic subunits PAF-AH1b2 and PAF-AH1b3 of the PAF-AH1b complex [168].

3.5.4.2 Cytosolic PLA₂ (cPLA₂)

Cytosolic PLA₂ enzymes are classified in group IV and contain a Ser-Asp catalytic dyad [156, 173]. In comparison to other PLA₂, they contain a Ca²⁺-binding C2 domain and require Ca²⁺ for their enzymatic activity [156, 173, 174]. cPLA₂ show elevated activity against long, poly-unsaturated *sn2*-FA, such as arachidonic acid and linoleic acid, and have also been shown to cleave oxidised *sn2*-FAs [102, 156, 175]. The inhibitors arachidonyl trifluoromethyl ketone (ATK) and methoxy arachidonyl fluorophosphonate (MAFP) were among the first reported inhibitors of cPLA₂ and have been widely studied in the literature [156]. They do not inhibit sPLA₂, but have been shown to target iPLA₂. MAFP targets Lp-PLA₂ as well [156, 163, 164]. ATK and MAFP are both derivatives of arachidonic acid with either a reversibly binding trifluoromethyl head group for ATK or a methoxy fluorophosphonate head group for MAFP, which forms a covalent bond with the active site serine (Figure 3.7C) [176–179].

3.5.4.3 Ca²⁺-independent PLA₂ (iPLA₂)

Ca²⁺-independent PLA₂ (iPLA₂) enzymes share homology with group IV cPLA₂ enzymes, but lack the C2 domain and have Ca²⁺-independent PLA₂ activity [156, 180]. Similar to cPLA₂, iPLA₂ contain a Ser-Asp catalytic dyad and show a similar selectivity for long unsaturated, as well as long oxidised *sn2* FAs [156]. Several iPLA₂ share homology with the potato storage protein patatin and are also called patatin-like phospholipases A (PNPLA) [156, 181]. Due to the similarity to cPLA₂, iPLA₂ are inhibited by the cPLA₂ inhibitors ATK and MAFP [156, 178, 182]. No specific iPLA₂ inhibitors are available so far [156].

3.5.4.4 Secreted PLA₂ (sPLA₂)

Secreted PLA₂ (sPLA₂) are small proteins ranging from 14–18 kDa which are secreted to the blood stream [156, 180]. In contrast to all other PLA₂ subfamilies, they contain a His-Asp catalytic dyad [156]. sPLA₂ have been shown to cleave oxidised lipids, especially bound to lipoproteins [183]. For selective inhibition of sPLA₂ enzymes, the inhibitor Varespladib was developed against sPLA₂ enzymes in the groups IIA, V and X (Figure 3.7B) [184].

3.5.4.5 Lysosomal PLA₂ (LPLA₂)

Lysosomal PLA₂ (LPLA₂) is classified in the PLA₂ group XV and predominantly found in lysosomes [156, 185]. It exhibits its maximum activity at acidic pH [156, 185]. Similar to Lp-PLA₂, it has a Ser-His-Asp catalytic triad and has been shown to cleave short-chain oxidised lipids [185, 186]. LPLA₂ has also been shown to cleave *sn1*-FAs and thus is not a selective PLA₂ [185]. LPLA₂ shares about 50% identity with lecithin:cholesterol acyltransferase (LCAT) [185, 187]. LPLA₂ is inhibited by MAFP, but no selective inhibitors have been identified [185].

3.5.4.6 Lecithin:cholesterol acyltransferase (LCAT)

Principally, lecithin:cholesterol acyltransferase (LCAT) catalyses the formation of cholesterol-acyl esters using PLs as donors for the acyl chains and shares 50% homology with LPLA₂ [185, 188, 189]. However, LCAT was also shown to cleave oxidised *sn2*-FAs without a subsequent formation of cholesterol esters [190]. The LCAT-PLA₂ activity seems to be selective for long-chain oxidised FAs, in contrast to PAF-AHs and LPLA₂, which cleave short-chain oxidised FAs [185, 191]. LCAT is a secreted serum protein and no selective inhibitors against LCAT have been developed so far [187].

3.6 Peroxiredoxin 6 – a trifunctional lipid oxidation repair enzyme

Peroxiredoxin 6 (PRDX6) is a unique enzyme as it exhibits both a cysteine-dependent peroxidase activity, as well as an independent PLA₂ activity [153, 192, 193]. There is additional evidence that PRDX6 also has a lysophosphatidylcholine acyl transferase (LPCAT) activity [154]. Neither the PLA₂ nor the LPCAT activity are found in other peroxidases, making PRDX6 a unique enzyme of its kind [153]. PRDX6 is known to repair oxidised membranes, a model for this process is shown in Figure 3.8 [107, 194]. In the initial state, PRDX6 is localised in the cytosol (Figure 3.8A). Upon oxidation of the membrane, PRDX6 can associate to the membrane by direct binding to OxPLs (Figure 3.8B) [107]. After binding, PRDX6 reduces lipid peroxides with its peroxidase activity by co-oxidation of glutathione (Figure 3.8C). The damaged FA is subsequently cleaved and replaced with an unoxidised FA using the PLA₂ and LPCAT functions (Figure 3.8D). Kinetic studies suggest that PLA₂-mediated acyl cleavage and LPCAT-mediated re-acylation occur sequentially without detachment of

PRDX6 or release of a lyso-PL [154]. The three enzymatic activities are described in detail in sections 3.6.1 to 3.6.3. The role of PRDX6 in repair of oxidised membranes has been shown using lungs of WT and PRDX6^{-/-} mice and pulmonary microvascular endothelial cells (PMVEC) [107, 194, 195]. For this, cells were artificially peroxidised using tert-butyl hydroperoxide (t-BOOH) or hypoxia (100% O₂). In WT cells, lipid oxidation damage levels returned to control level within 2 h, whereas PRDX6^{-/-} cells did not repair lipid oxidation damage, indicating a complete inhibition of membrane repair [107, 194, 195]. Mutations of PRDX6 which selectively inactivated either the peroxidase activity (C47S-PRDX6) or the PLA₂ activity (D140A-PRDX6) caused a reduction in lipid oxidation damage repair, but not complete inhibition [107].

3.6.1 PLA₂ activity of PRDX6

The active site of the PLA₂ function is comprised of a Ser-His-Asp catalytic triad, similar to Lp-PLA₂ and LPLA₂ [156, 193, 196–198]. In this triad, the serine is deprotonated by the aspartate-activated histidine which drastically increases the nucleophilicity of hydroxyl oxygen of the serine. This activated oxygen can facilitate the cleavage of electrophilic groups such as the carboxylic carbon of the *sn*2-esterified FA of a phospholipid [156]. Furthermore, inhibitors and activity-based protein profiling (ABPP) probes carrying a reactive fluorophosphonate group (e.g. MAFP and TAMRA-FP) can covalently and selectively bind this activated serine of PRDX6 [179, 199]. The active site for the PLA₂ activity of PRDX6 also contains an oxyanion hole which can further stabilise the charged transition state of the cleaved phospholipid [200]. Mutation of any of the catalytic triad residues (H26A, S32A and D140A) causes a complete loss of PLA₂ activity [196].

The PLA₂ activity of PRDX6 is Ca²⁺-independent and shows its greatest activity in acidic conditions [153, 198]. At pH 4, the activity for unoxidised and oxidised PL is similar.

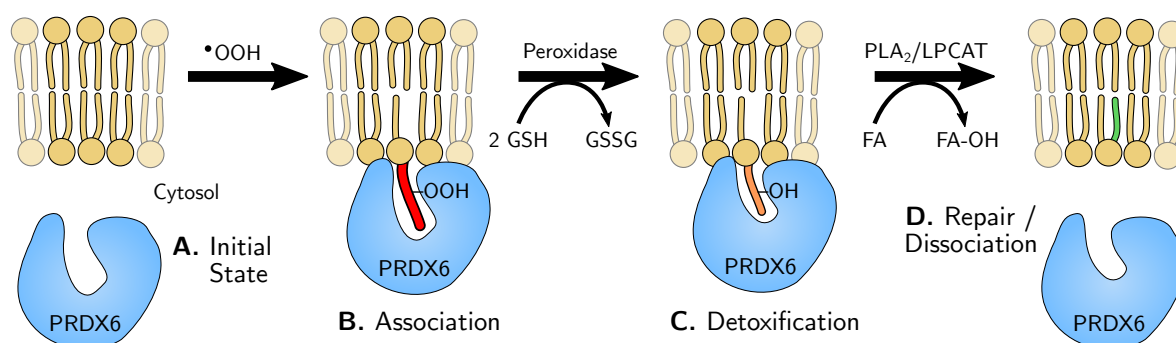


Figure 3.8: Model for OxPL detoxification by PRDX6. (A) In the initial state, PRDX6 is localised to the cytosol. (B) Upon lipid oxidation of membranes, PRDX6 associates with the oxidised membrane. (C) With its glutathione-dependent peroxidase function, PRDX6 reduces lipid peroxides to less toxic lipid hydroxides. (D) The oxidatively damaged FA is cleaved using the PLA₂ function and replaced with an unoxidised FA through its LPCAT activity. *Abb.:* FA, fatty acid; GSH, glutathione; PRDX6, Peroxiredoxin 6; LPCAT, lysophosphatidylcholine acyl transferase. Fig. adapted from [153]

At neutral pH, however, PRDX6 has been shown to retain a high activity for cleavage of Ox-PLs, whereas activity for unoxidised PL is greatly reduced [153,201]. Hyperoxidation drastically increases the PLA₂ activity of PRDX6 at neutral pH, but does not affect the activity at pH 4 [202,203]. Phosphorylation of PRDX6 by kinases such as mitogen-activated protein kinase (MAPK) greatly enhances the PLA₂ activity [198,204]. Phosphorylated PRDX6 has a 15–20-fold higher activity than unphosphorylated PRDX6 at pH 4 and also shows an equally high activity at neutral and acidic pH [153,198,204]. The PLA₂ activity of PRDX6 is independent of dimerisation [205].

Despite similarities between LPLA₂ and PRDX6, such as the Ca²⁺-independent activity at acidic pH and the Ser-His-Asp catalytic triad, both enzymes differ substantially in other characteristics [153,186]. While PRDX6 is localised in both cytosol and lysosomes, LPLA₂ has been exclusively characterised in lysosomes [153,185]. In contrast to LPLA₂, PRDX6 does not have PAF-AH or PLA₁ activity [153,185]. PRDX6 readily cleaves OxPLs at neutral pH, whereas LPLA₂ has a greatly reduced activity at neutral pH [153,186].

The compound MJ33 has been described as a PRDX6 inhibitor in the literature [198,206]. MJ33 is a charged phospholipid mimicking the tetrahedral transition state of phospholipids during PLA₂-mediated FA cleavage [207]. Due to its hydrophobic phospholipid structure, MJ33 has a low bioavailability and does not readily cross membranes. The IC₉₀ for inhibition of PRDX6 by MJ33 is about 1 mol%, thus in a liposome-based PLA₂ activity assay, MJ33 makes up 1% of the total lipid composition of the liposome [153,198]. Taken together, MJ33 does not serve as an effective inhibitor outside the *in vitro* liposome-based activity assay and has limited application in complex biological systems.

3.6.2 Peroxidase activity of PRDX6

PRDX6 is a non-selenium cysteine-peroxidase and uses glutathione as the reductant (Figure 3.5B) [107,192,194]. In contrast to most other peroxidases which use two cysteines for their peroxidase activity (2-Cys peroxidase), PRDX6 only contains one cysteine and is thus also called a 1-Cys peroxidase [192,208,209]. The peroxidase activity of PRDX6 requires the dimerisation of the enzyme [205]. Replacement of the active cysteine at position 47 with a serine (C47S) causes a complete loss of the peroxidase function of PRDX6 [192,194,195,209]. No selective inhibitors of the PRDX6-peroxidase activity are known.

3.6.3 Lysophosphatidylcholine acyl transferase (LPCAT) activity of PRDX6

The acyl transferase activity of PRDX6 was shown to be specific for lysophosphatidylcholine and thus termed lysophosphatidylcholine acyl transferase (LPCAT) activity [154]. This LPCAT activity of PRDX6 shows a similar pH- and phosphorylation-dependency as the PLA₂ activity and shows a specificity for the transfer of palmitoyl-CoA [154]. The inhibitor of the PLA₂ activity of PRDX6, MJ33, did not inhibit the LPCAT activity [154]. The D31A mutation of PRDX6 causes a complete loss of the LPCAT activity [154].

3.6.4 Physiological roles of PRDX6

As discussed previously, PRDX6 is involved in the repair of oxidised membranes [107]. Both the PLA₂ and LPCAT activities of PRDX6 have been shown to play a pivotal role in degradation and remodelling of lung surfactant, which is a lipid-protein complex [107]. Lung surfactant facilitates pulmonary compliance (ability to expand during inhalation) and reduces the surface tension in lung alveoli allowing efficient gas exchange [107]. The PLA₂ activity of PRDX6 is essential for activation of NADPH oxidase 1 and 2 (NOX1/2) [210,211]. NOX1 and NOX2 catalyse the formation of the superoxide radical $\cdot\text{O}_2^-$ which is involved in the macrophage oxidant defense system against bacteria [212]. PRDX6-mediated activation of NOX1 and NOX2 might be involved in the response of the lung microvascular endothelium to mechanical stress [153]. Thus, PRDX6 can act as both a pro- and an antioxidant enzyme in certain cellular contexts [153]. It has been suggested that PRDX6 thus could be regarded as a “normalising” enzyme conferring balance between the protection against oxidative damage by ROS, while still allowing sufficient ROS generation for cellular signaling [153]. This double role of PRDX6 has been shown in the context of acute lung injury, where PRDX6 both contributes to ROS generation via activation of NOX2, but also has been shown to reduce oxidative stress through its peroxidase activity [153,194,210].

A recent study suggested that the PLA₂ activity of PRDX6 is important for male fertility and ROS control in spermatozoa [213]. In mice, PRDX6 expression has been shown to decrease with age which in turn corresponded to reduced male fertility and spermatozoa motility and viability [213]. Treatment of mice spermatozoa with the PRDX6 inhibitor MJ33 leads to increased lipid oxidation and reduced fertilisation rates [213]. For humans, male infertility has been linked to decreased PRDX6 levels in spermatozoa [214]. Taken together, PRDX6 might play a crucial role in male fertility by protection of spermatozoa from oxidative stress.

PRDX6^{-/-} mice have a reduced glucose-dependent insulin secretion and higher insulin resistance and thus show a phenotype similar to diabetes type 2 [215]. Furthermore, treatment of mice with streptozotocin-induced type 1 diabetes with recombinant PRDX6 alleviated diabetic symptoms [216]. These findings imply a role of PRDX6 in manifestation of diabetes [153].

In cancer, overexpression of PRDX6 is associated with increased proliferation, cell migration and cellular invasion with various types of cancer, including breast, lung, colorectal, gastric, ovarian, tongue, oesophagus, bladder, liver, gingiva, skin and mesothelium cancer [153,217–222]. Accordingly, the knockout of PRDX6 in various cancer models reduced cell viability and proliferation [217,219,220]. Carcinogenesis is generally connected to increased production of ROS due to the elevated metabolism in cancer cells [223,224]. Thus, overexpression of PRDX6 in cancer cells is may confer additional antioxidant protection and

to promote cancer cell proliferation [217]. In skin cancer, however, overexpression of PRDX6 has been shown to contrastingly prevent formation of new tumours, while promoting the growth of existing skin cancer tumours [225]. The detailed mechanistic role of PRDX6 in carcinogenesis is not yet fully understood [153]. Nonetheless, PRDX6 is generally linked with enhanced growth and survival of cancer cells and pharmacological inhibition of PRDX6 could help to reduce cancer cell proliferation and tumour growth [153, 217].

3.6.5 PRDX6 knockout models and natural PRDX6 mutants

The sequence of PRDX6 is highly conserved between mammals [153]. PRDX6 was successfully knocked out in C57/BL6JRj mice [226]. PRDX6^{-/-} mice show a reduced fertility with a significantly reduced litter size, increased pup mortality and increased sensitivity to lipid oxidation damage [227]. This phenotype can be alleviated with an α -tocopherol rich diet [227]. Mice with selective mutations conferring loss of either PLA₂ or peroxidase activity have been generated [153, 228, 229]. Natural homozygous loss-of-function (LoF) mutations of PRDX6 in humans have not been reported so far. As fertility in PRDX6^{-/-} mice is greatly reduced, the selection of a natural PRDX6 LoF mutation in human is unlikely due to the likely reproductive fitness cost. Several single-nucleotide polymorphisms (SNPs) of PRDX6 have been examined in the context of acute lung injury without finding a significant association [230].

3.7 Protective mechanisms against lipid oxidation and membrane repair in RBCs and *Plasmodium*

3.7.1 Antioxidant Protective Enzymes in RBCs and *Plasmodium*

RBCs contain several enzymes which directly detoxify ROS such as superoxide dismutase (SOD), which catalyses the dismutation of the superoxide radical (Equation 3.2a), or catalase, which cleaves H₂O₂ into water and oxygen (Equation 3.2b) [127]. While *Plasmodium spp.* express superoxide dismutase orthologues, no gene encoding for a *Plasmodium* catalase has been identified, yet [73].

3.7.2 Non-enzymatic antioxidants in RBCs and *Plasmodium*

α -tocopherol is the key antioxidant in RBCs and *P. falciparum* which confers protection against lipid oxidation [127, 140, 141, 231]. For a long time, it was believed that only photosynthesising plants, algae and cyanobacteria were able to synthesize tocopherols in their plastids [232]. This implied that a plant-based diet was the only source of tocopherols for *Plasmodium spp.* and humans. Recently, however, *P. falciparum* has been shown to synthesise α -tocopherol within its apicoplast [231, 233]. Accumulating evidence suggests that the

apicoplast originates from algae and has been acquired by *Plasmodium spp.* through secondary endosymbiosis [7]. Thus, the apicoplast harbours synthesis pathways which are not found in mammalian cells, such as the complete biosynthesis pathway of α -tocopherol [7, 231].

Next to α -tocopherol, coenzyme Q₁₀ (CoQ₁₀) has been shown to be involved in antioxidant protection against lipid oxidation in RBCs [111, 234–236]. Therapeutically, heme-induced lipid oxidation damage during ferroptosis can be inhibited by administration of artificial radical scavenging antioxidants such as ferrostatin-1 and liproxstatin [111, 142, 237]. Recently it was shown that ferrostatin-1 reduces exogenously triggered lipid oxidation and prevents cell death in liver stage *P. yoelii* parasites by conferring antioxidant protection [137].

3.7.2.1 Glutathione and thioredoxin peroxidases of RBCs and *Plasmodium*

RBCs contain various peroxidases which are recycled by the thiol-disulfide antioxidant system with glutathione (GSH) and thioredoxin (Trx) as the major reductants [73, 127]. Proteomic analysis provided evidence that RBCs contain the glutathione peroxidases GPx1, GPx4 and PRDX6 as well as the thioredoxin peroxidases PRDX1–5 [127, 238, 239]. GPx1 and 4 contain an active selenocysteine, whereas PRDX1–5 contain two cysteines and PRDX6 contains active cysteine [138]. GPx4, PRDX5 and PRDX6 are known to reduce lipid peroxides whereas GPx1 and PRDX1–4 efficiently reduce small ROS molecules like H₂O₂ [107, 138, 240, 241]. Oxidised glutathione and thioredoxin are recycled and reduced by oxidation of NADPH to NADP⁺ [127]. Thus, sufficient NADPH levels are crucial for the antioxidant activity of peroxidases [144]. In RBCs, glucose-6-phosphate dehydrogenase (G6PD) is the key enzyme for reduction of NADP⁺ to NADPH [145]. Genetic G6PD deficiency severely compromises the RBC antioxidant system conferring protection against infection with *P. falciparum* [145].

Similar to RBCs, the peroxidase antioxidant system of *Plasmodium spp.* is dependent on glutathione and thioredoxin [73, 80, 242]. In addition, *Plasmodium spp.* express a third di-thiol reductant called plasmoredoxin [243]. Within the parasite, the glutathione and thioredoxin systems are separated by compartmentalisation, but have overlapping functions [244, 245]. The relationship and balance between both systems is still widely debated in the literature [73, 144, 242, 245]. A recent publication provided evidence that both systems interact via cross-talk [246]. In contrast to RBCs, *Plasmodium spp.* express various peroxidases, of which most have been shown to use thioredoxin as the reductant [73, 242]. *Plasmodium spp.* do not have a classical glutathione peroxidase (GPx), but express glutaredoxins which are oxidised by substrates and then non-enzymatically reduced by glutathione [242, 247]. Interestingly, *P. falciparum* expresses five homologues of human peroxiredoxins (PRDX), including a 1-cys PRDX with homology to human PRDX6 [242]. However, in contrast to the trifunctional human PRDX6, the *P. falciparum* orthologue exclusively exhibits a peroxidase, but no PLA₂ or LPCAT activity [248]. Neither of the other four *Pf*PRDXs contains a PLA₂ or LPCAT motif or domain suggesting that all *Pf*PRDXs are mono-functional peroxidases.

3.7.2.2 PLA₂ enzymes in RBCs and *Plasmodium*

Only three PLA₂ enzymes are reported in the published RBC proteome: The PAF-AH1b complex, patatin-like phospholipase domain-containing protein 6 (PNPLA6, also called neuropathy target esterase, NTE) and PRDX6 [238]. Furthermore, the proteomic data indicates the presence of the PLA₂-activating protein (PLAA) [238]. The presence of the PAF-AH1b complex in RBCs has been confirmed independently [170]. As PNPLA6 has not been reported to cleave oxidised lipids, PRDX6 and PAF-AH1b are the only PLA₂ enzymes reported in RBCs which are known to cleave oxidised lipids [249]. The heterotrimeric structure of PAF-AH1b makes it structurally distinct from other PLA₂ enzymes and a selective inhibitor (P11) is available [168].

About 22 phospholipases have been described in *P. falciparum* in the literature (Overview in [129]). From these 22 enzymes, only four have been characterised as PLA₂ enzymes and all four are all classified in the patatin-like phospholipase domain-containing protein (PNPLA) family [129, 250]. *Pf*PNPLAs have not been described to cleave or repair OxPLs [181]. Recently, a *P. berghei* phospholipase (*Pb*PL) was found to facilitate rupture of the PVM during egress [251]. *Pb*PL contains an acyltransferase domain, but has not been demonstrated to exhibit specific PLA₂ or PLA₁ activity [129].

3.7.2.3 PLA₂ enzymes in other apicomplexans and related parasites

Multiple PLA₂ enzymes have been reported in the related apicomplexan parasite *Toxoplasma gondii*. In 1991, first evidence for the presence of a Ca²⁺-dependent phospholipase was presented [252]. Later on, the presence of a *T. gondii* iPLA₂-like PLB was reported [253]. In 2017, a *T. gondii* patatin-like phospholipase, called *Tg*PL2, was shown to localise to the apicoplast and to be essential for apicoplast integrity [254]. Recently, a third *T. gondii* patatin-like phospholipase called *Tg*PL3 was reported to be essential for host cell invasion and rhoptry secretion [255]. The presence of a sPLA₂-like phospholipase in the apicomplexan parasite *Cryptosporidium* was reported in 2003 [256]. The related parasite *Leishmania major* expresses an ortholog of human Lp-PLA₂ [257]. Furthermore, it was shown that the general PLA₂ inhibitor bromoenol lactone (BEL) killed promastigote and intracellular amastigote forms of *L. amazonensis* *in vitro* and decreased skin parasitism and lesion size during *in vivo* infection in mice [258]. The authors suggested the role of PLA₂ enzymes for virulence of *L. amazonensis*, but did not provide a candidate protein [258]. In a follow-up study, it was shown that BEL inhibited both endocytosis and exocytosis in *L. amazonensis* [259]. The authors did not provide a candidate PLA₂ as the target of BEL. While many PLA₁ enzymes have been characterised in the protozoan parasites *Trypanosoma brucei* and *Trypanosoma cruzi*, no PLA₂ has been identified in *Trypanosoma* spp. [260].

3.7.3 The antioxidant host-parasite relationship and uptake of host RBC antioxidant enzymes

The metabolic pathways of the parasite and its host RBC are closely linked, especially as the parasite internalises large parts of its host cell cytosol through endocytosis in order to digest hemoglobin in its food vacuole (cf. section 3.3.1) [42]. Thus, an interaction between the antioxidant systems of host RBCs and the parasite is very probable. So far, only few direct interactions have been reported in the literature [137, 261, 262]:

Infection of RBCs with *P. falciparum* prevents the *de novo* synthesis of glutathione within the RBC cytosol, as the infection increases the permeability of the RBC membrane causing the leakage of the synthesis intermediate γ -glutamyl-cysteine [261]. This lack of glutathione in the RBC cytosol is compensated by export of oxidised glutathione from the parasite which in turn requires *de novo* synthesis of glutathione within the parasite [261].

KONCAREVIC ET AL. reported in 2009 that *P. falciparum* directly imports human PRDX2 into its cytosol via an unknown pathway [262]. The authors presented evidence that after internalisation, human PRDX2 effectively uses *P. falciparum* thioredoxin-1 (*PfTrx1*) as a substrate and thus could support the *P. falciparum* antioxidative system [262]. Human PRDX2 has been shown to reduce small ROS molecules and is not known to be involved in repair of lipid oxidation [138].

Recently, it was shown by KAIN ET AL. that host human GPx4 is directly involved in liver stage infection of *P. yoelii* through modulation of lipid oxidation within the parasite [137].

3.8 Summary and thesis aim

The digestion of hemoglobin and the subsequent release of free heme during the blood stage growth of *P. falciparum* leads to a severe elevation of oxidative stress levels in the parasite and its host RBC [73, 242]. This elevated oxidative stress causes extensive cellular damage, such as lipid oxidation of unsaturated fatty acids (FA) [102, 135, 242]. To date, however, research on oxidative stress in *P. falciparum*-infected RBCs is mainly focussed on the glutathione and thioredoxin mediated detoxification of small (ROS) molecules such as H_2O_2 [73, 242]. Understanding of lipid oxidation in *P. falciparum*-infected RBCs is still limited and only few studies have been published in the last decades [126, 130, 133–136]. The most comprehensive and recent study on lipid oxidation during *P. falciparum* infection was published by FU ET AL. in 2009 and demonstrated vast lipid oxidation damage of parasite, but not RBC membranes in BODIPY^{581/591}-PC stained *P. falciparum* infected RBCs [126]. Beyond lipid oxidation, previous lipid-related studies in *P. falciparum* focussed on lipid uptake, *de novo* synthesis and metabolism, membrane homeostasis as well as lipid signalling [129, 250, 263–265].

The three membranes of a *Plasmodium* infected RBC – parasite membrane (PM), parasitophorous vacuole membrane (PVM) and RBC membrane (RBCM) – consist mainly of unsaturated phospholipids (PLs) and are thus prone to lipid oxidation damage [132]. The saturation of FA residues of PLs is asymmetric between the *sn1* and *sn2* position of the glycerol backbone [151]. Generally, the *sn1*-FA is saturated and cannot be oxidised, whereas the *sn2*-FA has varying degrees of unsaturation and is readily oxidised by ROS [151, 152]. Thus, selective cleavage of the oxidised *sn2*-FA by phospholipase A₂ enzymes is essential in detoxification of oxidised phospholipids (OxPL) and repair of lipid oxidation damaged membranes [102, 107, 153, 156]. The role of PLA₂ enzymes for lipid oxidation control in *Plasmodium* spp. has not been investigated, yet.

The aim of this thesis is to investigate the role of PLA₂ enzymes during the blood stage of *P. falciparum* with a focus on lipid oxidation control. Despite intense research of host parasite interactions in lipid metabolism, previous studies focussed on host-derived lipids and did not take host lipid enzymes into account [129, 264–267]. Thus, we were especially interested in the role of host RBC PLA₂ enzymes during host cell cytosol uptake (HCCU) which marks the initial step for hemoglobin digestion and is the main source of oxidative stress in infected RBCs. KONCAREVIC ET AL. reported that *P. falciparum* imports host PRDX2 and KAIN ET AL. showed that lipid oxidation during *P. yoelii* liver stage is modulated by host peroxidases [137, 262]. Based on these findings, we hypothesised that host RBC PLA₂ enzymes could play an important role in detoxification of hemoglobin-induced lipid oxidation.

Here, we provide evidence that the host RBC antioxidant PLA₂ enzyme peroxiredoxin 6 (PRDX6) is internalised by *P. falciparum* alongside hemoglobin during blood stage growth. We identified Darapladib as a suitable inhibitor of the PLA₂ activity of PRDX6. Darapladib completely inhibited parasite growth and raised oxidative stress levels during early schizont stage. We found that PRDX6 is localised to host cell cytosol-containing vesicles (HcV). Treatment with Darapladib disrupted transport of HcV to the food vacuole (FV) and blocked blood stage parasite growth. The identification of PRDX6 as an important host RBC enzyme for *P. falciparum* blood stage growth opens up possibilities for novel therapeutic approaches with host-enzyme targeting antimalarials. Targeting of host RBC enzymes will greatly impede the development of drug resistant parasites.

4 Material and Methods

4.1 Media and buffers

Table 4.1: Media and buffers

complete RPMI culture medium (cRPMI)		
5 mg/mL	Albumax I	Gibco Life Technologies
109 μ M	Hypoxanthine	c.c.Pro
20 μ M	Gentamicin	Sigma
in 1x	iRPMI	Gibco Life Technologies
sterile filtered		
complete RPMI culture medium with 2.5% human serum (cRPMI+HS)		
2.5%	AB ⁺ Human Serum	EFS, Rungis
in 1x	cRPMI	
sterile filtered		
incomplete RPMI culture medium (iRPMI)		
1x	RPMI-1640 powder	Gibco Life Technologies
2 g	NaHCO ₃	Fisher Scientific
in 1 L	ddH ₂ O	
sterile filtered		
65% Percoll solution for schizont isolation		
65%	100% Percoll	GE Healthcare
10%	10x PBS	Sigma
25%	ddH ₂ O (sterile)	
sterile filtered		

4.2 *Plasmodium falciparum* strains

If not otherwise indicated, the *P. falciparum* 3D7 strain was used. The *P. falciparum* Cambodia field isolate 3815 was a kind gift of DR. JEAN-CHRISTOPHE BARALE (Institut Pasteur, Paris). *P. falciparum* NF54-C580Y and the *P. falciparum* Cambodia field isolate 3601 were kind gifts of DR. DIDIER MÉNARD (Institut Pasteur, Paris).

Mice were infected with GFP-expressing *P. berghei* ANKA [268], or the *P. yoelii* YM lethal strain [269] which were kind gifts by DR. ROGERIO AMINO (Institut Pasteur, Paris).

4.3 Mice

PRDX6^{-/-} mice were a kind gift by DR. ARON B. FISHER (University of Pennsylvania, Philadelphia, USA) [226]. Age-matched control C57/BL6JRj WT mice were obtained from Janvier Labs (Le Genest-Saint-Isle, France).

4.4 Antibodies

Table 4.2: Antibodies

Primary Abs				
Target	Clone	Label	Host	Source
<i>h</i> Hb- β	polycl.	HRP	Goat	Bethyl
<i>h</i> PRDX6	1A11	-	Mouse	Santa Cruz
<i>mouse</i> CD71	R17217	APC	Rat	eBioscience
<i>Pf</i> NAPL	polycl.	-	Rabbit	Raised in lab
Secondary Abs				
Target	Clone	Label	Host	Source
Mouse	polycl.	Alexa Fluor 488	Goat	Invitrogen
Mouse	polycl.	HRP	Goat	Promega
Mouse	polycl.	15nm Gold	Goat	Sigma
Rabbit	polycl.	HRP	Goat	Promega

4.5 Drugs and Inhibitors

Table 4.3: Drugs and Inhibitors

Drug	Target	c _{Stock}	c _{final}	Solvent	Source
Apafant	PAF Receptor	20 mM	1–20 μ M	DMSO	Cayman
ATK	PLA ₂	10 mg/mL	0.5–300 μ M	EtOH	Cayman
Darapladib	PRDX6, Lp-PLA ₂	10 mM	0.25–2 μ M	DMSO	Selleck
Dihydroartemisinin	Multiple	700 μ M	700 nM	DMSO	Cayman
E64	Cys-Peptidases	1 mM	10 μ M	H ₂ O	Sigma
MAFP	PLA ₂	20 mM	50–300 μ M	DMSO	Enzo
P11	PAF-AH1b2/3	20 mM	1–20 μ M	DMSO	Cayman
Varespladib	sPLA ₂	10 mM	0.5–20 μ M	DMSO	Cayman
α -Tocopherol	Antioxidant	100 mM	0.1–75 μ M	DMSO	Sigma

4.6 Enzymes

Table 4.4: Enzymes

Enzymes	c _{Stock}	c _{final}	Source
MAPK (ERK2)	100 µg/mL	10 µg/mL	R&D Systems
PRDX6	2.57 mg/mL	250 ng/mL	see Sec. 4.13

4.7 Fluorescent Probes

Table 4.5: Fluorophores and fluorescent probes

Fluorophore	c _{Stock}	c _{final}	Source
BODIPY ^{581/591} C11	1 mM	5 µM	Invitrogen
Ethidium Bromide	0,7 mg/mL	2 µM	Eurobio
Hoechst 33342	10 mg/mL	5 µM	Molecular Probes
LysoSensor Yellow/Blue dextran 10kDa	50 mg/mL	0.5 mg/mL	Invitrogen
SYBR Green I	10000×	5×	Lonza
SYTO 61	5 mM	0.5 µM	Invitrogen
TAMRA-FP	100 µM	2 µM	Invitrogen

4.8 Lipids

Table 4.6: Lipids

Lipid	c _{Stock}	c _{final}	Solvent	Source
Cholesterol	11.6 mg/mL	-	EtOH	Sigma
DLPC	25 mg/mL	25 µg/mL	EtOH	Avanti Lipids
DOPC	25 mg/mL	25 µg/mL	EtOH	Avanti Lipids
[¹⁴ C]-DPPC	0.1 mCi/mL	0.5 µCi/mL	EtOH:toluene (1:1)	ARC
DPPC	73.4 mg/mL	-	EtOH	Avanti Lipids
DSPC	25 mg/mL	25 µg/mL	EtOH	Avanti Lipids
Egg-yolk PC	100 mg/mL	-	EtOH	Sigma
Egg-yolk PG	10 mg/mL	-	EtOH	Sigma

4.9 *In vitro* culture of *P. falciparum*

P. falciparum 3D7 was cultured in complete RPMI-1640 (cRPMI) medium using O⁺ human erythrocytes with a final hematocrit of 2–4% under mixed gas atmosphere (5% O₂, 5% CO₂ and 90% N₂) at 37°C as described previously by TRAGER & JENSEN [270]. *P. falciparum* NF54 C580Y and the field isolates 3815 and 3601 were cultured in cRPMI supplemented with 2.5% AB⁺ human serum (EFS, Rungis).

4.9.1 Giemsa staining of thin blood smears

Giemsa-stained thin smears were prepared from *P. falciparum*, *P. berghei* and *P. yoelii* cultures to follow the development of parasites and to determine parasitemia of the culture. For each smear 200 μ L of cultures was taken, briefly spun down and spread on a glass slide by using a second glass slide at a 40° angle. After air-drying of the thin smear, cells were fixed in 100% methanol and stained for 3 – 5 min in Giemsa staining solution. The staining time was dependent on the life cycle stage: slides of cultures with predominantly schizont stage were stained for 3 min, whereas slides of cultures with ring stages were stained for 5 min. Excess staining solution was washed off with distilled water and the slides were air-dried. Subsequently, slides were examined with a 100 \times oil immersion objective under a light microscope. To determine parasitemia, the percentage of infected RBCs in the culture was determined. RBCs infected with multiple parasites were counted as single infections.

4.10 Synchronisation and purification of parasites

4.10.1 Synchronisation of parasite culture with sorbitol

Parasites were synchronised at ring stage (8 – 24 hpi) by treatment with a 5% sorbitol solution as described by LAMBROS [271]. After centrifugation (800 g, 5 min, RT), the supernatant was discarded and the pellet was resuspended in 5 pellet volumes of 5% sorbitol solution (w/v in ddH₂O, sterile) and incubated for 15 min at 37°C with occasional shaking. The sorbitol-treated culture was washed for two times (800 g, 5 min, RT) in incomplete RPMI (iRPMI) and resuspended in cRPMI and cultured as described above (see 4.9).

4.10.2 Purification of schizonts with Percoll

P. falciparum schizonts have a lower density compared to uninfected RBCs or ring and trophozoite stages. Thus, they can be purified by overlaying a 65% Percoll solution with resuspended infected erythrocytes and subsequent centrifugation [272]. The schizonts can be isolated from the interphase forming between the Percoll solution and the iRPMI medium. For each 15 cm cell culture dish, 5 mL of 65% Percoll solution at 37°C was carefully overlaid with the culture resuspended in 5 mL iRPMI. After centrifugation (800 g, 20 min, RT, no brake), the interphase containing schizonts was withdrawn and washed two times (700 g, 5 min, RT) in iRPMI.

4.11 Flow cytometric measurement of *P. falciparum*

4.11.1 Screening of different fluorescent nucleic acid dyes

Fluorescent nucleic acid intercalating dyes (Table 4.7) were used to stain *P. falciparum* infected RBCs. Suitable final concentrations for the fluorescent nucleic acid dyes were found in the literature [273, 274]. Each dye was added to 200 μL of a 1:20 diluted culture of uninfected and infected RBCs in a 96-well plate in the final concentrations shown in Table 4.7 and incubated for 30 min at 37°C. After incubation, one plate was spun down (700g, 5 min, RT) and washed once with PBS (700g, 5 min, RT). Both plates were measured on the *MACSquant* flow cytometer as described in section 4.11.2.

Table 4.7: Screening of nuclear acid dyes

Dye	Final conc.	Stock conc.	V in 200 μL	Channel
SYBR Green I	5 \times	10,000 \times	5 μL of 1:50 in PBS	B1
Hoechst 33342	5 μM	10 mg/mL μM	5 μL of 1:100 in PBS	V1
EtBr	2 μM	0,7 mg/mL	4 μL of 1:10 in PBS	B2

4.11.2 Final protocol for flow cytometric measurement of different *P. falciparum* life stages

For flow cytometric measurement of *P. falciparum* blood stages, cultures were diluted to 0.2% hematocrit and transferred to a 96-well round bottom plate. 5 μL of 200 \times SYBR Green I (diluted in PBS) were added to 200 μL of the diluted culture for a final concentration of 5 \times SYBR Green I. The plate was then incubated for 30 min at 37°C, 5% O₂ and 5% CO₂ in the dark. Samples were measured on a calibrated *MACSquant* flow cytometer on the forward scatter (FSC), side scatter (SSC) and B1 fluorescent channel (B1: λ_{Ex} 488 nm and λ_{Em} 525/50 nm).

Data was processed with the FlowJo 10 Software (FlowJo, LLC). The gating strategy is shown in Figure 4.1 A. After exclusion of doublets, a gate for uninfected and infected RBCs based on the size of the cells in the FSC-A channel was set up to exclude debris and merozoites. Finally, gates for rings, trophozoites and multiply infected RBCs, and schizonts were set up. The total parasitemia was defined as the sum of the aforementioned gates.

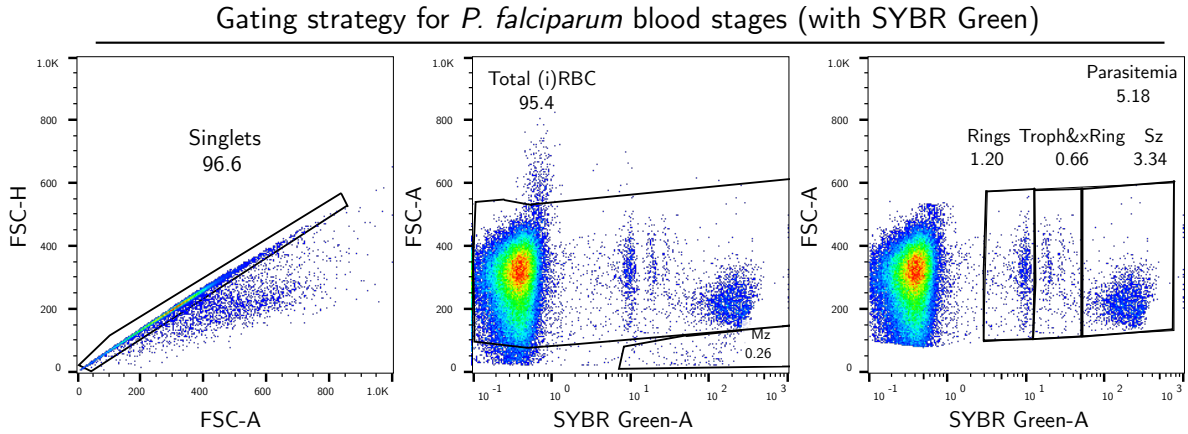


Figure 4.1: Gating strategy for flow cytometric measurement of different *P. falciparum* life stages. For the measurement of the different blood stage parasites, firstly doublets were excluded by comparing the FSC-area versus the FSC-height as the first step. Secondly, a gate for all RBCs and iRBCs was set up to exclude debris and merozoites. In the third step, gates for rings, trophozoites and multiply infected iRBCs, schizonts and the total parasitemia were set up.

4.11.3 Progression and growth assay

To assess the effect of inhibitors on the ring to schizont progression, and growth from ring stage to next generation ring stage, a tightly Percoll-synchronised culture with 2–4% parasitemia and 2% hematocrit was treated with different inhibitors at ring stage (14–20 hpi). The inhibitors were present throughout the assay. Concentrations and solvents of the used inhibitors are shown in Table 4.3. The concentration of the solvent was kept equal in all samples in a given experiment and maintained below 0.2% for DMSO and Ethanol to avoid toxic effects. For each condition, a triplicate set of 1 mL cultures was added into wells of a 24-well plate and kept at 37°C and 5% O₂, 5% CO₂ throughout the assay. In the beginning of the experiment, the initial ring stage culture was scored by flow cytometry as described in section 4.11.2 and by examination of Giemsa-stained blood smears. After 20h, the samples were measured again to assess progression to schizont stage. Further 24h later, the overall growth and development of next generation rings was measured. Data was analysed as described in section 4.11.2. Each experiment was performed with three biological replicates. Relative rate of progression was calculated as the fraction of schizonts in treated and control samples (Equation 4.1). Relative growth was calculated as the ratio of parasitemia in the treated and control samples after subtraction of the initial parasitemia (Equation 4.2).

$$\text{Relative Progression} = \frac{\% \text{ Schizonts (Treatment)}}{\% \text{ Schizonts (Control)}} \quad (4.1)$$

$$\text{Relative Growth} = \frac{\% \text{ rings (Treatment)} - \% \text{ rings (Initial)}}{\% \text{ rings (Control)} - \% \text{ rings (Initial)}} \quad (4.2)$$

4.11.4 Re-Invasion Assay with pretreated RBCs

Fresh RBCs were washed and pelleted in RPMI. 10 μ L of packed RBCs were resuspended in 190 μ L cRPMI and treated with different concentrations of the irreversible, covalently binding PLA₂ inhibitor methoxy arachidonyl fluorophosphonate (MAFP, Enzo), or its reversible analogue arachidonyl trifluoromethyl ketone (ATK, Cayman) or DMSO for 60 min at 37°C with occasional mixing. Afterwards, the cells were washed two times with cRPMI to remove unbound drug. Schizonts were isolated from 30 mL of a 4% hematocrit highly synchronous, late stage (44–48 hpi) *P. falciparum* 3D7 culture using a Percoll gradient (cf. Section 4.10.2). The resulting schizont pellet was resuspended in cRPMI and equal amounts were added to the pre-treated RBCs and cultured for 20 h at 37°C, 5% O₂, 5% CO₂ to allow egress, re-invasion and formation of next generation rings within the pre-treated RBCs. After 20 h, parasitemia was assessed using flow cytometric measurement with SYBR Green staining and by examination of Giemsa-stained blood smears. After another 24 h, the progression of rings to schizonts was assessed using flow cytometry and examination of Giemsa-stained blood smears. A flow chart of the assay procedure can be found in Figure 5.8.

4.11.5 Artemisinin ring stage survival assay

Ring stage survival upon treatment with Dihydroartemisinin (DHA, Cayman) was measured using the method described by WITKOWSKI ET AL. [275]. Ring stage survival was assessed in *P. falciparum* 3D7, NF54 C580Y and Art-resistant field isolate strains 3815 and 3801 (cf. Section 4.2). Late stage schizonts were purified from synchronous *P. falciparum* cultures which contained only late stage (44–48 hpi) schizonts and newly invaded rings. Purified schizonts were added to fresh RBCs and the culture was incubated for 3 h at 37°C, 5% O₂, 5% CO₂ to allow egress, re-invasion and development of rings. After 3 h, unegressed schizonts were removed by a second Percoll purification. The pellet containing highly synchronous 0–3 h old rings and RBCs was washed in cRPMI and was examined by flow cytometry and Giemsa-stained blood smears to confirm schizont depletion and to measure the parasitemia. Subsequently, the parasitemia was adjusted to 1% and the culture diluted 1:10 in cRPMI. Initial parasitemia was measured by flow cytometry and Giemsa-stained blood smears. In a 24-well plate, 1 mL aliquots of the culture were treated with 700 nM DHA, 1 and 2.5 μ M Darapladib, or combinations of both drugs for 6 h at 37°C, 5% O₂, 5% CO₂. The concentration of DMSO was kept equal in all samples. After 6 h, the drugs were removed by washing twice in cRPMI. After resuspension in cRPMI, the culture was incubated for further 66 h and parasitemia was assessed by flow cytometry and Giemsa-stained blood smears. Parasite survival was calculated as shown in equation 4.3.

$$\text{Relative Survival} = \frac{\% \text{ rings (Treatment)} - \% \text{ rings (Initial)}}{\% \text{ rings (Control)} - \% \text{ rings (Initial)}} \quad (4.3)$$

Table 4.8: Lasers and Filters for BODIPY^{581/591} C11 and Hoechst 33342 measurement

Fluorophore	Channel	λ_{Ex} [nm]	λ_{Em} [nm]	Colour
BODIPY ^{581/591} C11 reduced	B2	488	614/50	Red
BODIPY ^{581/591} C11 oxidised	B1	488	525/50	Green
Hoechst 33342	V1	405	450/50	Blue

4.12 Measurement of lipid oxidation

4.12.1 Parasite labelling with BODIPY^{581/591} C11 lipid oxidation sensor

To measure oxidative stress, parasites were labelled with the fluorescent lipid oxidation sensor BODIPY^{581/591} C11 (Invitrogen) based on the methods described in the literature [126, 276]. A *P. falciparum* 3D7 culture was highly synchronised via repeated Percoll gradient purifications. Parasites were treated with 0.5 μ M or 2 μ M Darapladib, 10 μ M Varespladib or DMSO for 2 h at ring stage (16–20 hpi), early trophozoite stage (30–34 hpi) or late trophozoite/early schizont stage (38–42 hpi). Synchronicity and parasitemia were confirmed at each step by flow cytometry and Giemsa-stained blood smears. After treatment for 2 h, parasites were pelleted by centrifugation and resuspended in labelling solution (5 μ M BODIPY^{581/591} C11, 10 μ M Hoechst 33342 in cRPMI) and incubated for 1 h at 37°C, 5% O₂, 5% CO₂. Parasites were measured on a MACSquant flow cytometer in the channels V1, B1 and B2 (see Table 4.8). Data was analysed using FlowJo 10 (FlowJo, LLC). After exclusion of doublets, debris and merozoites by size, infected RBCs were gated for by selecting Hoechst 33342 positive cells. The MFI of “Red” and “Green” channels of infected RBCs was calculated. Relative lipid oxidation was calculated as shown in equations 4.4.

$$\text{Lipid oxidation} = \frac{\text{MFI}(\text{Green})}{\text{MFI}(\text{Green}) + \text{MFI}(\text{Red})} \quad (4.4)$$

$$\text{Relative lipid oxidation} = \frac{\text{Lipid oxidation (Treated)}}{\text{Lipid oxidation (Control)}}$$

4.12.2 TBARS assay

Detection of thiobarbituric acid reactive substances (TBARS), such as malondialdehyde (MDA), was adapted from the method published by OHKAWA ET AL. [122]. To quench auto-oxidation, butylated hydroxytoluene (BHT, Sigma) was added to the reaction [277]. An 0.8% (w/v) aqueous solution of 2-thiobarbituric acid (TBA, Sigma) was prepared by heating the solution to 50°C for 2 h. A 20% parasitemia, 4% hematocrit *P. falciparum* 3D7 culture, or a 4% hematocrit RBC suspension were treated with 0.5 μ M or 2 μ M Darapladib, or DMSO for

8 h at 37°C, 5% O₂, 5% CO₂. Afterwards, 5 mL of each culture was pelleted by centrifugation. The pellet was resuspended in a 15 mL reaction tube with 1.5 mL 20% acetic acid pH 3.5 (v/v, Sigma), 200 µL 10% SDS (Sigma), 100 µL of 0.1% (w/v) BHT in EtOH, 1.5 mL of 0.8% TBA in H₂O and 600 µL H₂O for a total reaction volume of 4 mL. The samples were heated for 1 h in vigorously boiling water. To stop the reaction, the reaction mix was cooled down in an ice bath. The pink coloured reaction product, a condensated TBA/MDA 2:1 adduct, was extracted by addition of 5 mL 1-butanol (Sigma), vortexing and centrifugation (2000 g, 10 min, RT). 150 µL of the butane layer was transferred into a black-walled 96-well plate and fluorescence (λ_{Ex} 530 nm, λ_{Em} 550 nm) was measured on a Tecan Infinite M1000 Pro plate reader.

4.13 Recombinant expression of human PRDX6 in *E. Coli*

Recombinant human PRDX6 was produced based on the protocol published by KIM ET AL. [200]. The gene sequence for human PRDX6 was tagged with a 6x-His tag (sequence and map in section IV.i), synthesised and cloned into the *E. Coli* expression vector pET28a (GenScript, Piscataway, USA). The plasmid vector was transformed into *E. Coli* BL21 (DE3) competent cells. A single colony of transformed bacteria was picked from a LB-agar plate with Kanamycin (50 µg/mL) and grown in LB medium with Kanamycin at 37°C to an optical density of OD₆₀₀ of 0.6. Expression of recombinant PRDX6 was induced with 1 mM isopropyl- β -*d*-thiogalactopyranoside (IPTG, Sigma). The culture was incubated for further 20 h at 18°C. After this, bacteria were harvested by centrifugation (6000 g, 10 min, 4°C) and resuspended in lysis buffer (50 mM Tris/HCl at pH 8, 150 mM NaCl, 2 mM β -mercaptoethanol). After sonication and removal of cell debris by centrifugation, the supernatant was loaded onto a HisTrap FF nickel-nitrilotriacetic acid (NTA) affinity column (GE Healthcare) equilibrated with lysis buffer (see above). Recombinant PRDX6 was eluted with lysis buffer supplemented with 250 mM imidazole (Sigma). Subsequently, recombinant PRDX6 was purified by gel filtration chromatography on a Superdex 200 16/600 column (Sigma) equilibrated with 20 mM HEPES at pH 7.0, 2 mM EDTA and 1 mM DTT. The yield from a 2 L initial bacterial culture was about 25 mg of purified recombinant PRDX6.

4.14 Bioinformatic analysis of *P. falciparum* protein sequences

To identify homologues of human cPLA₂ (UniProt ID P47712) and human Lp-PLA₂ (UniProt ID Q13093), the respective primary human protein sequences were compared with *Plasmodium spp.* protein sequences in the PlasmoDB database using a basic local alignment search tool (BLAST) [278].

4.15 Enzyme activity assays

4.15.1 Lp-PLA₂ activity assay

The enzymatic activity of Lp-PLA₂ (also called Platelet-activating factor acetylhydrolase, PAF-AH) was measured using a colorimetric assay kit (Cayman, Ann Arbor, USA). Samples were diluted in assay buffer 2 (0.1 M Tris/HCl, pH 7.2). The solvent of the assay substrate 2-thio PAF was evaporated under a gentle stream of nitrogen. Dried 2-thio PAF was resuspended in 12 mL assay buffer 2 to make the substrate solution. For the assay, 10 μ L diluted sample was mixed with 200 μ L substrate solution, briefly mixed and incubated for 30 min at RT. The reaction was developed by addition of 10 μ L 5,5'-dithio-*bis*-(2-nitrobenzoic acid) (DTNB). The hydrolysis of the Sn2 position acetyl thioester bond by Lp-PLA₂ produces a free Sn2 thiol group which reacts with the disulfide bond of DTNB and forms the yellow dye 5-thio-2-nitrobenzoic acid, which effectively absorbs light at 414 nm. After allowing the reaction to develop for 1 min, enzymatic activity was read by measuring absorbance at 414 nm.

4.15.2 LDH activity assay

P. falciparum lactate dehydrogenase (LDH) activity was measured based on the method published by MAKLER & HINRICHS [279,280]. 9 mL of LDH assay buffer (100 mM Tris/HCl, 0.2 M L-lactic acid (Sigma-Aldrich), 0.2% (v/v) Triton X-100, pH 9.1) was mixed with 50 μ L of a 10 mg/mL stock of 3-acetylpyridine adenine dinucleotide (APAD, Sigma), 200 μ L of a 50 U/mL stock of diaphorase (Sigma) and 2 mg of Nitroblue tetrazolium (NBT, Sigma). Samples were added to 100 μ L of supplemented assay buffer in a 96-well plate and incubated for 30 min at RT. Absorbance was read at 655 nm.

4.15.3 PRDX6 activity assays

4.15.3.1 Phosphorylation of PRDX6

PRDX6 was phosphorylated according to the method described by WU ET AL. [198]. Recombinant human PRDX6 (150 μ g/mL final) and active MAPK (ERK2, R&D Systems, 10 μ g/mL final) were added to 30 μ L of a phosphorylation buffer containing 50 mM Tris/HCl (pH 7.5), 20 μ M EGTA, 10 mM MgCl₂ and 2 mM Mg-ATP (Sigma) and incubated for 90 min at 30°C.

4.15.3.2 PRDX6 PLA₂ activity assay

Measurement of PLA₂ activity of phosphorylated PRDX6 (pPRDX6) was based on the enzymatic PLA₂ assay described by FISHER ET AL. [208] and the rapid free fatty acid extraction method by KATSUMATA ET AL. [281]. Liposomes consisting of DPPC/egg yolk PC/egg yolk PG/cholesterol (6:3:1.2:0.95) with 0.6 μ Ci tracer [2-palmitoyl-1-¹⁴C]-dipalmitoyl phosphatidylcholine (¹⁴C-DPPC) were prepared by freezing/thawing three times in liquid

nitrogen. 100 μL diluted pPRDX6 (2.5 $\mu\text{g}/\text{mL}$ in PLA_2 assay buffer 40 mM NaOAc, 5 mM EDTA, pH 5), or blank PLA_2 assay buffer was added to 800 μL PLA_2 assay buffer containing different concentrations of Darapladib in DMSO. After addition of 100 μL liposome preparation, the samples were incubated for 2 h at 37°C. The enzymatic reaction was terminated by addition of 200 μL 5% Triton X-100 in PLA_2 assay buffer. The product of the PLA_2 enzymatic reaction, free ^{14}C -palmitic acid, was extracted by addition of 10 mL hexane with 0.1% acetic acid (v/v) and 200 mg of anhydrous Na_2SO_4 [282] and subsequent vortexing for 20s. 3 mL of the hexane layer were added to 10 mL UltimaGold liquid scintillation cocktail (PerkinElmer, Waltham, USA) and measured on a TriCarb 2800TR liquid scintillation counter (PerkinElmer, Waltham, USA).

4.16 Inhibitor binding studies

4.16.1 PRDX6 binding assays with activity-based protein profiling

The activity-based protein profiling (ABPP) protocol by NAGANO ET AL. was used for this assay [283]. Recombinant human PRDX6 (cf. Section 4.13) was diluted to 10 mg/mL in PBS. Aliquots of 50 μL were incubated for 5 min at RT with different concentrations of Darapladib (0.1–10 μM), Varespladib (1–50 μM), MAFP (1–100 μM), ATK (1–100 μM) or DMSO. TAMRA-fluorophosphonate (TAMRA-FP, Invitrogen) was solved in DMSO (100 μM), added to the sample (2 μM final) and incubated for 30 min at 37°C. After 30 min, the reaction was quenched by addition of 15 μL 4 \times Laemmli sample buffer (BioRad) and 7.5 μL 1 M DTT. The sample was heated to 95°C for 10 min and separated by SDS-PAGE on a 12% SDS polyacrylamide gel. After electrophoresis, the gel was imaged on a ChemiDoc MP imager in the Cy3 channel.

4.16.2 *In silico* PRDX6 docking studies

Docking of Darapladib was performed using Smina with Vinardo scoring function [284]. The docking study was designed in collaboration with Luis Checa Ruano and Olivier Sperandio (Institut Pasteur), calculations and data evaluation were performed by Luis Checa Ruano. An exhaustiveness setting of 15 was used and 10 poses per ligand were produced as output. Darapladib was docked on PRDX6 (PDB 5b6m), using a docking box of 27 \AA \times 31 \AA \times 19 \AA dimensions located on the surface close to Ser32 and Lys67, where a relatively shallow pocket is located. The list of residues located on this region are: 4, 19, 20, 21, 22, 23, 25, 27, 28, 29, 30, 31, 32, 36, 37, 51, 55, 58, 59, 61, 62, 65, 66, 67, 68, 69, 98, 99, 100, 101 and 103. Calculations were done with Darapladib in its protonated state, with diethylamine carrying a positive charge. Two docking runs with the mentioned parameters were performed on chain A and B of 5b6m. The resulting docking poses were visually inspected in order to identify favourable ligand-receptor contacts.

4.17 Infection of PRDX6 KO mice with rodent malaria

4.17.1 Infection and *in vivo* growth assay

PRDX6^{-/-} mice and age-matched control C57/BL6JRj WT mice (cf. Section 4.3) were infected with GFP-expressing *P. berghei* ANKA [268], or the *P. yoelii* YM lethal strain [269] via the tail vein for an initial parasitemia of 0.002%. Parasitemia was measured by Giemsa-stained blood smears and by flow cytometry. For *P. berghei* ANKA GFP, parasites were identified by GFP-fluorescence. For *P. yoelii* YM, cells were labelled with 5× SYBR Green I and 1:100 α-mouse CD71-APC for 30min at 37°C. To specifically assess intraerythrocytic growth, CD71⁺ reticulocytes were excluded. Infected RBCs were identified as SYBR Green⁺ and CD71⁻ cells.

4.17.2 *Ex vivo* *P. yoelii* YM progression assay

P. yoelii cannot egress from or invade RBCs outside its animal host. However, ring stage parasites can develop into schizonts *in vitro* [285]. PRDX6^{-/-} mice and age-matched control C57/BL6JRj WT mice were infected with *P. yoelii* YM as described above. When the parasitemia in the mice reached about 20%, 20µL blood was drawn from the chin and collected in heparinised tubes. 15 µL of the blood was diluted in 8 mL of cRPMI and added in 1 mL aliquots into a 24-well plate. The initial amount of schizonts was measured by Giemsa-stained blood smears and flow cytometry by labelling the parasites with 5× SYBR Green I and 1:100 α-mouse CD71-APC for 30min at 37°C. Infected RBCs were identified as SYBR Green⁺ and CD71⁻ cells. CD71⁺ reticulocytes were excluded by gating. Cells were treated with Darapladib (0.5–10 µM) or DMSO and incubated at for 16 h at 37°C, 5% O₂, 5% CO₂ to allow progression of parasites to schizont stage. After 16 h, schizont development in RBCs was assessed by Giemsa-stained blood smears and flow cytometry as described above.

4.18 Immunoblotting of parasite lysate

4.18.1 Selective lysis with Saponin and sample preparation

Late trophozoites and early schizonts from synchronous *P. falciparum* 3D7 cultures were purified with a Percoll gradient (cf. Sections 4.9 and 4.10.2). The resulting parasite pellet was resuspended in PBS. RBC membranes were lysed by exposure to 0.01% Saponin (Sigma, Stock 1% in H₂O) for 5 min at RT. Complete hemolysis was confirmed by Giemsa-stained blood smears. After washing two times with PBS, the hemolysed pellet was resuspended in 1× Laemmli SDS sample buffer (BioRad) with 200mM DTT (Sigma) and boiled at 95°C for 10 min.

4.18.2 SDS-PAGE and Immunoblotting

Samples were loaded onto a 12% SDS-polyacrylamide gel and gel electrophoresis was performed at 120V. Proteins were transferred onto a nitrocellulose membrane using a wet transfer system (BioRad) at 80 V for 1 h using a cold 1× Tris-glycine (TG) transfer buffer with 20% Ethanol. The membrane was blocked in PBS with 5% skimmed milk overnight at 4°C with continuous agitation. Following this, the membranes were incubated with mouse α -hPRDX6 (1:2000), rabbit α -PfNAPL (1:500) and goat α -hHb HRP (1:5000) in PBS with 2.5% skimmed milk and 0.05% Tween 20 for 2 h at RT (details for antibodies in Table 4.2). After washing in PBST (PBS, 0.1% Tween 20) three times for 10 min each, blots with α -PRDX6 and α -PfNAPL were incubated with respective α -mouse and α -rabbit HRP-coupled secondary antibodies (1:5000) for 1h at RT. After washing with PBST three times 10 min each, the membranes were developed with enhanced chemiluminescence (ECL) substrate (ThermoFisher Scientific) and imaged on a Amersham Imager 600 (GE Healthcare). Band intensity was calculated using ImageJ (NIH, Bethesda, USA).

4.19 Microscopy

4.19.1 Fluorescence microscopy

4.19.1.1 Immuno-fluorescence microscopy

P. falciparum 3D7 was cultured as described above (Section 4.9) and fixed by the method described by TONKIN ET AL. [286]. 1 mL of a 4% hematocrit, high parasitemia culture was pelleted by centrifugation (1.5 g, 3min, RT) and resuspended in freshly prepared PBS containing 4% para-formaldehyde (PFA, Electron Microscopy Sciences) and 0.0075% gluteraldehyde (GA, Sigma) and fixed for 30 min at RT. After washing in PBS once, fixed parasites were permeabilised with 0.1% Triton X-100 in PBS for 10 min at RT. Cells were washed in PBS again and blocked for 30 min in PBS with 2.5% BSA. Antibody dilutions were prepared in PBS with 2.5% BSA. After blocking, parasites were incubated with mouse α -hPRDX6 (1:500) for 1 h at RT. Parasites were washed twice in PBS and incubated with α -mouse AlexaFluor 488-coupled secondary antibody (1:2000) and Hoechst 33342 (2 μ M final), washed again twice in PBS and resuspended in 30 μ L PBS. From this suspension, 4 μ L were transferred onto a glass slide and covered with a glass coverslip. Samples were examined under a Deltavision Elite high resolution fluorescence microscope (GE Healthcare Lifesciences) using DAPI, FITC and differential interference contrast (DIC) channels. Hemozoin crystal size was measured in DIC images using ImageJ (NIH, Bethesda, USA).

Table 4.9: Lasers and Filters for LysoSensor Blue/Yellow and SYTO61 measurement

Fluorophore	Channel	Laser	λ_{Ex} [nm]	Filter	λ_{Em} [nm]	Colour
Microscopy						
LysoSensor pH 7	-	UV	390/18	DAPI	435/48	Blue
LysoSensor pH 5	-	UV	390/18	TRITC	597/45	Yellow
SYTO 61	-	Red	632/22	Cy5	679/34	Far Red
Flow Cytometry						
LysoSensor pH 7	V1	UV	405	DAPI	450/50	Blue
LysoSensor pH 5	V2	UV	405	YFP	525/50	Yellow
SYTO 61	Y3	Yellow	561	Cy5	695/50	Far Red

4.19.1.2 Preloading of RBCs with LysoSensor Blue/Yellow Dextran, infection with parasites and host cell cytosol-uptake assay

RBCs were preloaded with the pH-sensitive LysoSensor Blue/Yellow Dextran (10kD) as described by JONSCHER ET AL. [50]. Fresh RBCs (stored less than a week) were washed three times in cold PBS. From the pellet, 64 μ L packed RBCs were transferred to 128 μ L of freshly prepared preloading lysis buffer (5 mM K_2HPO_4 , 20 mM Glucose, pH 7.4). After addition of 2 μ L 30mM DTT, 4 μ L 50mM Mg-ATP (Sigma) and 2 μ L of 50mg/mL LysoSensor Blue/Yellow dextran 10kD (Invitrogen) on ice, the suspension was rotated at 4°C for 10min. For resealing, 50 μ L of 5 \times resealing buffer (750 mM NaCl, 25 mM Na_2HPO_4 , pH 7.4) was carefully added to the RBC suspension and incubated for 60 min at 37°C while gently rocking. Preloaded RBCs were washed three times in cRPMI and resuspended in 1 mL cRPMI.

For infection of preloaded RBCs, schizonts were isolated from 30 mL of a 4% hematocrit highly synchronous, late stage (44–48 hpi) *P. falciparum* 3D7 culture using a Percoll gradient (cf. Section 4.10.2). The resulting schizont pellet was resuspended in 1 mL cRPMI, mixed with the 1 mL preloaded RBCs and cultured for 20 h at 37°C, 5% O_2 , 5% CO_2 to allow re-invasion and formation of rings. Successful re-invasion was controlled with Giemsa-stained blood smears and flow cytometric measurement as described above.

At ring stage (16-20 hpi), the culture was split into two parts and treated with either 2 μ M Darapladib or DMSO control and further incubated until control parasites progressed to late trophozoite stage (32-40 hpi, large hemozoin crystals visible). To identify infected RBCs, the cells were stained with 0.5 μ M SYTO 61 for 30 min at 37°C and washed once in cRPMI. The resulting pellet was resuspended in 50 μ L cRPMI. From this suspension, 4 μ L were transferred onto a glass slide and covered with a glass cover slip. Images were taken with Deltavision Elite high resolution fluorescence microscope (GE Healthcare Lifesciences) with laser and filter sets combinations as indicated in table 4.9 as well as in the differential interference contrast

(DIC) channel. Fluorescent signal in the FV was quantified as the integrated density of the FV area in the “Yellow” and “Blue” channels using ImageJ. Relative successful transport of cytosolic LysoSensor to the FV was expressed as the ratio of integrated densities of “Yellow” and “Blue” channels.

For flow cytometric measurement, the cells were stained with 0.5 μM SYTO 61 for 30 min at 37°C, washed once in cRPMI afterwards and measured on a MACSquant flow cytometer in the channels V1, V2 and Y3 (see Table 4.9). Data was analysed using FlowJo 10 (FlowJo, LLC). After exclusion of doublets, debris and merozoites by size, infected RBCs were gated for by selecting SYTO 61 positive cells. The MFI of “Yellow” and “Blue” channels of SYTO 61⁺ infected RBCs was calculated. Relative successful transport of cytosolic LysoSensor to the FV was expressed as the ratio of the MFI of “Yellow” and “Blue” channels.

4.19.2 Transmission electron microscopy

4.19.2.1 Treatment of parasites for host cell cytosol uptake assay

A synchronous *P. falciparum* 3D7 culture at ring stage was treated with 2 μM Darapladib, 20 μM E64, a combination of both, or DMSO as control and incubated overnight at 37°C, 5% O₂, 5% CO₂ until control parasites progressed to schizonts. Giemsa-stained blood smears were prepared and examined by light microscopy.

4.19.2.2 Fixation of parasites

1 mL of *P. falciparum* 3D7 cultures was pelleted by centrifugation (1.5 g, 3 min, RT) and resuspended in freshly prepared PBS containing 4% EM-grade PFA (Electron Microscopy Sciences) and 0.1% EM-grade GA (Sigma) and fixed for 1 h on ice. After washing in PBS once, fixed parasites were stored in PBS with 1% PFA at 4°C. Following this, all steps for immuno-TEM and EPON resin embedding, as well as image acquisition were performed by Olivier Gorgette, Ultrastructural BioImaging Core Facility, Institut Pasteur.

4.19.2.3 Immuno-TEM

Fixed parasites were washed three times in PBS followed by an incubation for 15 min in 50 mM NH₄Cl at RT. Parasites were resuspended in PBS with 10% gelatin (Sigma) and incubated for 10 min at 37°C. The samples were allowed to solidify on ice and were infiltrated with 2.3 M sucrose at 4°C overnight, mounted onto sample pins and frozen in liquid nitrogen. Subsequently, the samples were cryo-sectioned (60 nm thickness) using a FC6/UC6 cryo-ultramicrotome (Leica) and a 35° diamond knife (Diatome). The sections were picked up using a 1:1 mixture of 2% methyl cellulose (Sigma) and 2.3M sucrose. Samples were quenched with 50 mM NH₄Cl, blocked in PBS with 1% BSA and immunolabeled with α -hPRXD6

1A11 (SantaCruz, 1:20) IgG1a monoclonal antibody in PBS with 1% BSA followed by a bridge step labelling with a polyclonal Rabbit Anti-Mouse Immunoglobulins (Dako, 1:50) and protein A-gold 10 nm (1:50) treatment for 15 min. Finally, samples were fixed with 1% glutaraldehyde in PBS for 5 min. The sections were thawed and stained/embedded in 4% uranylacetate/2% methyl cellulose mixture (1:9). Images were recorded with a Tecnai Spirit transmission electron microscope at 120 kV with bottom-mounted EAGLE 4Kx4K camera.

4.19.2.4 EPON resin embedding

Fixed parasites were treated again with 2.5% glutaraldehyde (Sigma) in PBS overnight, washed three times in PBS and mordanted with tannic acid 1% in PBS for 30min at RT. Cells were then washed three times in PBS, postfixed with 1% OsO₄ for 1.5 h and washed three times with distilled water and stored overnight at 4°C. Samples were dehydrated 15 min in a graded series of ethanol (25%, 50%, 75%, 95%, 3× 100%). Samples were incubated 1×15 min, then 2×10 min in propylene oxide and embedded in EMbed-812 epoxy resin (EMS; EPON/Propylene Oxide: r = 25/75 for 2 h; r = 50/50 overnight; r = 75/25 all the day and overnight with the tubes open under the chemical hood). Samples were then embedded 3× 2h at RT in pure EPON and subjected to heat polymerization for 5 days at 60°C. Thin sections were cut with a Leica Ultramicrotome Ultracut UC7' sections (60 nm), stained with uranyl acetate and lead citrate. Images were recorded with a Tecnai Spirit transmission electron microscope at 120 kV with bottom-mounted EAGLE 4Kx4K camera (FEI-Thermofisher).

5 Results

5.1 Establishment of a flow cytometry-based assay to score *P. falciparum* blood stages by nucleic acid staining

5.1.1 Selection of a fluorescent nucleic acid dye

Three commonly used nucleic acid staining dyes, SYBR Green I, Hoechst 33342 and Ethidium Bromide (EtBr) were tested to find a fluorescent dye that allows the separation of different *P. falciparum* intraerythrocytic life stages (Figure 5.1). Furthermore, the need for an additional washing step to reduce background staining was examined.

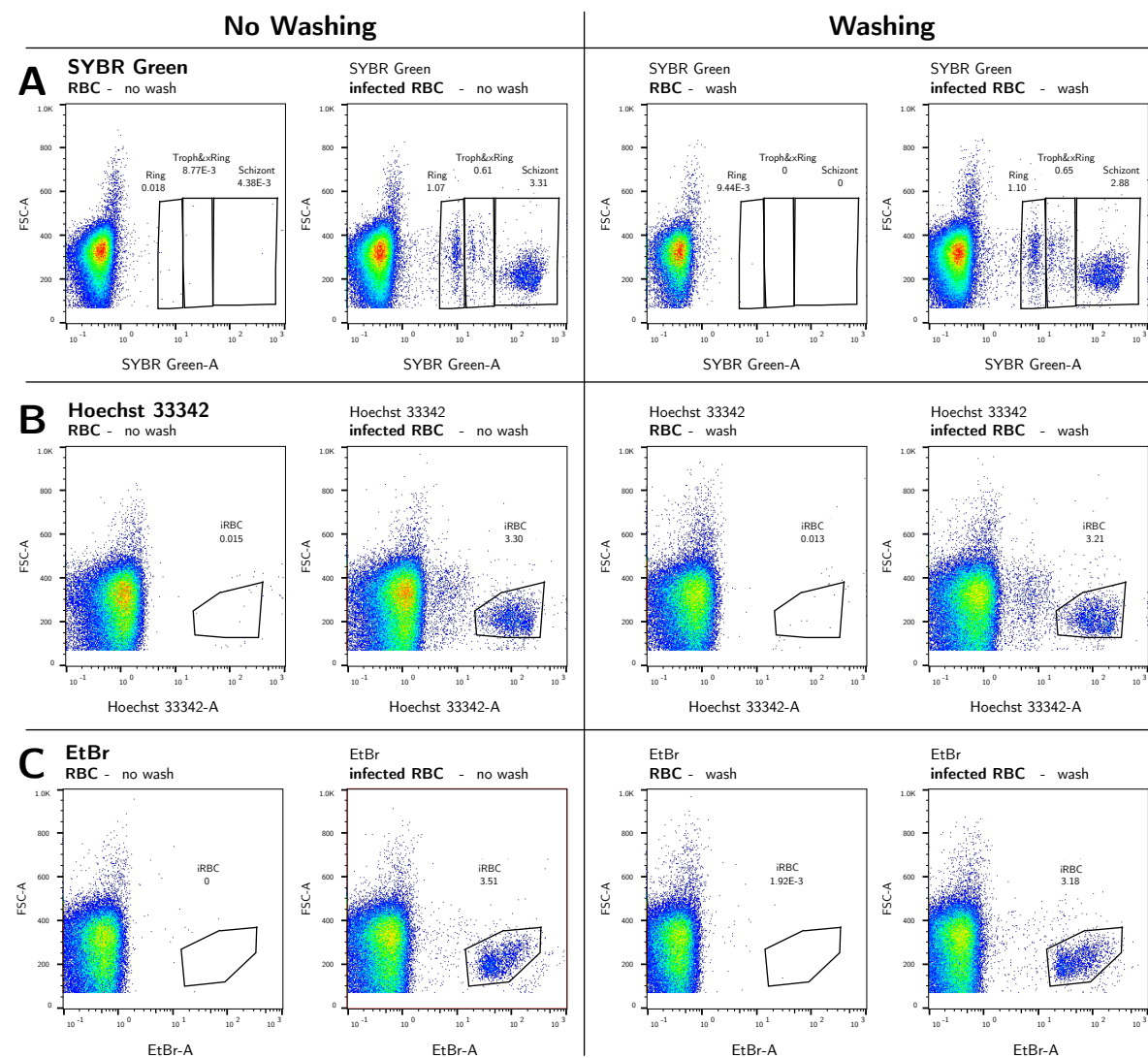


Figure 5.1: Screening of fluorescent nucleic acid dyes. Three of the most commonly used fluorescent nucleic acid dyes to score for infected RBCs were screened for their ability to separate the populations of different *P. falciparum* blood stages: (A) 5× SYBR Green I, (B) 5µM Hoechst 33342 and (C) 2µM Ethidium Bromide (EtBr). SYBR Green shows the best separation of different intraerythrocytic parasite life stages. Hoechst 33342 and EtBr only showed one indistinguishable population. A subsequent washing step with PBS did not improve the staining.

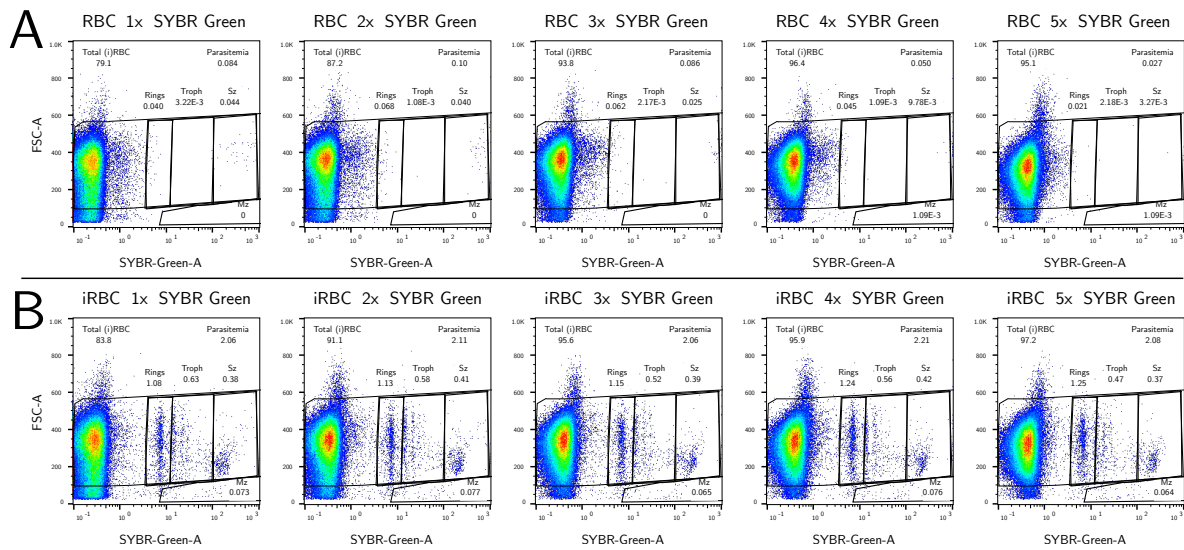


Figure 5.2: Establishment of the optimal SYBR Green concentration. Different concentrations of SYBR Green from 1× to 5× were screened for optimal staining of iRBCs, separation of blood stages and background staining. Non-infected RBCs (A) and an asynchronous culture of infected RBCs (B) were compared to assess the background staining of uninfected RBCs. A SYBR Green concentration of 5× was considered optimal as the background staining did not increase, the populations were well separated, and small impurities of leukocytes were shifted to the edges.

The results shown in figure 5.1 clearly show that SYBR Green is the only dye which shows distinct populations for the different blood stages. Staining with Hoechst 33342 and EtBr only yielded one indistinguishable population. None of the dyes showed significant background staining. Thus, a subsequent washing step with PBS only reduced the number of stained cells within the gates but did not reduce background staining and was considered unnecessary.

5.1.2 Establishment of the optimal SYBR Green concentration

In order to determine the optimal concentration of SYBR Green I, RBCs and iRBCs were stained with SYBR Green concentrations from 1× to 5×. The optimal final concentration of SYBR Green for staining of *P. falciparum* infected RBCs was 5× (Figure 5.2). The population of uninfected RBCs was well defined on the FSC-A axis, the background staining is negligible and blood stage parasite populations are well separated. Despite carefully washing the blood, some leukocytes can be found in the samples. Due to their high content of DNA, the leukocyte population is shifted to the right border of the chart and can be excluded by gating.

5.1.3 Validation of the gating strategy and separation of *P. falciparum* blood stages

In order to validate the flow cytometry protocol, especially the gating strategy described in section 4.11.2, three *P. falciparum* blood stage cultures in different states of synchronicity, life cycle progression and parasitemia were examined by both flow cytometry and by examination

of a thin layer Giemsa-stained blood smear by light microscopy (Figure 5.3). The results obtained by flow cytometry are consistent with the results from scoring by light microscopy. It was however not possible to distinguish multiply infected RBCs in ring stage and trophozoites by flow cytometry. It was also not possible to clearly differentiate between late trophozoites and early schizonts, as there is no boundary between these stages and individual schizonts can differ in size and DNA-content.

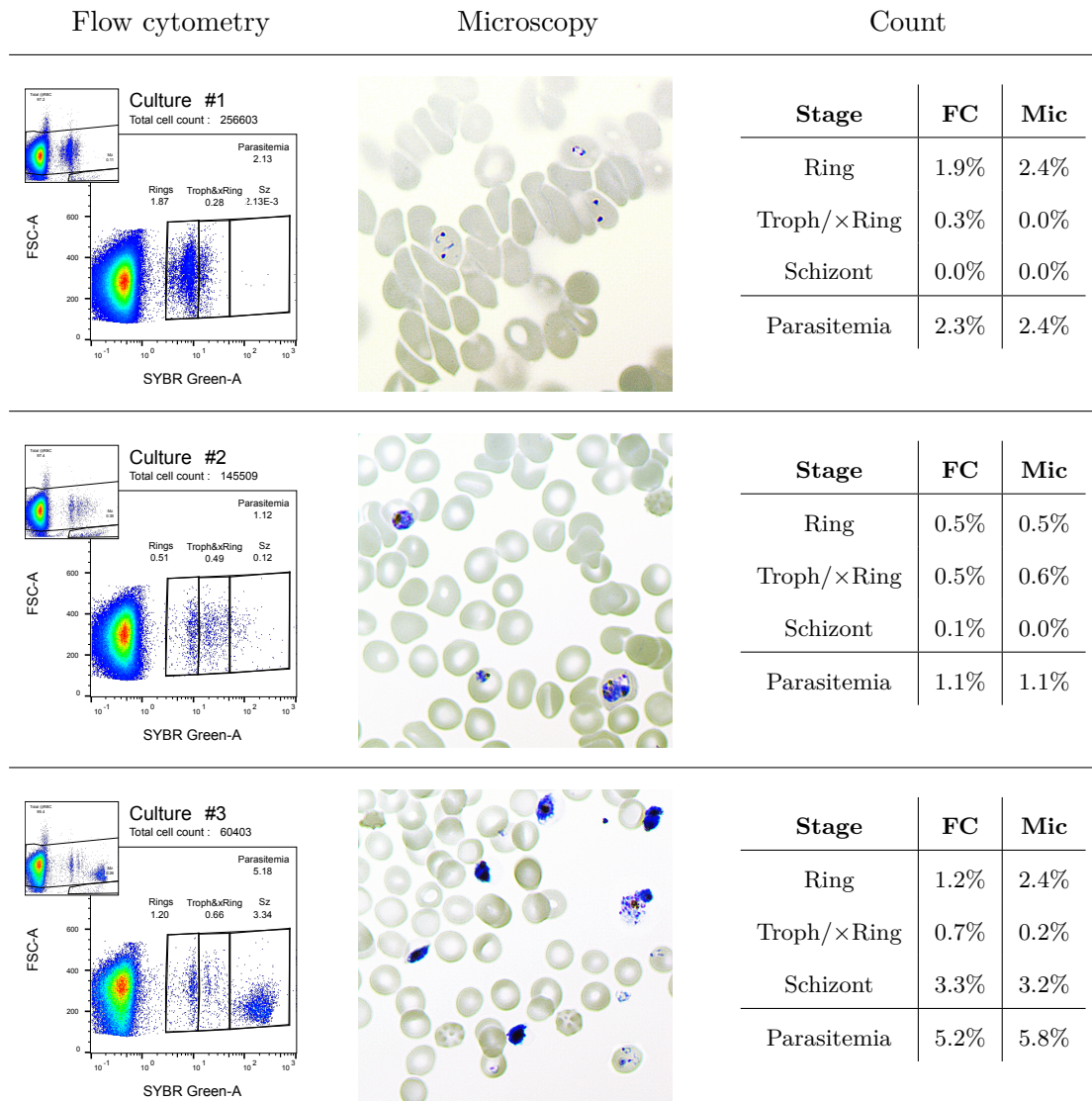


Figure 5.3: Validation of gating strategy and separation of *P. falciparum* blood stages. In order to validate the flow cytometry protocol, three cultures in different states of synchronicity, life cycle progression and parasitemia were examined by flow cytometry and by light microscopy of a thin layer smear ($n_{RBC}=2000$). The results obtained by flow cytometry are consistent with the results from scoring by light microscopy. *Abbr.:* FC, flow cytometry; Mic, microscopy

5.2 Phospholipase A₂ (PLA₂) inhibitors Darapladib, MAFP and ATK block *P. falciparum* blood stage progression and growth

PLA₂ enzymes play an important role in repair of membranes damaged by lipid oxidation. Therefore, we investigated the effect of known PLA₂ inhibitors on blood stage parasite development using the established flow cytometry-based assay to detect blood stage parasites. Synchronous *P. falciparum* 3D7 rings were treated with inhibitors and subsequently allowed to progress to schizont stage (“progression”) or to complete the full blood stage cycle until the next generation ring stage (“growth”) and measured quantitatively by flow cytometry as described above (Section 5.1). Inhibitors were present during the whole cycle. Of five inhibitors tested, only Darapladib, methoxy arachidonyl fluorophosphonate (MAFP) and arachidonyl

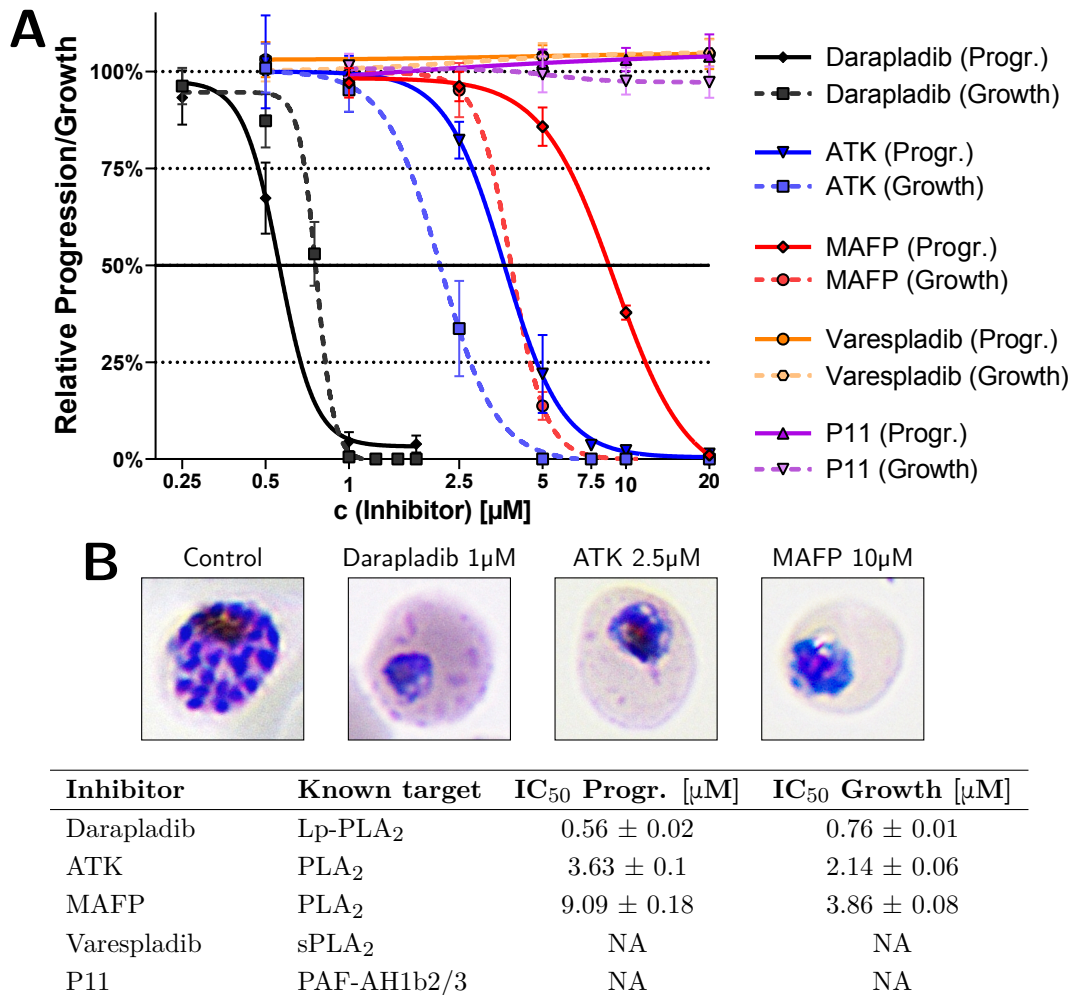


Figure 5.4: Effect of PLA₂ inhibitors on progression and growth. A synchronous *P. falciparum* culture was treated at ring stage. **(A)** PLA₂ inhibitors Darapladib, MAFP and ATK blocked *P. falciparum* progression to schizont and full-cycle growth. Varespladib and P11 did not exhibit an effect on parasite progression and growth. **(B)** Representative images of control and progression arrested *Pf* parasites after treatment with Darapladib, ATK and MAFP. Experiments were performed with at least three biological replicates. **Abb.:** ATK, Arachidonyl trifluoromethyl ketone; Lp-PLA₂, Lipoprotein-associated PLA₂; MAFP, Methoxy arachidonyl fluorophosphonate; PAF-AH1b, Platelet-activating factor acetylhydrolase 1b; sPLA₂, secreted PLA₂.

trifluoromethyl ketone (ATK) blocked *P. falciparum* progression and growth (Figure 5.4A). Varespladib and P11 did not exhibit an effect on parasite progression and growth. Of all inhibitors tested, Darapladib was the most effective and blocked progression and growth with an IC₅₀ of 0.56 μ M and 0.76 μ M, respectively. Upon treatment with Darapladib, MAFP and ATK at ring stage, parasites failed to develop beyond trophozoite stage and appeared as contracted, pyknotic parasites within their host RBC (Figure 5.4B). Treatment of schizonts with 1 μ M Darapladib did not inhibit egress of merozoites. Together with the finding that the IC₅₀ values of Darapladib for progression and growth inhibition were very close, this indicates that Darapladib exhibits its main killing action in early trophozoite stage.

5.3 Darapladib treatment raises oxidative stress levels in *P. falciparum* blood stages

During the trophozoite stage, which is the main time window of Darapladib action, the parasite takes up hemoglobin from the host RBC and transports it to the food vacuole (FV) where it is proteolytically digested to release amino acids and heme. This causes a drastic increase of oxidative stress levels in the parasite leading to lipid oxidation and membrane damage. PLA₂ enzymes are known to repair membranes damaged by lipid oxidation. Thus, we were interested whether treatment with the PLA₂ inhibitor Darapladib increased lipid oxidation during trophozoite stage. We assessed lipid oxidation in two ways: Direct measurement using the fluorescent lipid oxidation sensor BODIPY^{581/591} C11 and determination of malondialdehyde (MDA) levels with the TBARS assay.

5.3.1 Lipid oxidation sensor BODIPY^{581/591} C11

A highly synchronised *P. falciparum* 3D7 culture was treated for 2 h with Darapladib and Varespladib and then labelled for 1 h with BODIPY^{581/591} C11 and Hoechst 33342 with the drugs still present (Figure 5.5A). Oxidation of BODIPY^{581/591} C11 in Hoechst 33342-labelled infected RBCs was measured by flow cytometry. Treatment with Darapladib caused a dose-dependent increase in oxidation of BODIPY^{581/591} C11 in 38–42 hpi late trophozoites/early schizonts, but did not affect oxidation of BODIPY^{581/591} C11 in uninfected RBCs, 16–20 hpi rings and 30–34 hpi early trophozoites. The sPLA₂ inhibitor Varespladib, which did not affect parasite progression or growth, did not affect oxidation of BODIPY^{581/591} C11. These data suggest that inhibition of parasite progression and growth by Darapladib is due to inhibition of protective PLA₂ enzymes involved in lipid oxidation damage repair. Inhibition of these PLA₂ enzymes would prevent repair of oxidised phospholipids (oxPL), leading to the observed increased oxidative damage through unhindered propagation of the lipid oxidation chain reaction, which is detrimental to cells.

5.3.2 Measurement of MDA levels by TBARS assay

Malondialdehyde (MDA) is one of several degradation products from the decomposition of oxidised lipids. Elevated MDA levels correlate with increased degradation of oxidised lipids and thus reflect levels of overall lipid oxidation in a biological sample. An asynchronous *P. falciparum* 3D7 culture with about 20% parasitemia, or uninfected RBCs were treated for 8 h with Darapladiib or DMSO and MDA levels were determined with the thiobarbituric acid reactive substances (TBARS) assay (Figure 5.5B). Treatment with 2 μM Darapladiib led to a significant increase of MDA levels in infected RBCs, whereas MDA levels of uninfected RBCs remained unaffected. Neither treatment with DMSO nor 0.5 μM Darapladiib changed MDA levels in RBCs and iRBCs significantly. These findings suggest that Darapladiib treatment leads to increased lipid oxidation in *P. falciparum* infected RBCs.

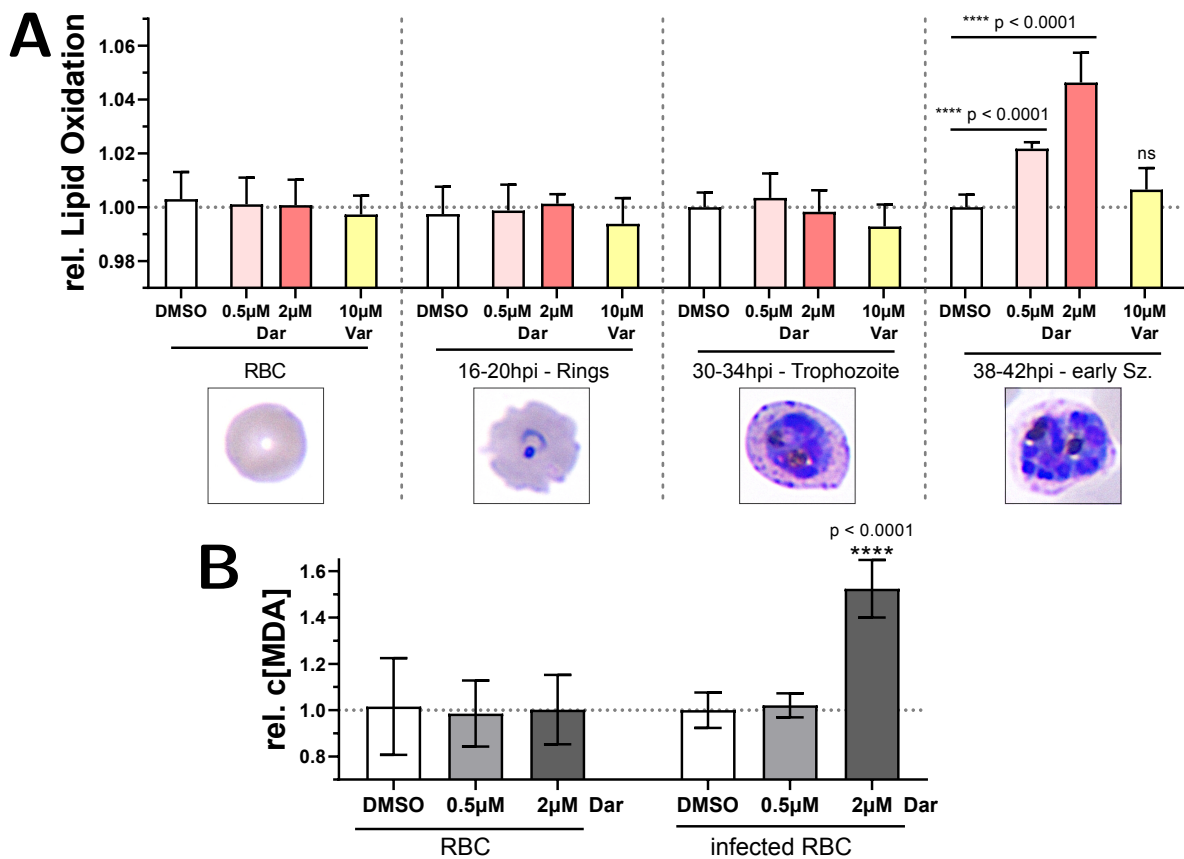


Figure 5.5: Darapladiib increases lipid oxidation. (A) Parasites were treated for 2 h with Darapladiib, Varespladiib or DMSO. Darapladiib significantly increased oxidation of the BODIPY^{581/591} C11 lipid oxidation sensor in 30–34 hpi late trophozoites/early schizonts in a dose-dependent manner. Lipid oxidation in rings, early trophozoites and uninfected RBCs was not elevated upon treatment with Darapladiib. The sPLA₂ inhibitor Varespladiib had no effect on lipid oxidation in any stage. (B) Treatment with 2 μM Darapladiib lead to a significant increase of MDA levels in infected RBCs, whereas uninfected RBCs remained unaffected. Experiments were performed with at least three biological replicates. **Abb.:** Dar, Darapladiib; hpi, hours post invasion; (i)RBC, (infected) Red Blood Cell; Var, Varespladiib; Sz, Schizont; Troph, Trophozoite.

5.4 Progression and growth of *P. falciparum* blood stages inhibited by Darapladib can be restored by addition of α -tocopherol and dioleoyl-PC

The lipophilic antioxidant α -tocopherol (vitamin E) prevents lipid oxidation by scavenging peroxy radicals and by interrupting propagation of the lipid oxidation radical chain reaction [141]. Given that treatment with Darapladib has been shown to increase lipid oxidation, we investigated whether addition of exogenous α -tocopherol restores parasite progression and growth. Synchronous *P. falciparum* 3D7 ring stage cultures were treated with the IC₇₅ concentration of Darapladib (0.75 μ M) and different concentrations of α -tocopherol ranging

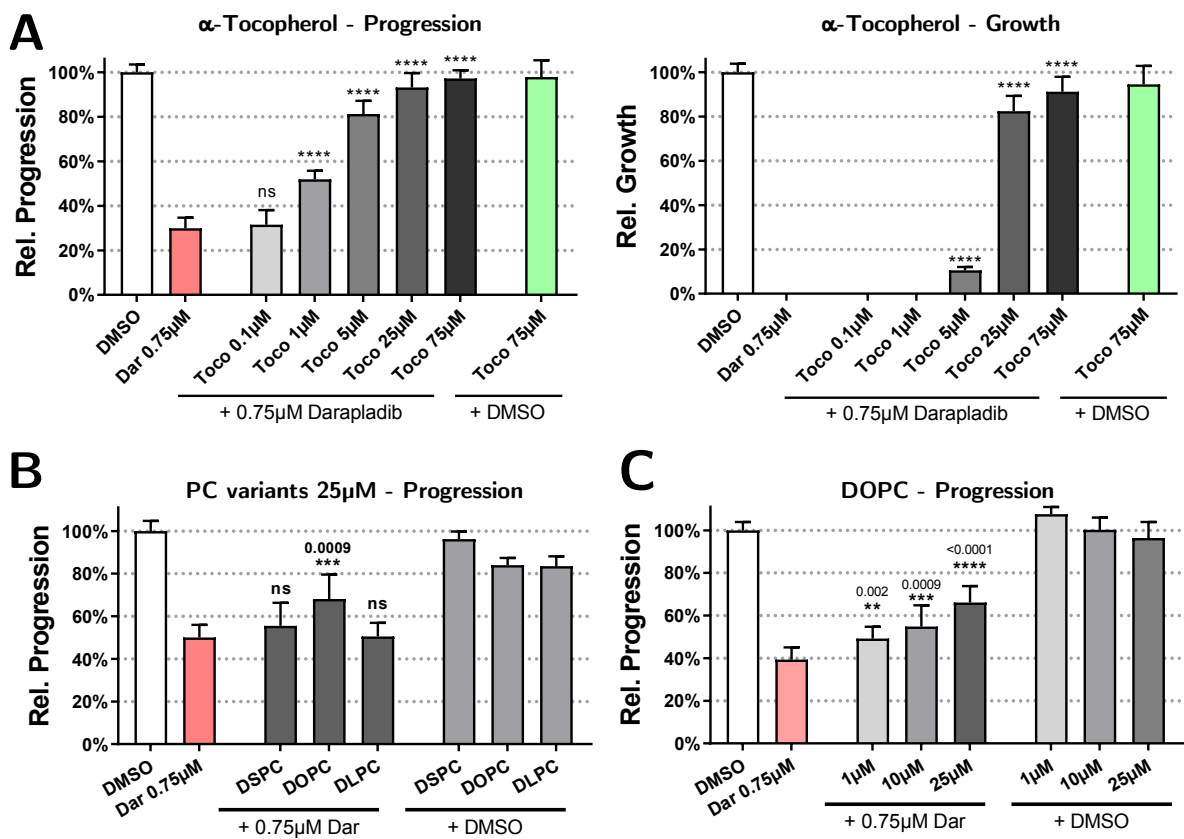


Figure 5.6: α -Tocopherol and DOPC restore *P. falciparum* blood stage progression inhibited by Darapladib. (A) Synchronous *P. falciparum* blood stage cultures were co-treated at ring stage with Darapladib and α -tocopherol. Addition of α -tocopherol restored Darapladib-inhibited progression and growth. Treatment with α -tocopherol alone did not have any effect on progression or growth. (B) Synchronous *P. falciparum* blood stage cultures were co-treated at ring stage with Darapladib and 25 μ M DSPC (18:0), DOPC (18:1) and DLPC (18:2). Only DOPC restored parasite progression significantly. (C) DOPC restored parasite progression in a dose-dependent manner in a co-treatment with Darapladib. Experiments were performed with at least three biological replicates. **Abb.:** Dar, Darapladib; DOPC, Dioleoyl phosphatidylcholine; DLPC, Dilinoleoyl phosphatidylcholine; DSPC, Distearoyl phosphatidylcholine; Toco, α -Tocopherol.

from 0.1 μM to 75 μM . Parasites were allowed to progress to schizont stage or to complete the full cycle. Addition of α -tocopherol completely restored both parasite progression and growth in a dose-dependent manner (Figure 5.6A). Treatment with α -tocopherol alone did not alter parasite progression and growth. These findings suggest that if lipid oxidation is prevented by co-treatment with antioxidant α -tocopherol, repair of lipid oxidation membrane damage becomes non-essential and inhibition of PLA₂ enzymes involved in lipid oxidation repair by Darapladib has no effect on parasite progression or growth.

If Darapladib indeed inhibits repair of oxidised *unsaturated* phospholipids, we hypothesised that addition of exogenous *unsaturated* phospholipids should alleviate the inhibition of progression by Darapladib, whereas *saturated* analogue phospholipids should have no effect. Phosphatidylcholine (PC) with oleic acid residues is the most abundant unsaturated phospholipid in infected RBCs and essential for parasite growth [106, 129, 263]. We investigated whether saturated disteareoyl-PC (DSPC, 18:0), mono-unsaturated dioleoyl-PC (DOPC, 18:1), or the di-unsaturated linoleoyl-PC (DLPC, 18:2) can restore Darapladib-inhibited parasite progression and growth.

Synchronous *P. falciparum* 3D7 rings were co-treated with the IC₇₅ concentration of Darapladib (0.75 μM) and 25 μM of DSPC, DOPC and DLPC (Figure 5.6B). Only mono-unsaturated DOPC restored parasite progression significantly in a co-treatment with Darapladib, while DSPC and DLPC had no significant effect.

To further investigate this, parasites were co-treated with 0.75 μM Darapladib and different concentrations of DOPC ranging from 1 μM to 25 μM (Figure 5.6C). Parasite progression of Darapladib treated cultures was partly restored in a dose-dependent manner by DOPC. These findings support the hypothesis that Darapladib inhibits lipid oxidation repair, as addition of exogenous DOPC could help to maintain the integrity of unrepaired, lipid oxidation-damaged membranes and counter the inhibitory effects of Darapladib.

5.5 Known targets of the PLA₂-inhibitors Darapladib, MAFP and ATK are absent in RBCs and *P. falciparum*

Darapladib has been developed as an inhibitor against human Lp-PLA₂ with an IC₅₀ of 0.25 nM and MAFP and ATK are known to inhibit serine hydrolases such as cPLA₂ and Lp-PLA₂ [160, 163, 164, 287]. Platelet-activating factor acetylhydrolase 2 (PAF-AH2) is an intracellular homologue of serum circulating Lp-PLA₂. However, neither cPLA₂, Lp-PLA₂ nor PAF-AH2 are reported in the proteome of human RBCs and reticulocytes [238]. The aforementioned enzymes were neither detected in RBC precursing erythroblasts by proteomics and RNAseq (MOHANDAS NARLA, personal communication). A recent report showed that extracellular *h*Lp-PLA₂ is not imported by the parasite from blood serum [288]. An in-depth

in silico search for *Plasmodium spp.* orthologues of human cPLA₂ (UniProt ID P47712), human Lp-PLA₂ (Q13093) and human PAF-AH2 (Q99487) in the PlasmoDB protein sequences database using a basic local alignment search tool (BLAST) did not yield any candidates.

To confirm that *P. falciparum* does not internalise human Lp-PLA₂ and also does not express an orthologue, we measured Lp-PLA₂ activity of a lysate of purified, saponised schizonts (Figure 5.7A). Recombinant Lp-PLA₂ served as the positive control and exhibited strong activity, which was successfully inhibited with Darapladib. No Lp-PLA₂ activity was detected in *P. falciparum* schizonts. To confirm the integrity of the schizont lysate and to compare the activity of biological replicates, we measured the activity of *P. falciparum* lactate dehydrogenase (LDH) (Figure 5.7B).

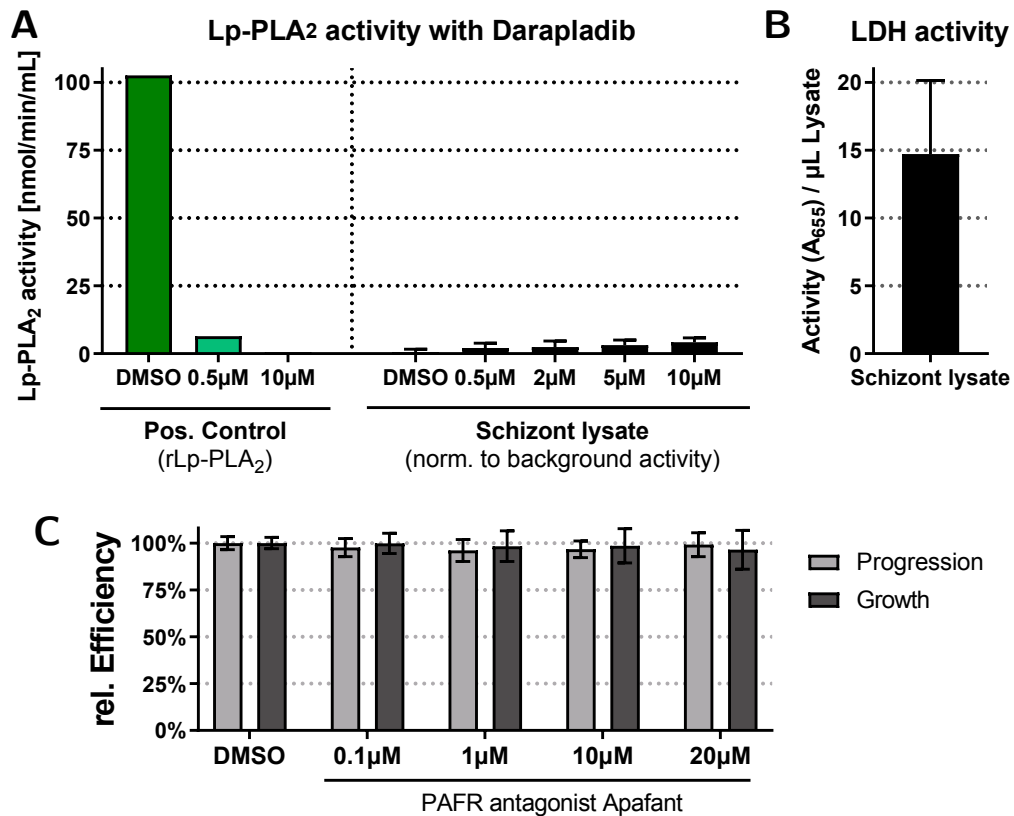


Figure 5.7: Lp-PLA₂ activity was absent in *Pf* schizont lysates. PAF-signalling is not essential for parasite development. (A) Lysate of purified, saponised *P. falciparum* schizonts did not exhibit specific Lp-PLA₂ activity. Recombinant Lp-PLA₂ was used as a positive control and was successfully inhibited by Darapladib. (B) *Pf*LDH activity was determined to validate integrity of the schizont lysate. (C) PAF receptor inhibitor Apafant does not inhibit parasite development. Experiments were performed with at least three biological replicates. *Abb.*: LDH, lactate dehydrogenase; Lp-PLA₂, Lipoprotein-associated PLA₂; PAF, platelet-activating factor; PAFR, PAF receptor

5.5.1 Lp-PLA₂-mediated platelet-activating factor signalling

The known target of Darapladib, Lp-PLA₂, regulates levels of the platelet-activating factor (PAF, acetyl-glycerol-ether-phosphorylcholine) which is involved in multiple signalling pathways [159]. We assessed whether PAF-related signalling could be involved in the antimalarial activity of Darapladib. Synchronous *P. falciparum* 3D7 cultures were incubated with the selective PAF receptor antagonist Apafant (Figure 5.7C). Neither progression nor growth were affected. This suggests that PAF signalling is not important for the antimalarial activity of Darapladib.

5.6 Pre-treatment of RBCs with MAFP inhibits *P. falciparum* blood stage progression, but not invasion

About 22 phospholipases have been described in *P. falciparum* in the literature [129]. From these phospholipases, only four have been characterised as PLA₂ enzymes and belong to the patatin-like phospholipase (PLP) family [129]. PfPLPs have not been described to cleave or repair oxidised phospholipids, but are thought to be involved in salvage of unoxidised phospholipids through β -oxidation and lipid signalling [181]. The RBC proteome, however, contains three PLA₂ enzymes, of which peroxiredoxin 6 (PRDX6) is known to repair OxPLs through its PLA₂ activity. In order to investigate whether a protective host RBC PLA₂ could be the target of the progression-blocking PLA₂ inhibitors, we pre-treated uninfected RBCs with the irreversible, covalently-binding PLA₂ inhibitor MAFP or its reversible analogue ATK (Figure 5.8A). After incubation with MAFP, RBCs were washed to remove unbound inhibitor and incubated with purified *P. falciparum* schizonts.

P. falciparum merozoites released from schizonts readily invaded pre-treated RBCs and formed rings regardless of MAFP or ATK treatment as observed by Giemsa-stained blood smears and flow cytometry (Figures 5.8A and 5.8B). However, progression of rings to schizont was significantly reduced in MAFP pre-treated RBCs. At 100 μ M MAFP pre-treatment, trophozoites did not exhibit segmentation and showed transparent vesicular structures in the cytosol (cf. markers in Figure 5.8A). Above 200 μ M MAFP, parasite size decreased, the FV was enlarged around the hemozoin crystal. At 300 μ M MAFP parasites exhibited a shrunken, pyknotic appearance with large transparent vesicular structures which did not contain visible hemozoin. Pre-treatment with the reversible analogue of MAFP, ATK, did not inhibit parasite invasion or progression supporting a specific target-directed action of MAFP (Figure 5.8B).

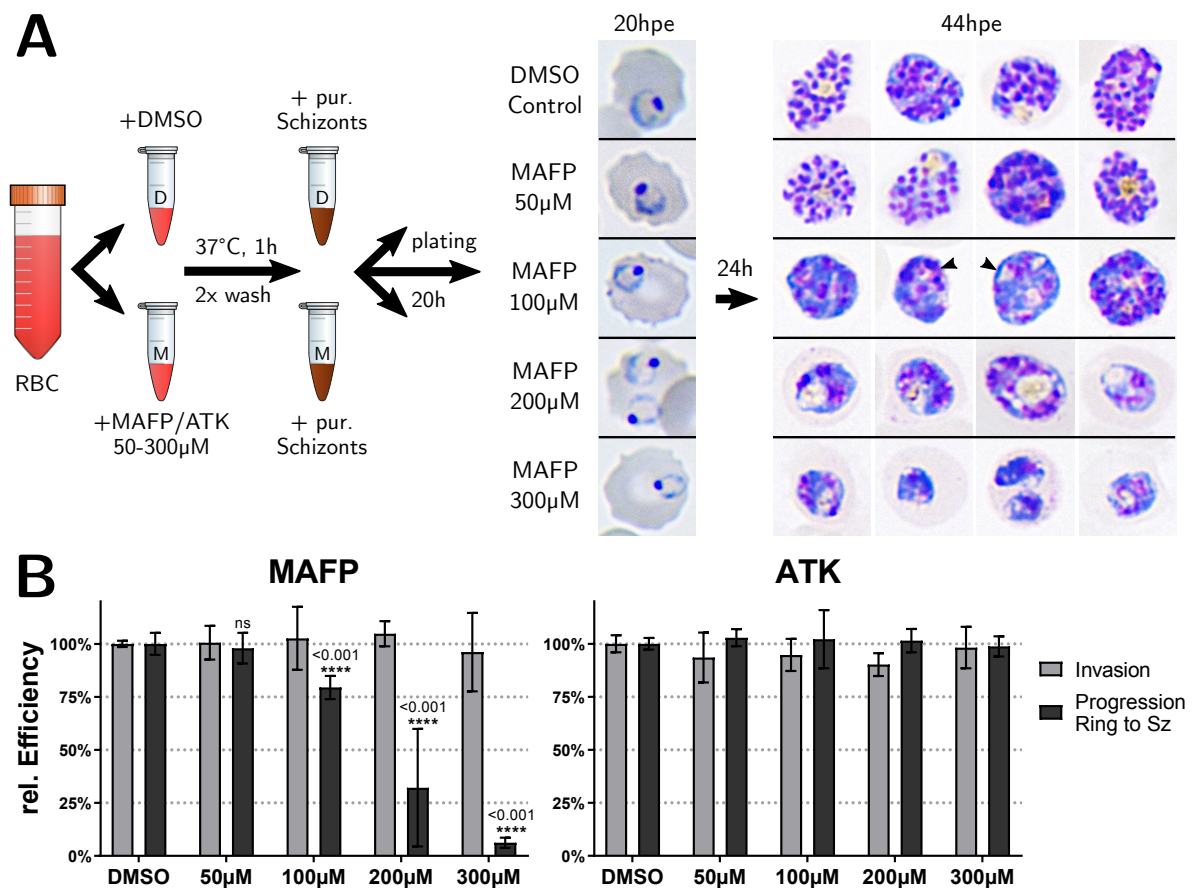


Figure 5.8: Pre-treatment of uninfected RBCs with MAFP allowed *P. falciparum* invasion, but inhibited ring to schizont progression. (A) Uninfected RBCs pre-treated with the irreversible, covalently-binding PLA₂ inhibitor MAFP allowed successful invasion and formation of rings. Parasites did not progress to schizont in MAFP pre-treated RBCs. (B) The reversible MAFP-analogue ATK had no effect on neither invasion nor progression. Experiments were performed with at least three biological replicates. *Abb.:* hpe, hours post egress; Lp-PLA₂, Lipoprotein-associated PLA₂; PAF-AH1b, Platelet-activating factor acetylhydrolase 1b; sPLA₂, secreted PLA₂.

5.7 Target identification of Darapladiib and MAFP

The RBC proteome contains only two PLA₂ enzymes which are reported to cleave OxPLs, PAF-AH1b and PRDX6 [153,238,241]. The selective inhibitor of PAF-AH1b had no effect on parasite growth indicating that PAF-AH1b is not a target for Darapladiib and MAFP. Thus, we hypothesised that Darapladiib and MAFP inhibit human PRDX6.

5.7.1 Production and validation of recombinant human PRDX6

Recombinant human PRDX6 with a C-terminal 6-His tag was produced in our laboratory by Christèle Huon using an *E. coli* expression system. The recombinant protein was purified by metal affinity chromatography to yield a single band that migrated at the expected size of

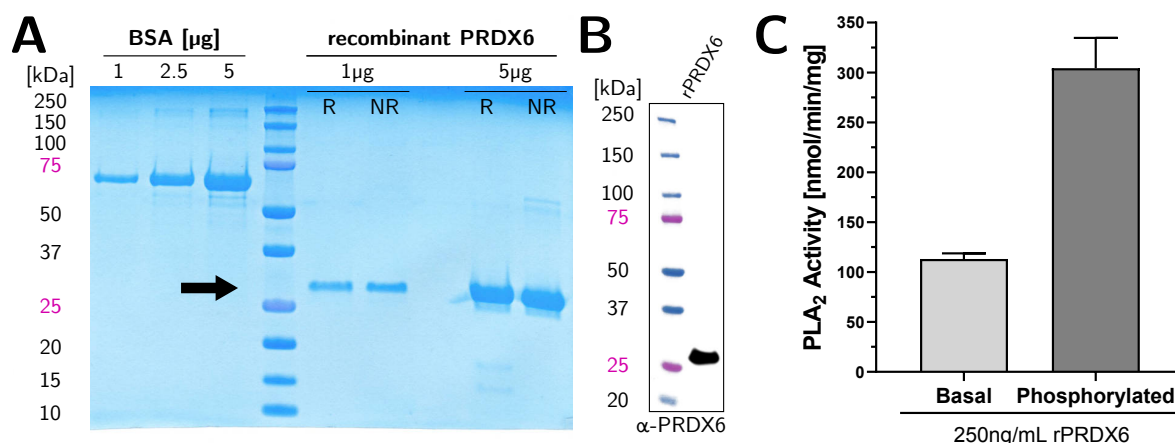


Figure 5.9: Recombinant expression and validation of human PRDX6. (A) rPRDX6 gave a single band at the expected size of 26 kDa. (B) Identity of rPRDX6 was confirmed by immunoblotting with a monoclonal α -hPRDX6 antibody. (C) Specific PLA₂ activity of basal and phosphorylated rPRDX6 was consistent with published data. *Abb.:* BSA, bovine serum albumin; R/NR, reducing (DTT)/non-reducing (w/o DTT).

26 kDa by SDS gel electrophoresis (Figure 5.9A). The yield from 2 L initial culture was about 25 mg. Recombinant PRDX6 was detected by immunoblotting with a monoclonal mouse α -hPRDX6 antibody confirming its identity (Figure 5.9B). The specific PLA₂ activity of rPRDX6 was measured using radioactively labelled liposomes at pH 5 before and after phosphorylation with MAFP. The specific PLA₂ activity of basal and phosphorylated rPRDX6 was consistent with published data (Figure 5.9C) [198].

5.7.2 Human PRDX6 is a target for Darapladib, MAFP and ATK, but not Varespladib

To assess if Darapladib targets human PRDX6, we employed activity-based protein profiling (ABPP). ABPP is based on the competitive and covalent labelling of the active site of the protein of interest (Figure 5.10A) [199]. PRDX6 is classified as a serine hydrolase and the active site of its PLA₂ function is comprised of a Ser-His-Asp catalytic triad [153]. In this triad, the serine is deprotonated, which drastically increases the nucleophilicity of its hydroxyl oxygen [289]. The activated serine can be targeted by electrophilic groups, such as fluorophosphonate, which selectively form a covalent bond with the reactive active site-serine, but not with serine residues outside the catalytic triad [199]. Probes for ABPP consist of an electrophilic covalently binding “warhead”, such as fluorophosphonate, which is linked to a reporter group, such as a fluorophore. The target protein is simultaneously incubated with the inhibitor of interest and the ABPP probe. If the inhibitor does not bind to the active site, the ABPP probe has access to the activated serine of the active site and forms a covalent bond (Figure 5.10A). If the inhibitor does bind to the active site, it blocks the access to the

active site and competitively reduces the labelling with the ABPP probe. After removal of unbound probe by washing, successful covalent fluorescent labelling of the target protein can be visualised via SDS gel electrophoresis followed by fluorescence gel-imaging. Summed up, if the inhibitor of interest reduces fluorescent labelling of the target protein, it binds to the active site of the target protein preventing access of the ABPP probe.

Darapladib, MAFP and ATK, but not Varespladib, reduced labelling of recombinant human PRDX6 with the fluorescent ABPP-probe TAMRA-fluorophosphonate (TAMRA-FP, Figure 5.10B and C). These data provide evidence that Darapladib, MAFP and ATK, but not Varespladib, bind to the active site of the PLA₂ activity of PRDX6.

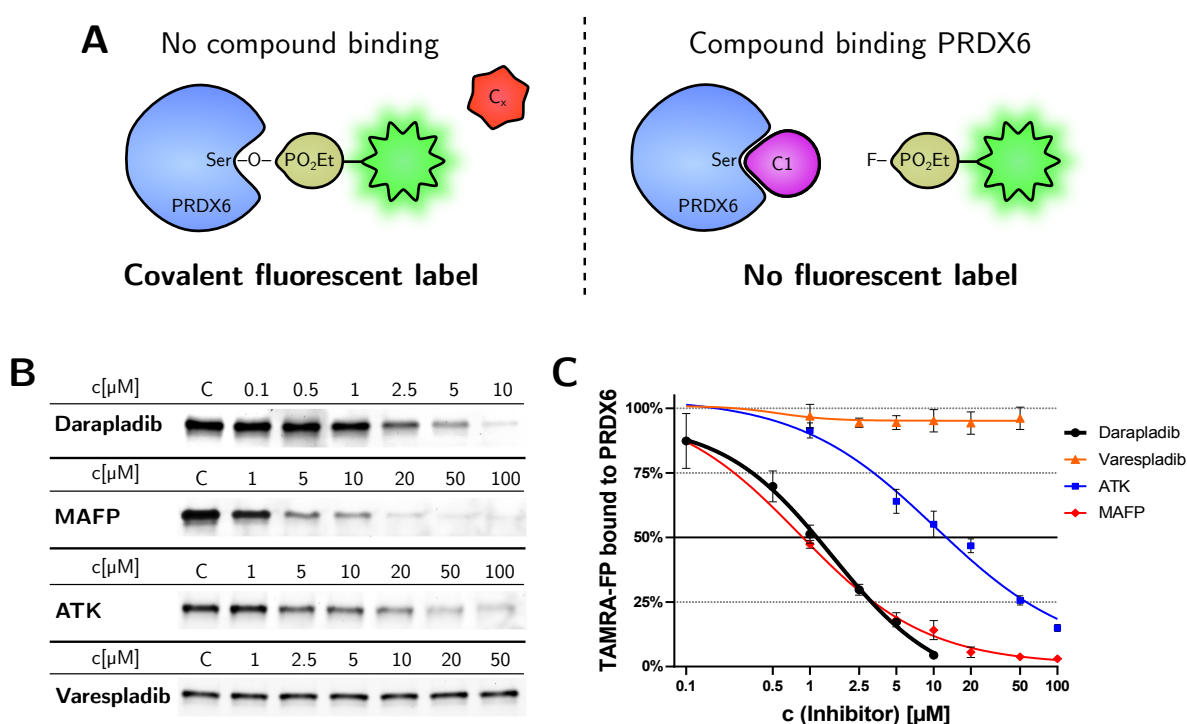


Figure 5.10: Darapladib, MAFP and ATK, but not Varespladib bind to human PRDX6. (A) Schematic principle of ABPP. (B) Recombinant human PRDX6 was incubated with Darapladib, MAFP, ATK and Varespladib and subsequently labelled with the fluorescent ABPP-probe TAMRA-FP. Darapladib, MAFP and ATK, but not Varespladib, reduced labelling of human PRDX6 indicating that bind to the active site of the PLA₂ function of PRDX6. (C) Quantified band intensities of fluorescent gels in (B). Representative gels from three independent experiments are shown. **Abb.:** ATK, arachidonyl trifluoromethyl ketone; MAFP, methoxy arachidonyl fluorophosphonate; PRDX6, peroxiredoxin 6.

5.7.3 Darapladib inhibits the PLA₂ activity of PRDX6

Given that Darapladib showed binding to the active site of the PLA₂ activity of PRDX6, we were interested if Darapladib also inhibits the enzymatic PLA₂ activity of PRDX6. To measure PRDX6 PLA₂ activity, we incubated phosphorylated recombinant PRDX6 with radioactively labelled unilamellar liposomes containing [2-palmitoyl-1-¹⁴C]-dipalmitoyl phosphatidylcholine (¹⁴C-DPPC) and measured release of free ¹⁴C-palmitic acid. Darapladib inhibited the PLA₂ activity of PRDX6 with an IC₅₀ of $0.56 \pm 0.03 \mu\text{M}$ (Figure 5.11).

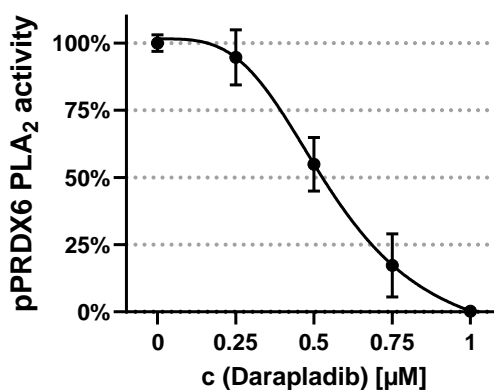


Figure 5.11: Darapladib inhibits the PLA₂ activity of PRDX6. Liposomes containing tracer (¹⁴C-DPPC) were incubated with phosphorylated PRDX6 and release of free ¹⁴C-palmitic acid was measured to assess PLA₂ activity. Darapladib inhibited the PLA₂ activity of recombinant PRDX6 with an IC₅₀ of $0.56 \pm 0.03 \mu\text{M}$. Results are based on three biological replicates. **Abb.:** DPPC, dipalmitoyl phosphatidylcholine; pPRDX6, phosphorylated Peroxiredoxin 6;

5.7.4 *In silico* docking of Darapladib to PRDX6

An *in silico* docking study to evaluate potential binding sites for Darapladib on PRDX6 was performed in collaboration with Luis Checa Ruano and Olivier Sperandio (Institut Pasteur, Paris). Darapladib was docked to hPRDX6 (PDB 5b6m) using Smina with Vinardo scoring function (Figure 5.12). The calculations and data evaluation were performed by Luis Checa Ruano. The docking study indicated that Darapladib could potentially bind at the predicted PLA₂ active site within PRDX6. One potential binding pocket was identified with two binding poses that had a similar docking score, -8.2 and -8.1 kcal/mol, respectively. The -8.1 kcal/mol pose was considered more relevant due to the greater proximity of Darapladib to the active site Ser32. In this pose, two H-bonds were present between the amide of the cyclopenta-pyrimidone ring of Darapladib and the Lys67 side chain, with a distance of 3.1 and 2.8 Å. Even if Lys67 is not directly involved in the catalytic triad, this residue formed a H-bond with Ser32 of the active site, with a distance of 3.7 Å. Some similarities could be established between the known structure of Darapladib bound to Lp-PLA₂

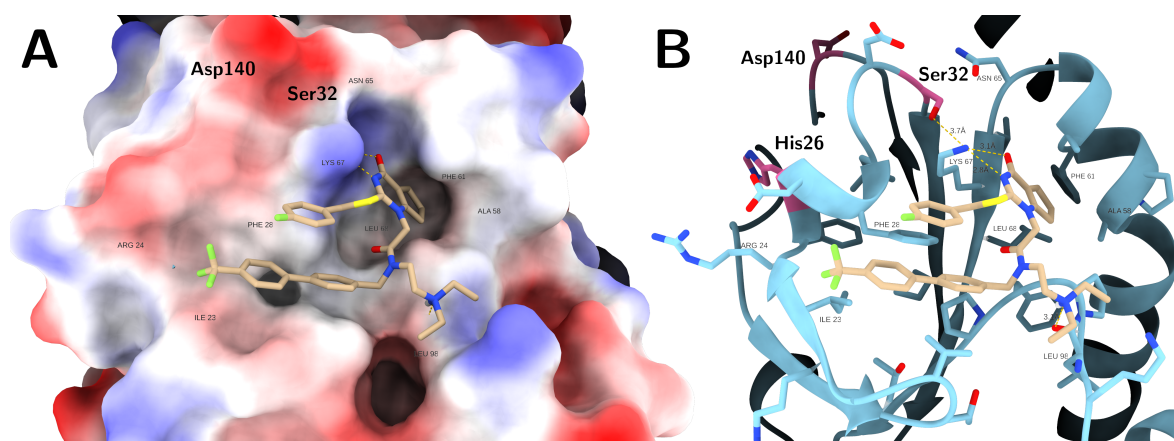


Figure 5.12: *In silico* docking of Darapladib to *hPRDX6*. Selected pose of Darapladib on PRDX6 (5b6m, chain B) showing (A) the electrostatic surface and (B) ribbon diagram. Residues involved in the catalytic triad are coloured in magenta.

and the Darapladib docking pose on PRDX6. For Lp-PLA₂, the carbonyl of the cyclopentapyrimidone ring forms an H-bond with the two residues of the oxyanion hole of the enzyme that stabilize the negative charge of a tetrahedral intermediate of the esterolysis reaction [290]. For PRDX6, Lys67 may be part of the oxyanion hole of the enzyme because of its proximity to Ser32 and its positive charge that could stabilize the tetrahedral intermediate of the reaction. If this hypothesis is right, Darapladib could also interact with the oxyanion hole of PRDX6. In addition, the cyclopentapyrimidone ring exhibited a good shape complementarity inside the cavity delimited between Lys67, Leu68, Ala58 and Phe61, with the cyclopentil moiety located in the deepest part of the cavity. Furthermore, the diethylamine group of Darapladib forms a H-bond with the carbonyl backbone of Leu98 (distance of 3.1 Å) and the biphenyl of Darapladib establishes hydrophobic contacts with Ile23, Val20 and Phe28. Taken together, these findings support the observation that Darapladib binds to PRDX6 and could inhibit its PLA₂ function.

5.8 Role of PRDX6 in a malaria mouse model using PRDX6^{-/-} mice

RBCs cannot be genetically altered, as they lack a nucleus and a protein expression machinery. Thus, it is not possible to validate PRDX6 as the target of Darapladib through genetic knockout. However, as PRDX6 has been successfully knocked out in mice, we used PRDX6^{-/-} mice and tested if blood stage rodent malaria parasites, *P. berghei* and *P. yoelii*, can infect and multiply in PRDX6^{-/-} mice. We examined *in vivo* blood stage growth of *P. berghei* and *P. yoelii* in PRDX6^{-/-} mice and *ex vivo* progression of *P. yoelii* infected RBCs from PRDX6^{-/-} mice.

5.8.1 *In vivo* growth assay

PRDX6^{-/-} mice and age-matched control C57/BL6JRj WT mice were infected with *P. berghei* ANKA or the *P. yoelii* YM lethal strain. Parasitemia was measured by Giemsa-stained blood smears and by flow cytometry. Growth of *P. berghei* ANKA in PRDX6^{-/-} and WT mice was not significantly different (Figure 5.13A). *P. berghei* preferably invades reticulocytes, in contrast to our target organism *P. falciparum*, which only invades mature RBCs. To assess intraerythrocytic growth in the mouse model, we used the *P. yoelii* YM lethal strain which invades both CD71⁺ reticulocytes and CD71⁻ mature erythrocytes. By labelling cells with

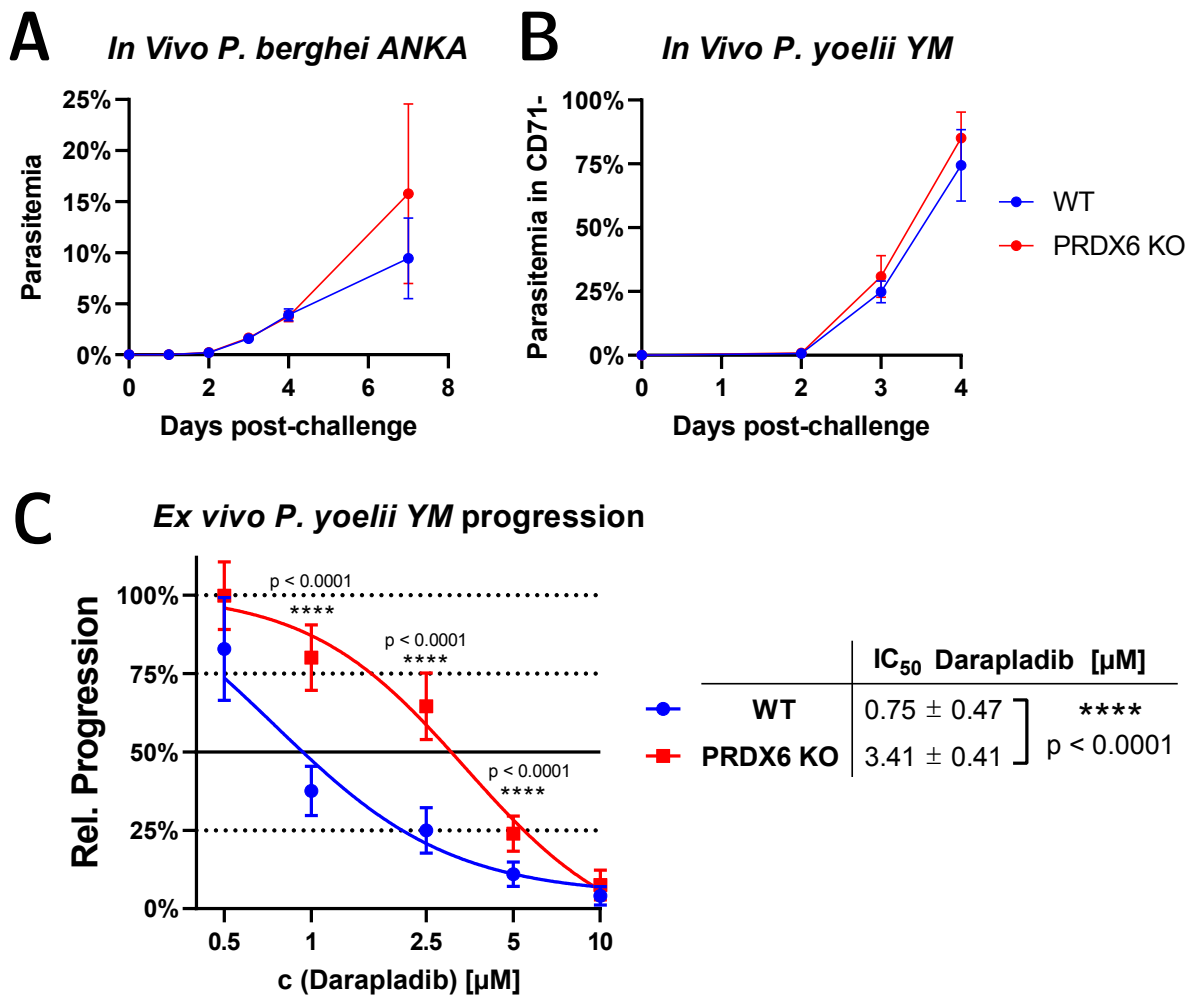


Figure 5.13: Growth of rodent malaria strains *P. berghei* ANKA and *P. yoelii* YM in PRDX6^{-/-} mice. (A) *In vivo* growth of *Pb* ANKA and (B) *Py* YM is not affected by knockout of PRDX6 in mice. (C) The IC₅₀ for inhibition of *Py* YM blood stage progression by Darapladib was significantly higher for infected PRDX6^{-/-} RBCs than for WT RBCs. Deletion of PRDX6 leads to compensatory expression of enzymes with a significantly lower affinity for Darapladib. Experiments were performed with at least five mice per group, *in vivo* *Pb* ANKA n=1 and *Py* YM n=2, *ex vivo* n=3. *Abb.*: KO, knockout; WT, wild type.

an α -CD71 antibody and excluding CD71⁺ reticulocytes in the analysis, we were able to specifically observe intraerythrocytic growth of *P. yoelii* YM in mature RBCs. Growth of *P. yoelii* YM was not significantly different between PRDX6^{-/-} and WT mice (Figure 5.13B).

5.8.2 *Ex vivo* progression assay with Darapladib

Darapladib has a very low bio-availability with a maximum plasma concentration in humans of about 20 nM [162]. As the IC₅₀ of Darapladib for the inhibition of the PLA₂ function of PRDX6 is about 560 nM and roughly 30 times higher than the maximum plasma concentration, we cannot test antimalarial activity of Darapladib in an *in vivo* growth assay. Thus, we tested the effect of Darapladib in an *ex vivo* ring stage progression assay using *P. yoelii* YM infected RBCs. Infected CD71⁺ reticulocytes were excluded in the analysis. Darapladib inhibited ring to schizont progression in WT RBCs (Figure 5.13C). Interestingly, Darapladib also blocked blood stage progression in PRDX6^{-/-} RBCs. This indicates that Darapladib has other targets besides PRDX6. However, the IC₅₀ of Darapladib for parasite progression in PRDX6^{-/-} RBCs was about 4.5-fold higher than for progression in WT RBCs. Thus, Darapladib appears to bind these other targets in PRDX6^{-/-} RBCs with lower affinity. PRDX6^{-/-} mice have been shown previously to compensate for the loss of PRDX6 with an increased expression of other antioxidant enzymes, such as PRDX3, PRDX4, Nuclear factor erythroid 2-related factor 2 (NRF2) and higher glutathione levels [291]. It remains to be seen if any of these upregulated enzymes can compensate for the loss of PRDX6 in PRDX6^{-/-} mice and if Darapladib targets these enzymes.

5.9 Internalisation and localisation of host RBC PRDX6

P. falciparum has been shown to import human peroxiredoxin 2 (PRDX2) from the host RBC cytosol [262]. We hypothesised that human PRDX6 may also be internalised by the parasite in a similar fashion.

5.9.1 Human PRDX6 is localised within the PVM of *P. falciparum* schizonts

To localise PRDX6 in *P. falciparum* infected RBCs, purified *P. falciparum* 3D7 early schizonts were treated with a 0.01% saponin solution to selectively lyse the host RBC membrane without affecting the parasitophorous vacuole membrane (PVM). After lysis, RBC cytosol was removed by centrifugation. Presence of human PRDX6 in protein extract from saponised and untreated schizonts was detected by immunoblotting. Human hemoglobin (Hb) served as a marker for complete lysis of the RBC membrane as it is the most abundant cytosolic protein in RBCs. *P. falciparum* nucleosome assembly protein L (NAPL) was used to normalise protein loading between samples. The bands for hPRDX6 and hHb in the immunoblots in

figure 5.14A and their quantified intensities (Figure 5.14B) show that human PRDX6 is only slightly reduced by saponin treatment, whereas hemoglobin is nearly completely removed. This suggests that human PRDX6 is indeed internalised by the parasite and localised within the PVM.

5.9.2 Vesicular hPRDX6 co-localises with the parasite in IFA

To study the localisation of human PRDX6 within infected RBCs, we examined infected RBCs by immunofluorescence microscopy. PRDX6-filled vesicular structures co-localised with the parasite suggesting selective endocytic uptake of human PRDX6 by the parasite (Figure 5.14C). The overall signal intensity of PRDX6 in the RBC cytosol was reduced in infected RBCs compared to uninfected RBCs, suggesting loss of PRDX6 from the RBC cytosol.

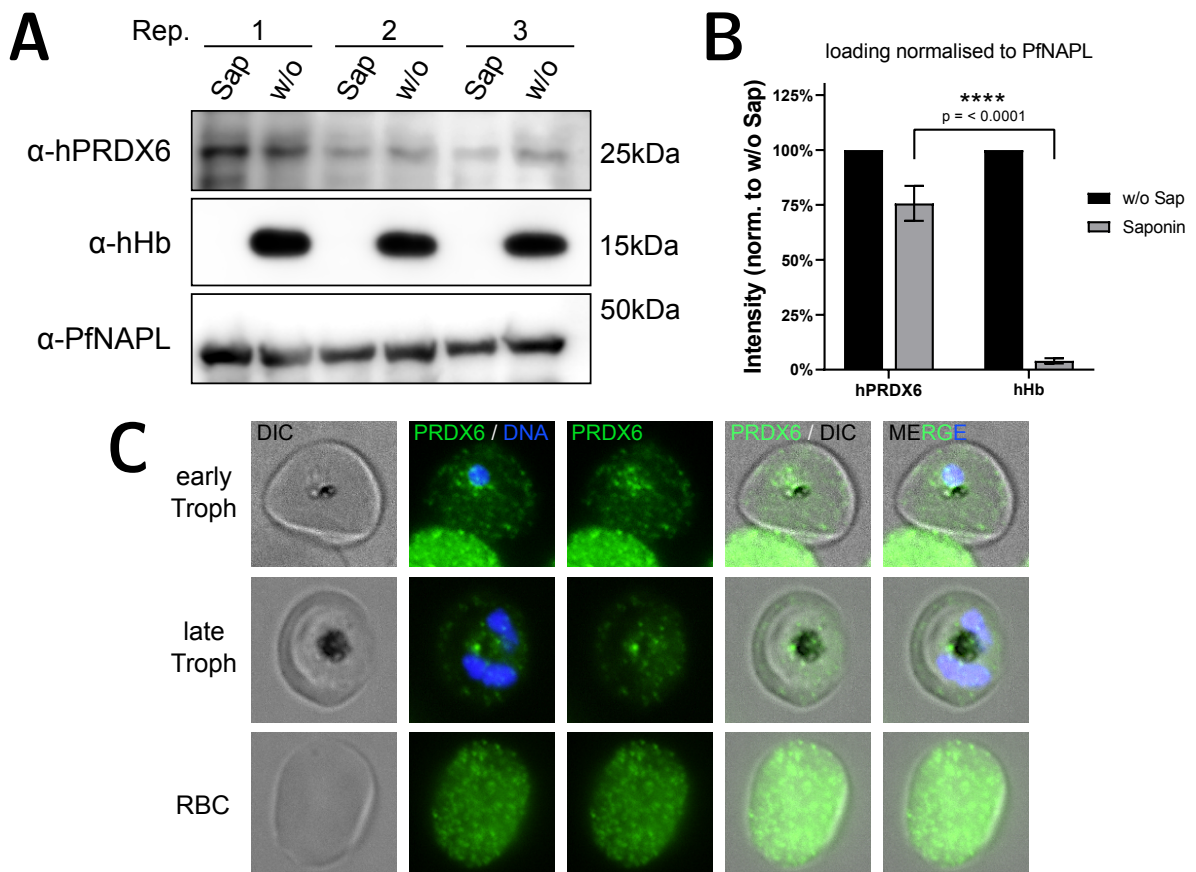


Figure 5.14: hPRDX6 is internalised by the parasite and shows vesicular co-localisation with the parasite. (A) Immunoblots of saponinised and untreated schizonts show internalisation of human PRDX6 within parasite PVM. (B) Quantified band intensities for human PRDX6 and Hb. (C) human PRDX6 filled vesicular structures co-localise with the parasite. Experiments were performed with at least three biological replicates. *Abb.:* Hb, Hemoglobin, NAPL, nucleosome assembly protein L.

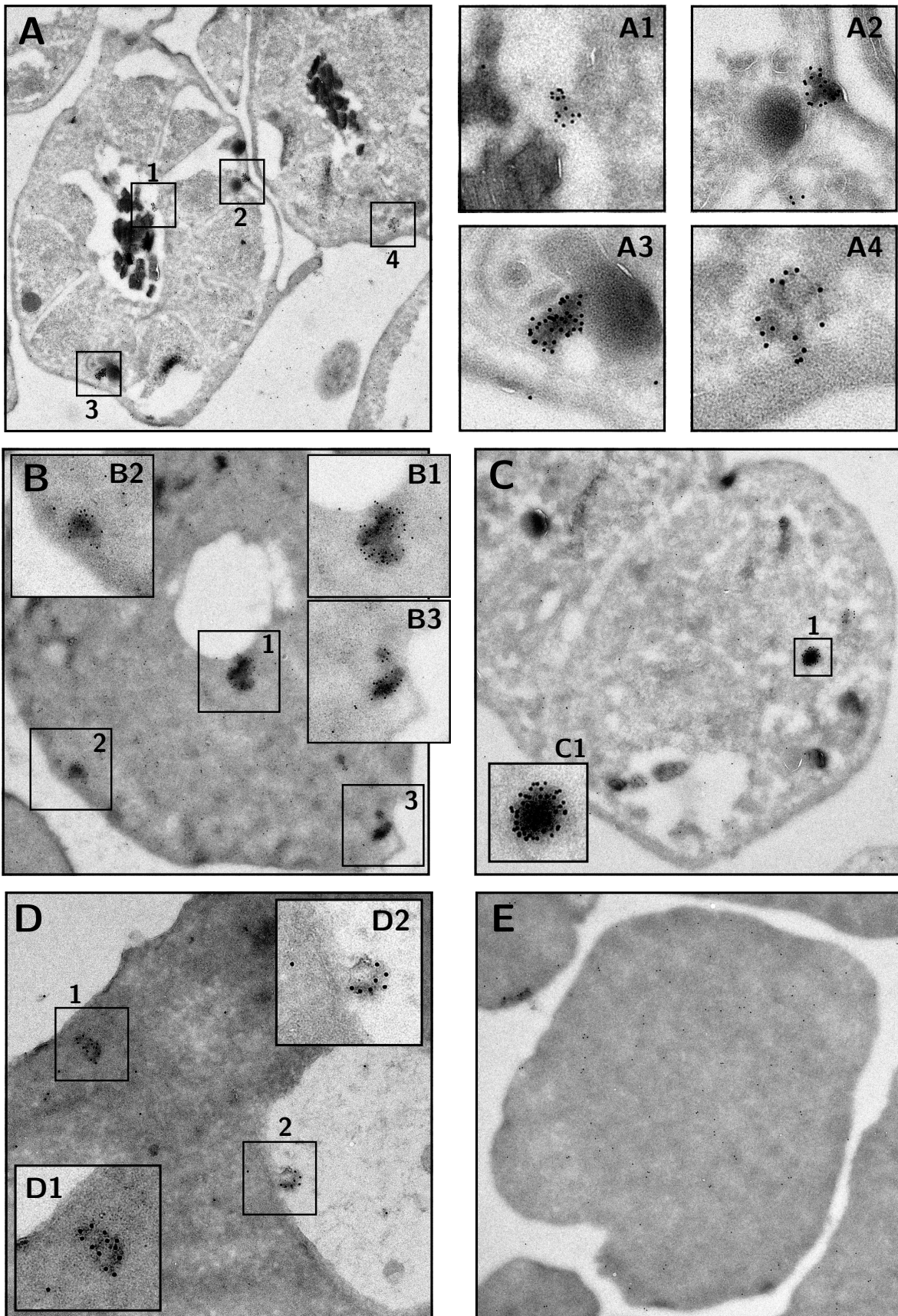
5.9.3 Immuno-EM shows human PRDX6 co-localises with host cell cytosol-containing vesicles

To further investigate the subcellular localisation of human PRDX6 within the parasite, we examined parasites by immuno-electron microscopy. Preparation of cells for electron microscopy and image acquisition was performed in collaboration with Olivier Gorgette, Ultrastructural BioImaging Core Facility, Institut Pasteur. Human PRDX6 was localised in dark-coloured vesicular structures within the parasite cytosol (Figure 5.15). These vesicles resembled cytotomes and were found at the inner surface of the PVM (Figure 5.15 A2, A4, B2, B3, D1), in the parasite cytosol (Figure 5.15 A3, C1) and adjacent to the FV membrane, both inside and outside the FV lumen (Figure 5.15 A1, B1, D2).

The data suggest that PRDX6 localises to host cell cytosol-containing vesicles (HcVs). Firstly, the dark colour of PRDX6-containing vesicles suggested the presence of hemoglobin, as the electron-dense iron atom of the heme group has low transmission for the electron beam (atomic number contrast). Secondly, the observed formation of one PRDX6-containing vesicle at the PVM surface (Figure 5.15 A4) suggests that PRDX6 is taken up alongside hemoglobin during host cell cytosol uptake (HCCU). Thirdly, PRDX6-containing vesicles were observed adjacent to the FV, and also within the FV lumen.

Taken together, this indicates that PRDX6 is internalised during HCCU and localises to HcVs which are then transported to the FV. However, PRDX6 was not detected in the FV, suggesting that PRDX6 is digested immediately after it is released into the FV lumen. Uninfected RBCs showed a uniform staining of PRDX6 in their cytosol (Figure 5.15 E). This is consistent with the reported cytosolic, non-vesicular localisation of PRDX6 in human cells [153].

Figure 5.15: (Next page) **Human PRDX6 is internalised by *P. falciparum* and localises to host cell cytosol-containing vesicles migrating towards the FV.** Cells were fixed according to the technique described by TOKOYASHU and probed with α -hPRDX6. (A2, A4, B2, B3, D1) PRDX6-containing vesicles resembling cytotomes were found at inner surface of the PVM. The dark colouration suggested the presence of iron-containing hemoglobin. (A4) One vesicles was observed during its formation at the PVM surface, suggesting that PRDX6-containing vesicles are formed during HCCU. (A3, C1) PRDX6-containing vesicles were also localised in the parasite cytosol, and (A1, B1, D2) adjacent to the FV membrane, both inside and outside the FV lumen. Non-vesicular PRDX6 was not detected inside the FV, suggesting immediate digestion of PRDX6 within the FV lumen. (E) Uninfected RBCs showed a uniform presence of PRDX6 in their cytosol. Representative images from three independent experiments are shown. **Abb.:** HcV, host cell cytosol-containing vesicles; FV, food vacuole.



5.10 Darapladib treatment disrupts HcV transport to the FV

5.10.1 Co-treatment of parasites with E64 and Darapladib

Given that human PRDX6 co-localises with hemoglobin in HcVs, we hypothesised that PRDX6 may play a role in the transport of HcVs to the FV. To test our hypothesis, we treated rings with either Darapladib or the protease inhibitor E64 individually, or with Darapladib and E64 together and analysed the cultures 20 h later by electron microscopy and light microscopy of Giemsa-stained smears. E64 inhibits the digestion of haemoglobin in the FV. As shown previously, treatment of rings with E64 results in parasites with a swollen FV containing accumulated, undigested hemoglobin [51]. These swollen FVs appear dark and electron-dense by electron microscopy (EM) and translucent in light microscopy (LM) of Giemsa-stained blood smears.

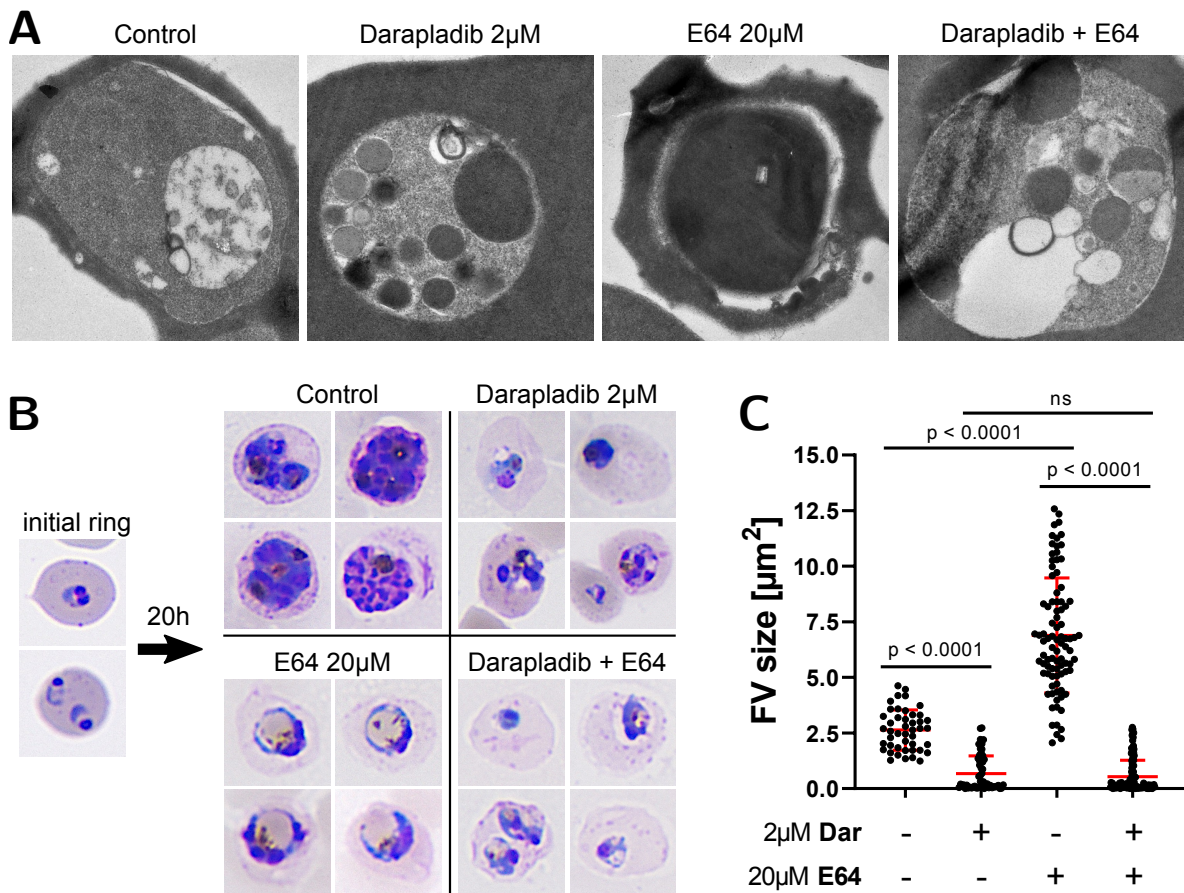


Figure 5.16: Darapladib treatment disrupts HcV transport. *Pf* 3D7 rings were treated with Darapladib, E64, the combination of both or DMSO as the control, incubated for 20 h until control parasites were late trophozoites and examined by electron (A) and (B) light microscopy. Treatment with Darapladib resulted in shrunken and pyknotic parasites and accumulation of HcVs in the parasite cytosol. E64-treated parasites contained a swollen, hemoglobin-filled FV as expected. Co-treatment with E64 and Darapladib precluded FV swelling supporting the hypothesis that Darapladib treatment disrupts transport of HcVs to the FV. (C) Quantification of the FV size upon treatment. **Abb.:** HcV, host cell cytosol-containing vesicles; FV, food vacuole.

Here, DMSO-treated control parasites successfully progressed to late trophozoites and their FVs contained hemozoin crystals visible both by EM and LM (Figure 5.16A,B). No HcVs were observed in the parasite cytosol by EM. Treatment with Darapladib alone drastically decreased the size of parasites and caused a shrunken and pyknotic appearance (Figure 5.16B). Multiple dark-coloured HcVs within the parasite cytosol were observed indicating the disruption of HcV transport by Darapladib and thus causing HcVs to accumulate in the parasite cytosol (Figure 5.16A). This suggests that Darapladib inhibits the transport, but not the formation of HcVs. Treatment with E64 alone resulted in the expected swelling of the FV (Figure 5.16A,B). Swollen FVs contained hemozoin both visible by EM and LM. The co-treatment with Darapladib and E64 resulted in shrunken, pyknotic parasites with a very similar phenotype to parasites treated only with Darapladib (Figure 5.16A,B). These observations suggest that Darapladib treatment allows HcV formation, but causes the disruption of HcV transport and prevent delivery of sufficient hemoglobin to the FV.

The size of the FV in treated parasites was quantified using ImageJ (Figure 5.16C). Treatment with Darapladib significantly reduced FV size, whereas the FVs of E64-treated parasites were enlarged. Co-treatment with both inhibitors prevents FV swelling and leads to shrunken small FVs. These data indicate that Darapladib treatment disrupts HcV transport.

5.10.2 Darapladib inhibits delivery of host cell cytosol to the FV

To validate the finding that Darapladib treatment disrupts transport of host cell cytosol-containing vesicles (HcV) to the FV, we pre-loaded RBCs with the pH-sensitive, cell impermeant fluorescent probe LysoSensor Blue/Yellow 10 kDa dextran. Pre-loaded RBCs were infected with *P. falciparum* 3D7 parasites, treated with 2 μ M Darapladib or DMSO and subsequently allowed to develop into trophozoites. The pH-sensitive LysoSensor Blue/Yellow emits blue fluorescence ($\lambda \approx 440$ nm) at neutral pH, but its emission wavelength shifts to yellow ($\lambda \approx 540$ nm) in an acidic environment. The RBC and parasite cytosol have a neutral pH, in contrast to the acidic parasite FV. Thus, when the parasite successfully internalises and transports host cell cytosol containing the fluorescent probe to its acidic FV, a yellow fluorescent signal is detectable in the FV. Equally, if transport of host cell cytosol to the FV is disrupted, the fluorescent probe is not transported to the acidic FV and no yellow fluorescence is detected. Parasite DNA was stained with the far-red DNA dye SYTO61. Parasites were examined by fluorescence microscopy (Figure 5.17A). DMSO-treated control parasites exhibited a bright yellow signal in their FV which co-localised with hemozoin crystals. This indicates the successful uptake and transport of host cell cytosol to the FV. The yellow fluorescence signal did not overlap with the SYTO61 stained nucleus. Darapladib treatment greatly reduced yellow fluorescence signal intensity and parasites appeared shrunken and pyknotic without visible hemozoin. These findings support the hypothesis that Darapladib disrupts

transport of host cell cytosol to the FV. Uninfected RBCs showed an evenly distributed blue, but no yellow fluorescence as expected. The ratio of yellow and blue fluorescence in the FV was quantified using the integrated signal density in ImageJ (Figure 5.17B). Yellow fluorescence intensity was significantly reduced in Darapladib-treated parasites. Parasites were also examined by flow cytometry (Figure 5.17C). Yellow fluorescence was significantly decreased in SYTO61⁺ infected RBCs upon treatment with Darapladib.

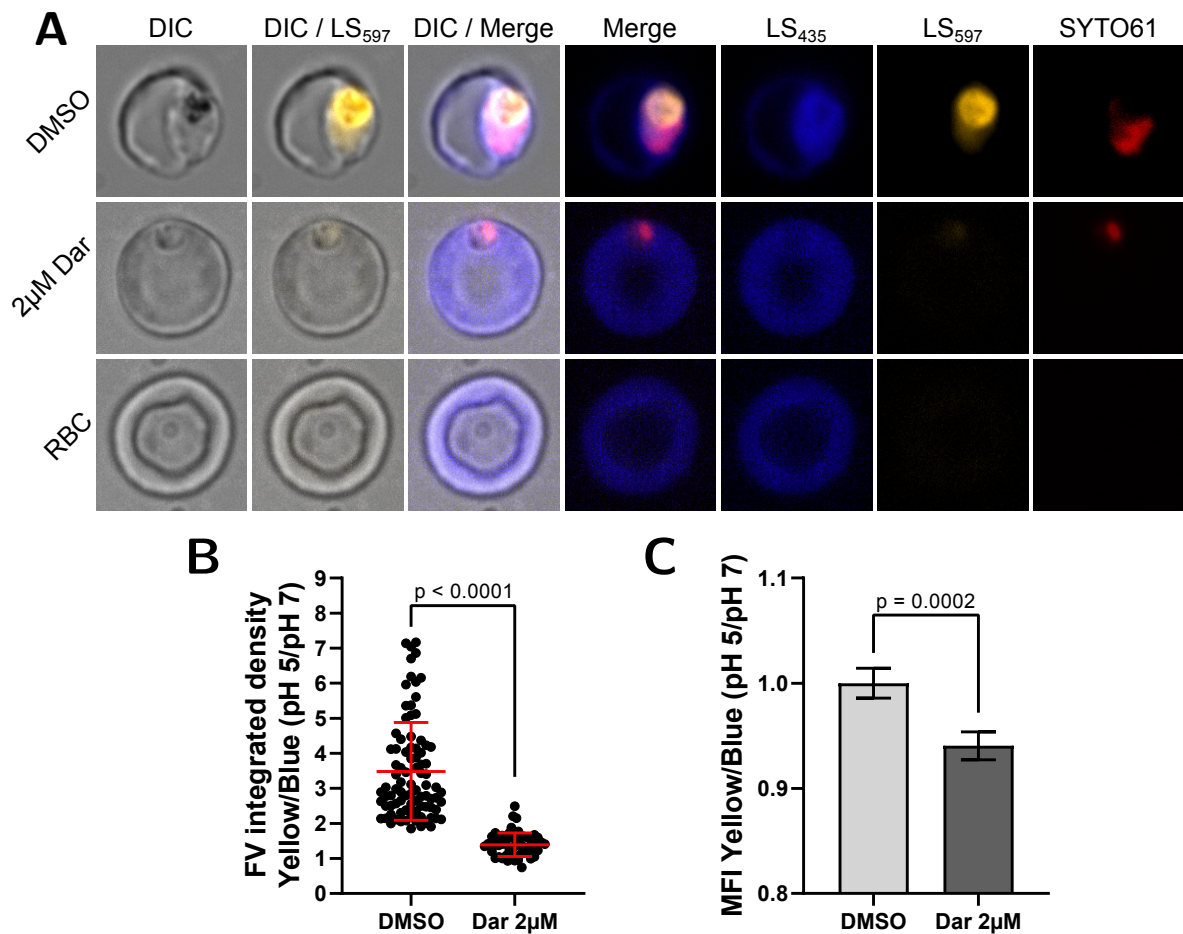


Figure 5.17: Darapladib inhibits delivery of host cell cytosol to the FV. (A) RBCs were preloaded with fluorescent LysoSensor-dextran, which emits blue fluorescence at neutral pH and yellow fluorescence at acidic pH. Preloaded RBCs were infected with *P. falciparum* 3D7 parasites. DMSO-treated control parasites exhibited a bright yellow fluorescence signal in their acidic FV, proving successful internalisation and transport of host cell cytosol containing the fluorescent sensor. Parasites treated with Darapladib only showed weak yellow fluorescence, suggesting the disruption of host cell cytosol transport. Uninfected RBCs showed an evenly distributed blue fluorescence. (B) Image quantification of yellow to blue ratio of the FV. Yellow fluorescence is significantly reduced upon treatment with Darapladib. (C) Flow cytometric quantification of yellow to blue ratio in parasites. Darapladib significantly reduced yellow fluorescence signal in parasites. Representative images from three independent experiments are shown. **Abb.:** FV, food vacuole.

5.10.3 Hemozoin crystal size is reduced upon Darapladib treatment

For further validation, the size of hemozoin crystals in Darapladib treated parasites was measured. *P. falciparum* 3D7 rings were treated with Darapladib or DMSO and allowed to progress to schizont stage. Hemozoin crystals were imaged using differential interference contrast (DIC) microscopy (Figure 5.18A) and quantified using ImageJ (Figure 5.18B). DMSO-treated parasites exhibited large hemozoin crystals with an average size of $2.5 \mu\text{m}^2$. The average hemozoin crystal size was significantly reduced to less than $0.5 \mu\text{m}^2$ upon treatment with Darapladib. These findings further confirm the hypothesis that treatment of Darapladib causes a disruption of HcV transport.

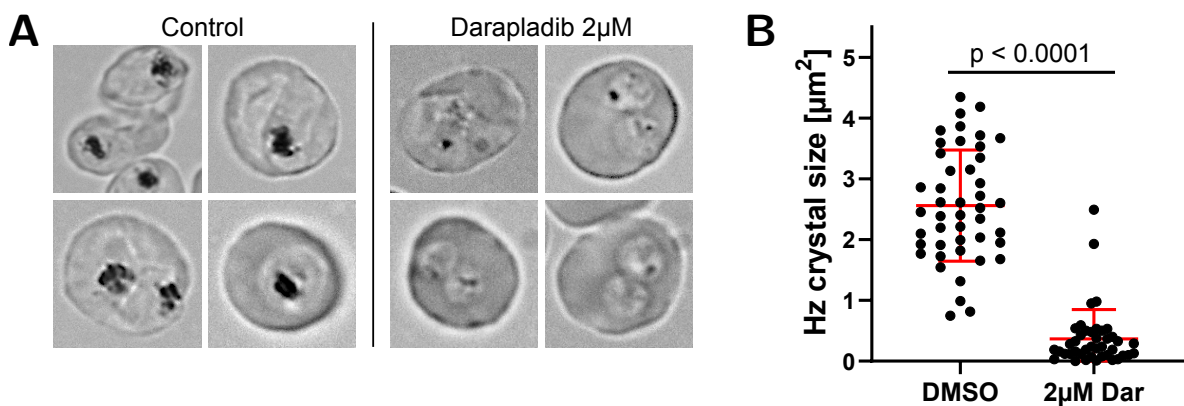


Figure 5.18: Treatment with Darapladib decreases hemozoin crystal size. (A) DIC images show that *Pf* 3D7 parasites contain smaller Hz crystals upon treatment with Darapladib. (B) The average size of Hz crystals is greatly reduced by treatment with Darapladib. Representative images from three independent experiments are shown. *Abb.:* Hz, hemozoin

5.11 Co-treatment of Artemisinin with Darapladib shows synergism

Synchronised rings (0–3 hpi) of *P. falciparum* 3D7 or ART-resistant strains were co-treated for 6 h with Dihydroartemisinin (DHA) and Darapladib in a ring stage survival assay (RSA). Artemisinin-susceptible *P. falciparum* 3D7 did not survive treatment with DHA (Figure 5.19A). Treatment with Darapladib reduced *P. falciparum* 3D7 survival in a dose-dependent manner, with about 80% survival at $1 \mu\text{M}$ Darapladib. *P. falciparum* NF54 Kelch13 C580Y had a survival rate of around 7% with DHA alone. *Pf*NF54 C580Y survival was significantly reduced to less than 1% by co-treatment with $1 \mu\text{M}$ and $2.5 \mu\text{M}$ Darapladib, respectively (Figure 5.19B and Table 5.1). Treatment with $1 \mu\text{M}$ and $2.5 \mu\text{M}$ Darapladib alone reduced parasite survival to around 80% and 60%. ART-resistant *P. falciparum* field isolate 3815

showed a survival of 7% with DHA alone. Addition of 1 μM and 2.5 μM Darapladib significantly reduced survival to 3% and 1%, respectively (Figure 5.19C). Parasite survival for 1 μM and 2.5 μM Darapladib without DHA was 95% and 85%. ART-resistant *P. falciparum* field isolate 3601 survived DHA treatment with about 29% (Figure 5.19D). Addition of Darapladib to DHA did not significantly reduce survival of *P. falciparum* field isolate 3601.

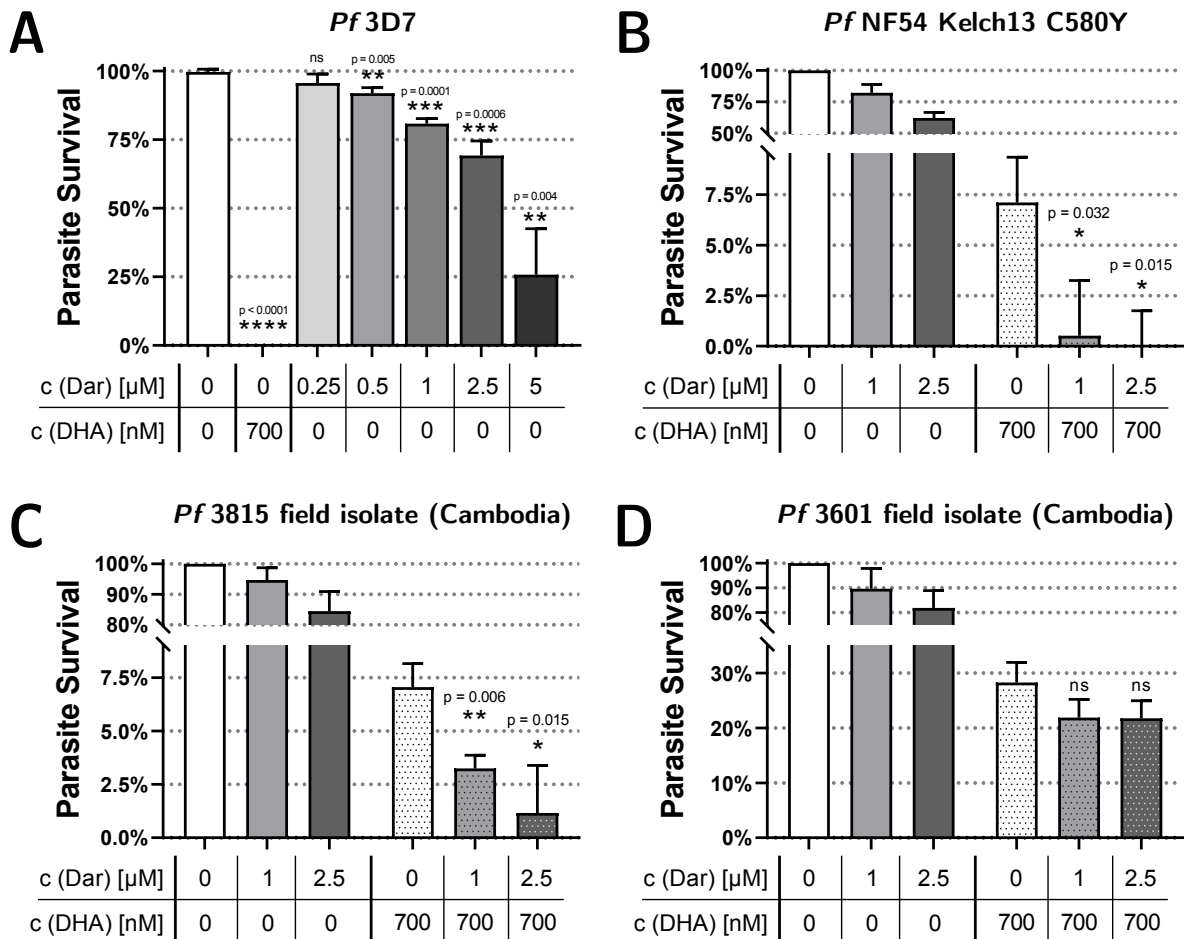


Figure 5.19: Co-treatment of ART-resistant parasites with DHA and Darapladib synergistically reduces parasite survival. (A) *Pf NF54 C580Y* had a survival rate of around 7.5% for treatment with DHA alone, which was reduced to less than 1% survival by addition of Darapladib. 1 μM and 2.5 μM Darapladib alone reduced parasite survival to 80% and 60%, respectively. (B) ART-resistant field isolate 3815 showed a survival of 7% with DHA alone, addition of 1 μM and 2.5 μM Darapladib significantly reduced survival to 3% and 1%, respectively. (C) About 29% of the *P. falciparum* field isolate 3601 survived DHA treatment. Treatment with Darapladib and DHA did not significantly reduce parasite survival. Experiments were performed with at least three biological replicates. **Abb.:** ART, Artemisinin; Dar, Darapladib; DHA, Dihydroartemisinin.

Table 5.1: Co-treatment with Darapladib and Artemisinin shows synergism. The survival rate for treatment with (A) 1 μ M or (B) 2.5 μ M Darapladib alone and 700 nM DHA alone was multiplied to calculate a theoretical survival rate if both drugs acted together exclusively additive (“Calc. Additive”). The experimentally measured survival rate for the co-treatment (“Measured”) was divided by the calculated theoretical additive survival rate. A ratio < 1 indicates synergism, a ratio = 1 an additive effect.

Table A	Parasite survival				
	Drugs Alone		Combination		Ratio
Strain	Dar 1 μ M	DHA	Calc. Additive	Measured	Calc./Measur.
NF54 C580Y	82.3 \pm 5.3%	7.1 \pm 1.8%	5.8 \pm 1.9%	0.5 \pm 2.2%	0.09 * (p=0.03)
3815	94.7 \pm 3.2%	7.1 \pm 0.9%	6.7 \pm 1.1%	3.3 \pm 0.5%	0.49 ** (p=0.008)
3601	89.6 \pm 6.7%	28.3 \pm 3.0%	25.4 \pm 4.6%	21.9 \pm 2.7%	0.89 ns

Table B	Parasite survival				
	Drugs Alone		Combination		Ratio
Strain	Dar 2.5 μ M	DHA	Calc. Additive	Measured	Calc./Measur.
NF54 C580Y	62.5 \pm 3.6%	7.1 \pm 1.8%	4.4 \pm 1.4%	0.0 \pm 1.9%	0.0 * (p=0.02)
3815	84.5 \pm 6.2%	7.1 \pm 0.9%	6.0 \pm 1.1%	1.2 \pm 1.8%	0.19 * (p=0.01)
3601	81.8 \pm 5.8%	28.3 \pm 3.0%	23.2 \pm 4.1%	21.8 \pm 2.6%	0.94 ns

To investigate, if both drugs act together in an additive or synergistic relationship, the theoretical parasite survival for an exclusively additive effect was calculated by multiplication of the survival rates for the individual drugs (“Calc. Additive”, Table 5.1). The experimentally measured survival rate for the combination of both drugs (“Measured”) was divided by the value for calculated additive survival rate. A ratio < 1 indicates synergism, a ratio = 1 an additive effect and a ratio > 1 antagonistic action. The ratios for *P. falciparum* NF54 Kelch13 C580Y and 3815 strains were significantly < 1 for 1 μ M Darapladib (Table 5.1A) and 2.5 μ M Darapladib (Table 5.1B) indicating a synergistic relationship of co-treatment with DHA and Darapladib.

6 Discussion

6.1 Context of this study

The occurrence of lipid oxidation in *Plasmodium spp.* infected RBCs and the general importance of PLA₂ enzymes in lipid oxidation repair have been reported in the literature [126,153]. Thus, a role for PLA₂ enzymes in the management of lipid oxidation repair during the *P. falciparum* blood stage is highly likely. However, the link between PLA₂-mediated lipid oxidation damage repair, and lipid oxidation during *P. falciparum* blood stage growth has not yet been investigated. Furthermore, despite comprehensive evidence for transfer of *lipids* between the host RBC and *P. falciparum*, the role of host RBC lipid *enzymes* in the context of *P. falciparum* infection has not yet been studied [129,264,266,267]. It is well established that the parasite internalises host cell cytosol to acquire hemoglobin, which is then digested. Thus, we were interested in investigating the potential role of other cytosolic host RBC proteins, which could be taken up alongside hemoglobin during host cell cytosol uptake (HCCU). The potential role of host cell enzymes in oxidative stress management during different stages of *Plasmodium spp.* has already been proposed in the literature [137,262].

Here, we provide evidence that the host RBC antioxidant PLA₂ enzyme peroxiredoxin 6 (PRDX6) is taken up by the parasite during HCCU and plays an important role during *P. falciparum* blood stage growth. We identified Darapladib as an efficient inhibitor of the PLA₂ activity of PRDX6. Treatment of *P. falciparum* with Darapladib blocks transport of host cell cytosol-containing vesicles (HcV) to the parasite food vacuole (FV) and leads ultimately to the death of the parasite. The identification of a host RBC target which is essential for *P. falciparum* blood stage growth enables the development of completely novel host-enzyme targeting drugs for malaria treatment. Targeting of host RBC enzymes would preclude the development of drug-resistant parasites, which is a major limitation of drug development strategies that target parasite enzymes and pathways.

6.2 Establishment of flow cytometric scoring of life stages by nucleic acid staining

We first established a protocol to quantify *P. falciparum* life cycle stages by flow cytometry in order to assess the effect of inhibitors on parasite development. For this, we tested three nucleic acid staining dyes: SYBR Green I, Hoechst 33342 and Ethidium Bromide (EtBr). Staining of parasites with SYBR Green I yielded the best separation of life cycle stages and allowed scoring of rings and schizont populations as well as total parasitemia (Figure 5.1). Background staining of uninfected RBCs was negligible and no lysis was observed during the staining procedure. In contrast to previous reports, neither permeabilisation of infected RBCs nor a separate washing step was necessary for efficient staining [273,292]. To validate our gating protocol, we scored three *P. falciparum* cultures in parallel by flow cytometry and examination of Giemsa-stained blood smears. The results obtained by flow cytometry and microscopy were consistent (Figure 5.3).

6.3 PLA₂ inhibitors block *P. falciparum* ring to schizont progression and blood stage growth

Using the established flow cytometric protocol, we tested the effect of several PLA₂ inhibitors on *P. falciparum* blood stage ring to schizont progression (“progression”) and completion of the full blood stage cycle with appearance of next generation ring stage parasites (“growth”). Of the tested inhibitors, the Lp-PLA₂ inhibitor Darapladib showed the highest efficacy and blocked *P. falciparum* blood stage progression and growth with an IC₅₀ of 0.56 μM and 0.76 μM, respectively (Figure 5.4). Darapladib-treated ring stage parasites did not develop beyond early trophozoite stage and appeared as pyknotic, shrunken dead parasites with little to no hemozoin visible. Treatment with arachidonyl trifluoromethyl ketone (ATK) and methoxy arachidonyl fluorophosphonate (MAFP) caused similar phenotypes and arrested parasite progression and growth, but with a significantly higher IC₅₀ than Darapladib. Neither the sPLA₂ inhibitor Varespladib, nor the PAF-AH1b2/3 inhibitor P11 had an effect on blood stage progression and growth, indicating that the action of Darapladib, ATK and MAFP was specific and that neither sPLA₂-like nor the PAF-AH1b-like enzymes are essential for blood stage growth of *P. falciparum*. Subsequent investigations were focussed on Darapladib, as it showed the lowest IC₅₀ of the tested inhibitors. MAFP was also of interest because of its irreversible covalent binding to the active site of serine hydrolases.

Darapladib, ATK and MAFP arrested parasite progression in the trophozoite stage, which is the metabolically most active stage during *Plasmodium spp.* blood stage growth. Membrane remodelling and lipid metabolism, as well as oxidative stress levels and lipid oxidation due to hemoglobin digestion reach their peak during the trophozoite stage. PLA₂ enzymes are involved in membrane remodelling as well as lipid oxidation repair [102,107,129,250]. Thus, we were interested to know whether the inhibition of PLA₂ enzymes arrested parasite progression due to inhibition of membrane remodelling and insufficient generation of lipid nutrients, or due to reduced lipid oxidation repair.

6.4 Darapladib treatment raises oxidative stress levels in *P. falciparum*

We labelled synchronous *P. falciparum* rings with the fluorescent lipid oxidation sensor BODIPY^{581/591} C11 to observe changes in lipid oxidation in blood stages. Labelled rings were treated with Darapladib, Varespladib or DMSO as control and allowed to progress to schizont stage. Treatment with Darapladib increased oxidation of BODIPY^{581/591} C11 in a dose-dependent fashion in early schizonts, but not in uninfected RBCs, rings or trophozoites (Figure 5.5). This indicates that Darapladib treatment elevates oxidative stress levels in early schizonts. Based on this observation we hypothesised that the progression arrest by treatment with Darapladib is caused by inhibition of PLA₂-mediated lipid oxidation repair which

could lead to unhindered propagation of the lipid radical chain reaction and oxidative damage. Treatment with Varespladib did not increase oxidation of BODIPY^{581/591} C11. This is consistent with the finding that parasite progression is not inhibited by Varespladib.

Oxidation of the lipid oxidation sensor BODIPY^{581/591} C11 does not quantitatively reflect increased lipid oxidation, as the sensor has been shown to be significantly more susceptible to lipid oxidation than endogenous unsaturated phospholipids [125]. However, increased oxidation of BODIPY^{581/591} C11 does serve as a marker of increased oxidative stress [125, 126]. Also, BODIPY^{581/591} C11 has been shown to rapidly shuttle between RBC and parasite membranes [126]. Thus, the oxidation status of RBCs and parasite membranes cannot be distinguished. The related sensor BODIPY^{581/591} PC, which allows selective assessment of RBCs and parasite membranes, is unfortunately not available anymore.

To validate the finding that Darapladib treatment increases oxidative stress in *P. falciparum* infected RBCs, we measured the level of the secondary lipid oxidation degradation product malondialdehyde (MDA) after treatment with Darapladib. MDA serves as an indirect readout of lipid oxidation damage and was measured using the thiobarbituric acid reactive substances (TBARS) assay [122]. Treatment with Darapladib significantly increased MDA levels in infected RBCs, but not in uninfected RBCs. These findings suggest that Darapladib increases lipid oxidation levels in *P. falciparum* infected RBCs.

6.5 Inhibition of progression and growth of *P. falciparum* blood stages by Darapladib can be restored by α -tocopherol and dioleoyl-PC

To further validate if Darapladib inhibits PLA₂ enzymes involved in oxidative stress control and detoxification of lipid oxidation damage, we tested whether parasite progression and growth can be restored by addition of exogenous α -tocopherol (vitamin E). The lipophilic radical scavenger α -tocopherol is the key antioxidant in RBCs and has been shown to confer protection against lipid oxidation by prevention and interruption of the lipid radical chain reaction [103, 127, 141]. α -tocopherol is not involved in lipid metabolism or membrane remodelling [141]. We hypothesised that if we prevent lipid oxidation damage by addition of exogenous antioxidant α -tocopherol, lipid oxidation *repair* by PLA₂ enzymes is rendered non-essential and inhibition of PLA₂ repair enzymes by Darapladib would become less important. Consequentially, co-treatment of Darapladib with α -tocopherol would restore parasite progression and growth.

As predicted, addition of α -tocopherol significantly and completely restored both Darapladib-inhibited *P. falciparum* progression and growth (Figure 5.6A). Treatment with α -tocopherol alone did not exhibit a significant effect on progression or growth. The complete restoration by

addition of antioxidant α -tocopherol indicates that Darapladib indeed targets PLA₂ enzymes which are essential for lipid oxidation repair and oxidative stress control, but not for lipid metabolism or membrane remodelling.

Only unsaturated lipids are prone to lipid oxidation [151]. Thus, we hypothesised that if Darapladib interferes in lipid oxidation repair, addition of exogeneous unsaturated, but not saturated phospholipids, could reduce the inhibitory effect of Darapladib. Hence, we tested whether mono-unsaturated dioleoyl phosphatidylcholine (DOPC, 18:1) or its saturated (disteareoyl-PC, DSPC, 18:0) and di-unsaturated analogues (linoleoyl-PC, DLPC, 18:2) restore Darapladib-inhibited progression. Indeed, DOPC, but not DSPC or DLPC, restored parasite progression in a dose-dependent manner (Figure 5.6B/C). The observation that addition of unsaturated DOPC, but not saturated DSPC, restored progression underlines that Darapladib could interfere in lipid oxidation repair, as only unsaturated lipids, but not saturated lipids would be damaged in the case of increased lipid oxidation due to Darapladib treatment. Interestingly, di-unsaturated DLPC did not restore parasite progression. This could be due to the fact that DLPC itself has an inhibitory effect on *P. falciparum* blood stage growth when administered *in vitro* [136]. DOPC is the most abundant unsaturated phospholipid in infected RBCs and is essential for *P. falciparum* growth [132,263,264]. Thus, the restoration observed with DOPC could also be due to the generally improved viability of the parasite due to availability of abundant DOPC as a lipid nutrient.

The restoration of progression and growth by α -tocopherol and DOPC suggests the Darapladib inhibits PLA₂ enzymes which are involved in lipid oxidation repair and management of oxidative stress. However, it remained completely unclear whether the main target of Darapladib is a *P. falciparum* PLA₂ or a human PLA₂ from the host RBC.

6.6 Established targets of PLA₂ inhibitors are not present in *Plasmodium spp.* and RBCs

To identify the targets for Darapladib, MAFP and ATK during *P. falciparum* blood stage growth, we first investigated whether *Plasmodium spp.* express orthologues of the established targets of these drugs. No parasite orthologues of human Lp-PLA₂, PAF-AH2, cPLA₂ or LPLA₂ were identified in *Plasmodium spp.* by *in silico* BLAST search. Recently, an in-depth computational study identified only four PLA₂ enzymes in *Plasmodium spp.*, which are classified as patatin-like phospholipases that are known to be involved in lipid oxidation repair [129,181]. Darapladib was developed as a selective inhibitor of human Lp-PLA₂ [160]. To confirm the absence of Lp-PLA₂-like enzymes in the parasite, we measured the Lp-PLA₂ specific platelet-activating factor acetylhydrolase activity in lysates of saponin-treated *P. falciparum* schizonts. No PAF-AH activity was detected, suggesting that neither human Lp-PLA₂ nor an

orthologue are present in *P. falciparum* schizonts (Figure 5.7A). This is further supported by a recent study that showed that extracellular Lp-PLA₂ is not internalised by *P. falciparum* from blood serum [288]. These findings suggest that Darapladib, MAFP and ATK may not inhibit *P. falciparum* enzymes. Although, it cannot be completely ruled out that these inhibitors target an unidentified PLA₂-like or unrelated parasite enzyme.

The established Darapladib target Lp-PLA₂ is an essential regulatory enzyme of the inflammatory lipid messenger platelet-activating factor (PAF) [102, 118]. Thus, we wondered if inhibition of PAF-mediated signalling could cause the observed phenotype of increased lipid oxidation and parasite death during blood stage progression. To test this hypothesis, we used the selective PAF receptor (PAFR) inhibitor Apafant [119]. Treatment of *P. falciparum* blood stages with Apafant had no effect on blood stage growth, indicating that PAF-mediated signalling is not essential for *P. falciparum* blood stage parasites (Figure 5.7C).

As we were unable identify suitable targets in *Plasmodium spp.*, we hypothesised that Darapladib, MAFP and ATK could target host RBC PLA₂ enzymes. A comprehensive study of the RBC proteome reported the presence of only three PLA₂ enzymes: The PAF-AH1b complex, patatin-like phospholipase domain-containing protein 6 (PNPLA6, also called neuropathy target esterase, NTE) and peroxiredoxin 6 (PRDX6) [238]. PNPLA6 has neither been shown to cleave oxidised lipids nor to be involved in lipid oxidation repair [249]. Thus, inhibition of PNPLA6 by the tested inhibitors would not explain the observed phenotype of increased lipid oxidation, which can be restored by addition of α -tocopherol. This makes PNPLA6 unlikely to be a target for Darapladib. For PAF-AH1b, we provided evidence that the selective PAF-AH1b inhibitor P11 does not inhibit *P. falciparum* blood stage growth. PAF-AH1b is a trimeric complex and thus structurally different from other PLA₂ enzymes, including the known targets of Darapladib, MAFP and ATK [168]. Thus, PAF-AH1b is unlikely to be the target of Darapladib, MAFP or ATK and is presumably not essential for blood stage growth.

The host RBC enzyme PRDX6, however, has been reported to be a dedicated lipid oxidation repair enzyme with PLA₂ activity [107, 153]. Inhibition of lipid oxidation repair by PRDX6 following Darapladib treatment could explain the observed increased oxidation of BODIPY^{581/591} C11, the growth arrest during the peak of hemoglobin digestion in trophozoite stage, and the restoration of growth with antioxidant α -tocopherol and DOPC. The active sites of both PRDX6 and Lp-PLA₂ consist of a Ser-His-Asp triad, which could explain affinity of the Lp-PLA₂ inhibitor Darapladib to PRDX6 [156]. In addition to the mechanistic similarities, the presence of this catalytic triad allows the covalent binding of MAFP to the active site serine of PRDX6. The only other known PLA₂ enzymes with a Ser-His-Asp triad are PAF-AH2 and LPLA₂, which are both not reported in the RBC, reticulocyte and erythroblast proteomes [156, 238, MOHANDAS NARLA, personal communication].

Furthermore, RBCs contain glutathione peroxidase 4 (GPx4), which is known to be involved in lipid oxidation control and to reduce lipid peroxides [137, 241]. However, GPx4 is

structurally and mechanistically different from PLA₂ enzymes as its active site contains a selenocysteine and no serine-containing catalytic triad [293]. No selective and efficient inhibitors of GPx4 have been reported so far [293]. Taken together, inhibition of GPx4 by Darapladib, MAFP or ATK is unlikely.

In summary, known targets of Darapladib, MAFP and ATK were absent in *Plasmodium spp.* and RBCs and no suitable orthologues were identified in *Plasmodium spp.* However, a promising candidate target with demonstrated PLA₂ activity was identified in the host RBC proteome, namely, human PRDX6. Thus, we explored the possibility that a host RBC PLA₂ could be the target of Darapladib, MAFP and ATK.

6.7 Pre-treatment of RBCs with MAFP suggests that a host RBC PLA₂ is essential for *P. falciparum* blood stage progression, but not invasion

In order to confirm that a host RBC PLA₂ is the target of the tested PLA₂ inhibitors during *P. falciparum* blood stage growth, uninfected RBCs were pre-treated with the irreversible, covalently-binding PLA₂ inhibitor MAFP or its reversible analogue ATK. After incubation with the inhibitors, RBCs were washed to remove unbound inhibitor and incubated with purified *P. falciparum* schizonts. Thus, the parasite was not exposed to MAFP or ATK. Pre-treatment of RBCs with MAFP or ATK did not inhibit invasion and formation of rings (Figure 5.8B). However, progression of rings to schizont stage was inhibited in a dose-dependent manner in MAFP pre-treated RBCs (Figure 5.8A/B). While parasites in DMSO-treated control RBCs developed successfully into segmented late stage schizonts, parasites in MAFP pre-treated RBCs did not develop beyond trophozoites and exhibited a shrunken, pyknotic appearance. This phenotype is very similar to the phenotype observed after continuous treatment of *P. falciparum* rings with Darapladib, MAFP or ATK (cf. Figures 5.4 and 5.8). These findings indicate that inhibition of RBC PLA₂ enzymes by MAFP blocks blood stage growth of *P. falciparum*. The IC₅₀ for inhibition of progression after pre-treatment of RBCs with MAFP is about 150 µM, which is considerably higher than the observed IC₅₀ of MAFP for continuous treatment of *P. falciparum*-infected RBCs from ring stage. This can be explained by the fact that MAFP is a lipophilic derivate of arachidonic acid with a low solubility in the aqueous phase. It is, thus, primarily present within the membrane bilayer (cf. Figure 3.7). Binding of membrane-localised MAFP to cytosolic PLA₂ enzymes, such as PRDX6, would thus be quite inefficient and mainly occur when target enzymes localise to the membrane surface. To allow covalent binding of target enzymes during the 1 h long treatment, the concentration of MAFP may need to be considerably higher than for continuous treatment. Toxic effects of treatment with high concentrations of MAFP were considered

unlikely, as pre-treatment of RBCs at similar concentrations did not inhibit merozoite invasion. Invasion of RBCs by merozoites is a tightly regulated process and relies on the integrity of the RBC membrane and its lipid composition [294]. For example, artificially increased cholesterol levels within the RBC membrane were shown to effectively inhibit *P. falciparum* merozoite invasion [294]. Merozoite invasion into pre-treated RBCs was unaffected at different concentrations of MAFP. This suggests, that MAFP-treated RBCs retain an intact plasma membrane and are viable.

To further control for non-specific toxic effects of MAFP, we pre-treated RBCs with ATK, the reversible analogue of MAFP. Both MAFP and ATK are derivatives of arachidonic acid and only differ in their head group (cf. Figure 3.7). Pre-treatment with up to 300 μM ATK did not inhibit either parasite invasion or progression supporting a specific target-directed action of MAFP and the absence of non-specific toxic effects such as altered membrane fluidity or increased permeability with these inhibitors.

The observed inhibition of *P. falciparum* progression in MAFP pre-treated RBCs supports the hypothesis that a host RBC PLA₂ enzyme could be the target for the tested PLA₂ inhibitors. More specifically, the phenotype could be explained by inhibition of host PRDX6, which was previously identified as the sole RBC PLA₂ involved in lipid oxidation repair. Thus, we tested whether Darapladib, MAFP and ATK can directly bind and inhibit PRDX6.

6.8 Darapladib, MAFP and ATK target human PRDX6

To assess the binding of Darapladib, MAFP and ATK to PRDX6, we successfully produced recombinant human PRDX6 in *E. Coli* (Figure 5.9). The production process provided yield of 12.5 mg purified human PRDX6 from 1 L bacterial culture. The identity of PRDX6 was confirmed by immunoblotting and the specific PLA₂ activity of basal and phosphorylated PRDX6 corresponded to published data (Figure 5.9). We employed activity-based protein profiling (ABPP) to investigate the binding of inhibitors to the active site of the PLA₂ activity of PRDX6. Darapladib, MAFP and ATK, but not Varespladib reduced labelling of PRDX6 with the ABPP probe TAMRA-FP, indicating competitive binding of the PLA₂ active site (Figure 5.10). Notably, Darapladib reduced the labelling of PRDX6 with an IC₅₀ of about 1 μM . MAFP prevented labelling of PRDX6 with a similar IC₅₀ as Darapladib. However, for inhibition of *P. falciparum* progression, MAFP has an about 16-fold higher IC₅₀ as compared to Darapladib (cf. Figure 5.4). The different IC₅₀ of MAFP in the ABPP binding assay and the *in vitro* progression and growth assay can be explained by the fact that MAFP is an irreversible inhibitor and forms a covalent bond with the active site serine. In fact, MAFP carries the same fluorophosphonate head group as the ABPP-probe used in the assay, TAMRA-FP. During the ABPP assay, recombinant PRDX6 was pre-incubated for 5 min with the inhibitors before addition of TAMRA-FP. Thus, MAFP presumably forms a covalent

bond to the active site serine of PRDX6 during the pre-incubation and inhibits the binding of the ABPP-probe TAMRA-FP by uncompetitive inhibition. This, however, might not reflect the binding of MAFP to PRDX6 *in vitro* where the substrate and inhibitors of PRDX6 are present at the same time and access of MAFP to PRDX6 might be limited. The observation that the sPLA₂ inhibitor Varespladib did not show binding to PRDX6 and correspondingly neither inhibited *P. falciparum* blood stage progression and growth supports the hypothesis that inhibition of PRDX6 is responsible for the growth inhibition observed with Darapladib, MAFP and ATK.

Consistent with the binding of Darapladib to the PRDX6-PLA₂ active site, Darapladib inhibited the PLA₂ activity of phosphorylated PRDX6 in a dose-dependent manner with an IC₅₀ of around 0.5 μ M (Figure 5.11). Notably, this IC₅₀ for inhibition of the PLA₂ activity of PRDX6 is very similar to the IC₅₀ for inhibition of blood stage progression and growth which provides further evidence that inhibition of the PLA₂ activity of PRDX6 is deleterious for blood stage development of *P. falciparum*. Remarkably, Darapladib is the first inhibitor shown to inhibit the PLA₂ activity of PRDX6 with an IC₅₀ in the sub-micromolar range.

In order to understand the structural basis for the interaction of Darapladib with PRDX6, we performed *in silico* docking studies. A potential binding pocket in close proximity to the active site residues was identified with a binding pose of Darapladib allowing the formation of multiple H-bonds and hydrophobic interactions (Figure 5.12). We compared the reported binding of Darapladib to its classical target Lp-PLA₂ with the binding of Darapladib to PRDX6 and identified similarities in the binding to the oxyanion hole which is essential for the stabilisation of the tetrahedral intermediate during hydrolytic de-esterification [290]. However, the distances between the residues of the catalytic site in the crystal structure of PRDX6 were found to be too large to allow efficient enzymatic activity [200]. We tried to find a conformation with closer proximity of the catalytic triad residues using dynamic simulations, but could not find such a conformation. It has been shown that phosphorylation of PRDX6 greatly enhances its PLA₂ activity. Thus, it is possible that the determined protein crystal structure of unphosphorylated PRDX6 does not accurately reflect the monomeric conformation of activated, phosphorylated PRDX6. The protein structure of phosphorylated PRDX6 has not yet been determined. Nonetheless, these *in silico* docking studies further underpin the finding that the PLA₂ activity of PRDX6 can be inhibited by Darapladib.

Taken together, we provide evidence that human PRDX6 is a target for Darapladib, MAFP and ATK. Furthermore, Darapladib inhibits the PLA₂ activity of PRDX6. In the literature, inhibition of PRDX6 was shown to result in impeded oxidative stress management and lipid oxidation repair. This in turn would explain the observed phenotype of increased oxidative stress following Darapladib treatment and the restoration of progression and growth by addition of exogenous α -tocopherol. These observations support the hypothesis that host RBC PRDX6 is essential for blood stage growth of *P. falciparum*.

6.9 Role of host PRDX6 in a rodent malaria model using PRDX6^{-/-} mice

Mature RBCs are unique cells, as they lose their nucleus, ribosomes and protein translation machinery during erythropoiesis [295]. Thus, all proteins present in mature RBCs have been translated in erythropoietic progenitor cells before the loss of the translation machinery in reticulocytes [295]. This means in turn that mature RBCs themselves cannot be genetically altered.

6.9.1 Available approaches for genetic studies in RBCs

Three systems are available to perform molecular genetic studies on RBCs: Firstly, naturally occurring polymorphisms of the gene of interest expressed in RBCs in human populations can be used to observe differences in phenotypes associated with specific polymorphisms to understand the function of the gene. Secondly, it is possible to manipulate genes in erythroid progenitor cells and study the phenotypes of RBCs derived from them. Thirdly, one can study transgenic knockout animal models to study the functional roles of genes in RBC biology.

Polymorphisms of PRDX6 in human populations are rare and individuals with a PRDX6^{-/-} genotype are not reported. The approach to study genetic polymorphisms in PRDX6 in humans to understand its function in RBCs was thus not feasible.

Genetically altered, nucleated RBCs can be obtained by genetic manipulation of erythroid progenitor cells via CRISPR/Cas9 followed by directed differentiation and enrichment of transgenic RBCs [296]. For example, the immortalised JK-1 erythroleukemia cell line has been shown to spontaneously differentiate into a sub-cell type resembling young, nucleated RBCs (called jkRBCs by the authors), which can be enriched by a Percoll gradient [296]. While jkRBCs allow effective invasion of *P. falciparum* merozoites, further development of invaded parasites into trophozoites and schizonts is impaired with only occasional observation of parasites beyond ring stage [296]. Recently, a second immortalised erythroid progenitor cell line, called EJ, was shown to differentiate into nucleated RBCs and to be amenable for CRISPR/Cas9 knockout of target genes [297]. Similar to jkRBCs, EJ-derived nucleated RBCs were shown to be readily invaded by *P. falciparum* and *P. vivax* merozoites, but invaded ring stage parasites did not develop into trophozoites or schizonts [297]. For the matter of this study, the phenotype of hypothetical PRDX6 inhibition by Darapladib, MAFP and ATK blocks progression from trophozoite to schizont stages. As neither of the two erythroid progenitor cell derived nucleated RBCs supports effective development of *P. falciparum* beyond ring stage, the use of this approach for our study is unfortunately limited.

Thus, the only other option available to us was the use of transgenic PRDX6^{-/-} mice in a rodent malaria model. PRDX6^{-/-} mice have been successfully generated in the lab of

Table 6.1: Host cell tropism of different human and rodent malaria species and strains. The host cell preference of different malaria species and strains for mature RBCs (mRBC) or reticulocytes (Retic.), as well the respective duration of the blood stage life cycle is shown [309,311].

Species	Strain	Host	Host cell preference	Blood stage cycle
<i>P. falciparum</i>	3D7	Human	mRBCs	46–48 h
<i>P. berghei</i>	ANKA	Rodent	Retic., also infects mRBCs	22–24 h
<i>P. yoelii</i>	17X-NL	Rodent	Retic.	18 h
<i>P. yoelii</i>	17XL / YM	Rodent	mRBCs and Retic.	18 h

PROF. ARON B. FISHER, University of Pennsylvania, and are viable, but show reduced male fertility and a generally increased susceptibility to oxidative stress (overview in Section 3.6.5) [226, 229]. However, the use of PRDX6^{-/-} mice in a rodent malaria model has three major limitations and shortcomings.

Firstly, murine and human RBCs are significantly different in multiple aspects: Human RBCs are about twice as large as murine RBCs, have a roughly three times longer life span than mice RBCs and show a higher affinity to oxygen [295, 298, 299]. While mice can *de novo* synthesise antioxidant ascorbic acid (vitamin C), humans have lost the ability to synthesise ascorbic acid about 20–25 million years ago [300]. Accordingly, the glucose transporter protein GLUT1, which has been shown to also transport dehydroascorbic acid into RBCs, is highly abundant in human RBCs, but not found in murine RBCs [301, 302]. Furthermore, human and murine RBCs exhibit differences in ion-transport, signalling pathways and regulation of erythropoiesis [303–306].

Secondly, despite a remarkable similarity between human and rodent-infecting malaria parasites, multiple biological processes have been shown to be fundamentally different [307, 308]. While the lipid enzyme phosphoethanolamine-N-methyltransferase (PMT) has been shown to be crucial for the sexual blood stage in human-infecting *P. falciparum*, the corresponding gene has been lost in rodent malaria parasites, such as *P. berghei* and *P. yoelii* [266, 307]. Furthermore, host cell tropism of malaria parasites, which refers to the ability to infect mature RBCs and/or reticulocytes, also varies greatly between *Plasmodium* species and strains as shown in Table 6.1. For example, *P. falciparum* exclusively infects mature RBCs, while the rodent malaria strain *P. berghei* ANKA shows a preference for reticulocytes, but can infect mature RBCs as well [309, 310]. The duration of the blood stage cycle is also different between human and rodent malaria species: The blood stage cycle of *P. falciparum* and *P. vivax* is around 48 h and 72 h for *P. malariae*. Contrastingly, all rodent-infecting *Plasmodium* species have a cycle length of less than 24 h (Table 6.1) [309, 311].

Thirdly, PRDX6^{-/-} mice have been shown to compensate the loss of PRDX6 with increased expression of other antioxidant enzymes and higher glutathione levels [291]. In a study on

dextran sodium sulphate (DSS)-induced colitis in PRDX6^{-/-} mice, the authors hypothesised that PRDX6 should have a protective role during intestinal inflammation and PRDX6^{-/-} mice therefore should be more susceptible to colitis-induced oxidative stress during inflammation [291]. Surprisingly, the study found that knockout of PRDX6 confers protection against colitis and inflammation. When challenged with DSS, PRDX6^{-/-} mice showed a significantly increased expression of antioxidant enzymes such as PRDX3, PRDX4, Nuclear factor erythroid 2-related factor 2 (NRF2), glutathione synthetase (GSS) on both the mRNA and protein level and had overall higher glutathione levels than WT mice [291]. Increased expression of PRDX3 and PRDX4 in PRDX6^{-/-} mice was also reported for a hepatic ischaemia/re-perfusion injury model and in the cigarette smoke-mediated lung inflammatory response [312, 313]. Thus, PRDX6^{-/-} mice cannot be viewed as “wild-type mice without PRDX6” and it remains unclear if observed phenotypes in PRDX6^{-/-} mice are due to the knockout of PRDX6, or due to compensatory responses leading to increased expression of complementary antioxidant enzymes.

Summed up, the available models to validate the importance of host RBC PRDX6 for blood stage growth using genetic approaches are limited. Genetically altered erythroid progenitor-derived nucleated RBCs do not support complete intraerythrocytic growth which would be essential to investigate the role of PRDX6 during trophozoite stage. Thus, we did not employ this approach. The only available option for us was to use PRDX6^{-/-} mice in a rodent malaria model. Infection of PRDX6^{-/-} mice with rodent malaria species, such as *P. berghei* and *P. yoelii*, has not been investigated, yet. Despite the caveats of this model as described above, we decided to test growth of rodent malaria strains *P. berghei* ANKA and *P. yoelii* YM in PRDX6^{-/-} mice.

6.9.2 *In vivo* growth and *ex vivo* progression in rodent malaria models

Blood stage *P. berghei* ANKA and *P. yoelii* YM infected mouse RBCs were used to infect PRDX6^{-/-} and WT mice by intravenous transfer and parasite growth was monitored by flow cytometry. Growth of *P. berghei* ANKA was not significantly different in PRDX6^{-/-} and WT mice (Figure 5.13A). As *P. berghei* ANKA preferably invades reticulocytes, we also assessed the growth of *P. yoelii* YM, which primarily infects mature RBCs. Growth of *P. yoelii* YM was also not significantly different between RBCs from PRDX6^{-/-} and WT mice (Figure 5.13B). Due to the biological differences between mouse and human RBCs (e.g. size and ascorbic acid metabolism) and between human and rodent-infecting *Plasmodium* species (e.g. blood stage cycle duration), the unaffected growth of *P. berghei* and *P. yoelii* in PRDX6^{-/-} mice does not rule out a role for PRDX6 in the growth of *P. falciparum* in human RBCs. Additionally, PRDX6^{-/-} mice have been shown to compensate the loss of PRDX6 with an increased expression of complementary antioxidant enzymes and glutathione, especially

when challenged with increased oxidative stress. This could explain why PRDX6 is not essential for growth of *P. berghei* and *P. yoelii* in PRDX6^{-/-} mice.

We hypothesised that if Darapladib specifically inhibits PRDX6, the loss of PRDX6 in PRDX6^{-/-} mice should lead to a reduced efficacy of Darapladib for inhibition of progression. As Darapladib has a very low bioavailability, it is not possible to reach sufficient concentrations in blood plasma *in vivo* in WT and PRDX6^{-/-} mice [162]. Thus, we assessed the effect of Darapladib on the *ex vivo* ring to schizont progression of *P. yoelii* YM infected PRDX6^{-/-} and WT RBCs (Figure 5.13C) [285]. The *ex vivo* IC₅₀ of Darapladib for *P. yoelii* progression in WT RBCs is 0.75 μM and similar to the IC₅₀ observed *in vitro* for *P. falciparum* of 0.76 μM, suggesting a similar affinity of Darapladib to mouse and human PRDX6. Interestingly, Darapladib also inhibited *ex vivo* progression of *P. yoelii* in PRDX6^{-/-} RBCs, but with a significantly higher IC₅₀ of 3.4 μM compared to WT RBCs. In the absence of PRDX6, 1 μM Darapladib had no effect on progression in PRDX6^{-/-} mice. This suggests that PRDX6 is a specific target of Darapladib. However, Darapladib also inhibited progression in PRDX6^{-/-} RBCs at higher concentrations, suggesting that Darapladib can also target the compensatory mechanisms that allow parasite progression in absence of PRDX6 in PRDX6^{-/-} RBCs. However, higher concentrations of Darapladib are required to target these compensatory enzymes compared to PRDX6. Furthermore, these compensatory mechanisms do not appear to be active in WT RBCs, as Darapladib efficiently blocks progression below 1 μM in WT RBCs. The observation that the deletion of PRDX6 in the host RBC changes the IC₅₀ for progression inhibition by Darapladib further underpins the hypothesis that the target of Darapladib is indeed a host enzyme, and not primarily a parasite enzyme.

Taken together, the use of PRDX6^{-/-} mice in a rodent malaria model is ambiguous as it does not entirely reflect *P. falciparum* infection in humans. In particular, the reported compensatory upregulation of antioxidant enzymes in PRDX6^{-/-} mice limits the relevance of this model to study the specific role of PRDX6 [291]. *In vivo* growth of *P. berghei* ANKA and *P. yoelii* YM was not different between PRDX6^{-/-} and WT mice. On the other hand, Darapladib showed a significantly reduced efficacy for *ex vivo* progression inhibition in PRDX6^{-/-} RBCs as compared to WT RBCs. This supports our hypothesis that host PRDX6 is a specific target of Darapladib and essential for blood stage progression of *P. falciparum* in human RBCs. To understand the potential role of PRDX6 in blood stage growth, we investigated the localisation of PRDX6 in *P. falciparum* infected RBCs.

6.10 PRDX6 is internalised by *P. falciparum* and co-localises with host cell cytosol-containing vesicles

In 2009, KONCAREVIC ET AL. reported that *P. falciparum* internalises host RBC PRDX2 by an unknown mechanism [262]. Human PRDX2 is involved in the detoxification of small molecule ROS like H₂O₂ and was shown to localise to the parasite cytosol [138,262]. We hypothesised that PRDX6 could be internalised by *P. falciparum* in a similar manner. To study internalisation of PRDX6, we selectively lysed the RBC membrane (RBCM) with saponin, without affecting the integrity of the parasitophorous vacuolar membrane (PVM) or the parasite membrane (PM) [314]. Thus, PRDX6 internalised by the parasite would be detectable in the cytosol of saponin-treated parasites. Indeed, PRDX6 was detected in lysates of both untreated and saponin-treated schizonts by immunoblotting (Figure 5.14A/B). This clearly indicated that PRDX6 is internalised by the parasite. We used hemoglobin as a control for complete removal of the RBC cytosol from saponin-treated samples. Hemoglobin was not detected in saponin-treated schizonts, confirming complete lysis of the RBCM. However, *P. falciparum* internalises hemoglobin during HCCU and was furthermore shown to synthesize hemoglobin itself [315,316]. The absence of a band for hemoglobin in saponin-treated schizonts could be explained by the much higher abundance of hemoglobin in the RBC cytosol as compared to the parasite [315].

Having established that PRDX6 is internalised by *P. falciparum*, we investigated the cellular localisation of human PRDX6 within infected RBCs by immuno-fluorescence microscopy. We found that PRDX6 localises to vesicle-like structures with multiple foci around the hemozoin-containing FV (Figure 5.14C). This suggested that PRDX6 is internalised via an endocytotic pathway like HCCU. The RBC cytosol in infected RBCs showed a generally reduced staining for PRDX6 as compared to uninfected RBCs. This is consistent with the observation that the RBC membrane is highly permeabilised in infected RBCs, ultimately leading to loss of RBC cytosol proteins through diffusion [33,34]. The loss of PRDX6 from the RBC cytosol was also observed during storage of preserved RBCs [317]. Furthermore, host RBC cytosol is digested by the parasite to create space for the intracellular development of the parasite [34].

To validate the vesicular localisation and investigation of a possible endocytotic pathway, we examined infected RBCs by immuno-electron microscopy. PRDX6 was found to localise to host cell cytosol-containing vesicles (HcV) within the parasite (Figure 5.15). Notably, nascent vesicles, which were still connected to the RBC cytosol, were identified and found to contain a higher concentration of PRDX6 as compared to the RBC cytosol, indicating that PRDX6 may be selectively loaded into HcVs during HCCU (Figure 5.15 A4). PRDX6-containing HcVs were also observed simultaneously at the PVM and FV surface in the same cells, suggesting that after internalisation of PRDX6 at the PVM surface, PRDX6 is transported to the FV

within HcVs (Figure 5.15 A,B and D). PRDX6-containing HcVs were also observed within the FV lumen at the inner surface of the FV membrane (Figure 5.15 A and D). Non-vesicular PRDX6 was not detected within the FV lumen, suggesting that PRDX6 is immediately digested after the release of HcVs into the FV lumen.

Summed up, the immuno-electron microscopy images clearly indicated that host RBC PRDX6 is taken up alongside hemoglobin during HCCU and transported to the parasite FV within HcVs. We hypothesised that if PRDX6 plays an important role for antioxidant protection within HcVs, inhibition by Darapladib might interfere either in HCCU or transport of HcVs to the FV.

6.11 Darapladib blocks HcV transport and delivery of hemoglobin to the FV

We investigated the putative role of PRDX6 in HcV transport in *P. falciparum* blood stage parasites using the protease inhibitor E64 and Darapladib. E64 blocks hemoglobin digestion within the FV which leads to the accumulation of undigested hemoglobin in the FV and swelling of the FV [51]. However, if HcV – and thus hemoglobin – transport to the FV is disrupted by Darapladib treatment, hemoglobin cannot accumulate in the FV precluding the swelling of the FV due to E64. We examined parasites both by electron and light microscopy. As expected, treatment with E64 resulted in large, swollen FVs filled with electron dense hemoglobin (Figure 5.16). Interestingly, treatment with Darapladib completely precluded the swelling of the FV, indicating that Darapladib acts upstream of E64 by disrupting transport of hemoglobin to the FV. The cytosol of parasites treated with Darapladib, or Darapladib and E64 both contained multiple dark-coloured HcVs, which are not found in untreated parasites. Hemoglobin did not accumulate in the FV upon co-treatment with E64 and Darapladib indicating that hemoglobin does not reach the FV in parasites treated with Darapladib. The observed phenotype of accumulated HcVs within the parasite cytosol shows striking similarities to the phenotype described in a recent report by JONSCHER ET AL. where the deletion of *PfVPS45* interrupted hemoglobin transport and arrest of HcVs in the cytosol of *P. falciparum* parasites [50]. In their study, the authors specified translucent structures observed in Giemsa-stained blood smears as arrested, hemoglobin-filled vesicles. Similar translucent structures were visible in Giemsa-stained blood smears of Darapladib-treated parasites suggesting the presence of arrested HcVs in the cytosol after treatment with Darapladib (Figure 5.16).

The disruption of host cell cytosol transport to the FV was confirmed using the pH sensitive, cell-impermeant fluorescent probe LysoSensor Blue/Yellow 10kDa dextran. To study vesicular transport in *P. falciparum* infected RBCs, we preloaded RBCs with LysoSensor Blue/Yellow

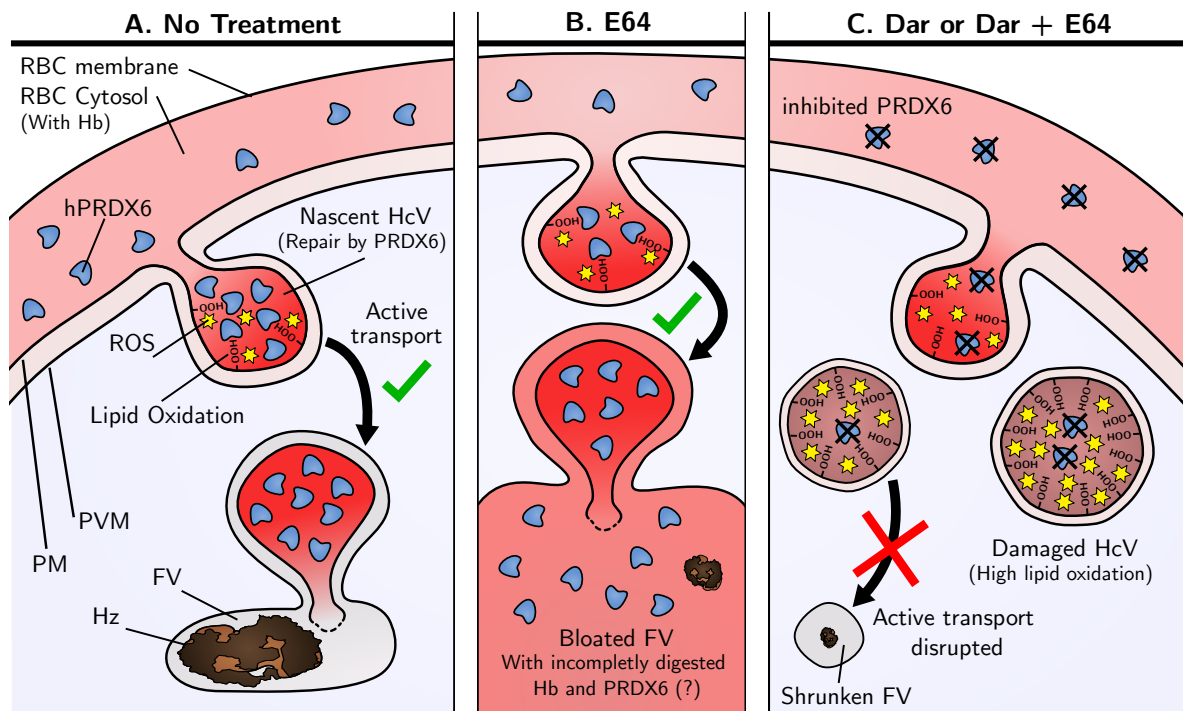


Figure 6.1: Model for Darapladib-inhibited host cell cytosol uptake in *P. falciparum*. (A) Human PRDX6 is internalised alongside hemoglobin (Hb) in host cell cytosol-containing vesicles (HcV). The increased density of hemoglobin in HcVs leads to elevated oxidative stress levels causing membrane damage. PRDX6 is crucial for the repair of vesicular membranes to assure membrane integrity and successful active transport. Without inhibition of PRDX6, the active transport is functional and HcVs are delivered to the FV. Hb is digested and detoxified into hemozoin crystals in the FV. (B) Upon treatment with E64, digestion of Hb is inhibited leading to the accumulation of Hb and swelling of the FV. (C) Inhibition of PRDX6 by Darapladib prevents the detoxification and repair of oxidised HcV membranes leading to the disruption of active transport of HcVs to the FV. Thus, no hemoglobin is delivered to the FV and the FV appears shrunken and contains little to no hemozoin. **Abb.:** *Dar*, Darapladib; *FV*, food vacuole; *Hb*, Hemoglobin; *HcV*, host cell cytosol-containing vesicle; *Hz*, Hemozoin; *PM*, parasite membrane; *PVM*, parasitophorous vacuole membrane; *RBC*, red blood cell; *ROS*, reactive oxygen species.

and subsequently allowed invasion by *P. falciparum* merozoites. DMSO-treated *P. falciparum* infected RBCs successfully internalised the probe from the host RBC cytosol and transported it to their acidic FV, yielding a strong yellow signal from the probe within the FV. Treatment of *P. falciparum* infected pre-loaded RBCs with Darapladib, however, greatly reduced the yellow signal in the parasite indicating the disruption of transport of host cell cytosol to the acidic FV (Figure 5.17). Another line of evidence that Darapladib inhibits hemoglobin transport was provided by the observation that Darapladib significantly reduced the size of hemozoin crystals in the FV (Figure 5.18).

Based on these findings, we formulated a hypothetical model for the role of PRDX6 and Darapladib in HCCU and transport of HcVs (Figure 6.1): During HCCU, host RBC PRDX6 is internalised alongside hemoglobin in HcVs. The increased density of oxidant hemoglobin

in HcVs leads to an increase of oxidative damage, ROS production and lipid oxidation. Internalised PRDX6 plays an important role in the repair of oxidised vesicle membranes and detoxification of ROS in HcVs. After budding off, HcVs are transported to the FV via an active transport machinery, potentially involving actin, dynamin, phosphatidylinositol 3-kinases (PI3K) and SNARE proteins [51–54]. PRDX6 protects the integrity of the HcV membrane and enables active transport of HcVs to the FV (Figure 6.1A). Ultimately, HcVs fuse with the FV and release their contents into the FV lumen where hemoglobin and other proteins such as PRDX6 are digested by proteases [36]. Free heme is detoxified by crystallisation into hemozoin in the FV. Upon treatment with E64, HcV transport to the FV is functional (Figure 6.1B). However, the inhibition of FV proteases by E64 leads to accumulation of host cell cytosolic proteins and swelling of the FV. In contrast, upon treatment with Darapladib, the repair of HcV membranes and detoxification of ROS within HcVs by PRDX6 is inhibited (Figure 6.1C). This leads to extensive oxidative damage and disruption of active transport of HcVs to the FV. Consequentially, HcVs accumulate in the parasite cytosol. As hemoglobin is not successfully delivered to the FV, the FV remains small and shrunken with little or no visible hemozoin. The disruption of HcV transport by inhibition of PRDX6 ultimately leads to the death of the parasite. The observed phenotype of the co-treatment with Darapladib and E64 is similar to the phenotype of treatment with Darapladib alone. This suggests that Darapladib acts upstream of E64, as disruption of hemoglobin transport by Darapladib prevented the E64-mediated accumulation of undigested hemoglobin in the FV.

Taken together our data suggests that host RBC PRDX6 serves as a kind of "transport protection" for HcVs, which are especially prone to oxidative damage due to the increased density of hemoglobin. Darapladib, as an inhibitor of the PLA₂ activity of PRDX6, prevents the lipid oxidation repair and oxidative stress relief in HcVs, leading to the disruption of the active transport of HcVs. As a result, hemoglobin-filled HcVs accumulate in the parasite cytosol and hemoglobin is not delivered to the FV. This is in line with the finding that Darapladib-treated parasites die during trophozoite stage, where HCCU and HcV transport are the key active processes for parasite development. Disruption of HcV transport by Darapladib treatment blocks blood stage parasite development and growth.

6.12 Reversal of Artemisinin resistance by co-treatment with Darapladib

As discussed in section 3.3.3, hemoglobin uptake and digestion is crucial for the activation of the current state-of-the-art antimalarial drug Artemisinin. Resistance against Artemisinin has been linked to reduced hemoglobin uptake in early ring stage leading to a decrease in heme-induced oxidative stress and thereby impairing the activation of Artemisinin [45].

For example, ART-resistance in *P. falciparum* NF54 C580Y is caused by impaired HCCU in ring stages due to the C580Y mutation in the β -propeller of Kelch13 (K13), a protein directly involved in ring stage HCCU complex formation [43,98]. The mutation is also found in the ART-resistant *P. falciparum* field isolate 3815 (JEAN-CHRISTOPHE BARALE, personal communication). Our findings suggested that Darapladib interrupts the transport of hemoglobin to the FV and interferes in the detoxification of oxidative stress by inhibition of the PLA₂ activity of PRDX6. Thus, we explored whether co-treatment of ART-resistant parasite strains with a Darapladib-Artemisinin combination could reduce parasite survival in a ring stage survival assay (RSA).

Co-treatment of Darapladib and Artemisinin significantly and synergistically reduced survival of the *P. falciparum* ART-resistant strains NF54 C580Y and 3815. The measured parasite survival for both NF54 C580Y and 3815 for co-treatment was significantly lower than the calculated theoretical survival rate in case of a purely additive drug interaction [318]. Both NF54 C580Y and 3815 contain the K13 C580Y mutation, suggesting that for this mutation, Darapladib reverses Artemisinin-resistance and shows synergistic inhibition of parasite growth. However, Darapladib did not significantly reduce survival of the highly ART-resistant *P. falciparum* strain 3601. In contrast to NF54 C580Y and 3815 strains, ART-resistance of 3601 is linked to the K13 R539T mutation, which confers a higher level of parasite survival than the C580Y mutation [98,319, DIDIER MÉNARD, personal communication]. It remains unclear if Darapladib failed to reduce survival of *P. falciparum* 3601 due to the K13 R539T mutation, or if other ART-resistance mechanisms could play a role in *P. falciparum* 3601.

We will assess whether Darapladib blocks progression of the ART-resistant strains in continuous treatment and predict that Darapladib would effectively kill ART-resistant parasite strains when administered continuously during the blood stage growth, as ART-resistance is only observed in early ring stages and the effect of K13 mutations seems to be limited to reducing HCCU during early ring stage. This remains to be tested experimentally.

The finding that Darapladib can restore ART-susceptibility and significantly decrease parasite survival could have significant implications as Artemisinin-resistance is one of the major threats in the control of malaria. An Artemisinin-based combination therapy (ACT) with a PRDX6-targeting partner drug would be effective in two ways: Firstly, it could help to restore ART-susceptibility during early ring stage and secondly inhibition of PRDX6 should block parasite blood stage growth of ART-resistant strains of *P. falciparum* by impeding HcV transport during trophozoite stage.

6.13 Summary

Previously, the role of PLA₂ enzymes during blood stage of *P. falciparum* was unclear in the literature. Here, we have provided evidence that the host RBC enzyme PRDX6 is essential for *P. falciparum* blood stage growth. Human PRDX6 is internalised by the parasite alongside hemoglobin during HCCU and was found to localise to HcVs. To our knowledge, PRDX6 is the first host enzyme shown to play an important role within HcVs. An effective inhibitor of PRDX6, Darapladib, was identified and disrupted transport of HcVs to the FV, suggesting that PRDX6 could play a pivotal role in maintaining membrane integrity to allow active vesicular transport. Furthermore, Darapladib significantly reduced survival of ART-resistant parasites in a co-treatment with Artemisinin. Combined with the finding that Darapladib raises oxidative stress in *P. falciparum* infected RBCs, we demonstrate that Darapladib treatment restores ART-susceptibility.

The identification of a host RBC target which is essential for *P. falciparum* blood stage growth allows the development of completely novel strategies for pharmacological treatment and control of malaria. Targeting of host RBC enzymes would have the great advantage, that parasites cannot attain resistance by mutation of target genes.

6.14 Outlook and outstanding questions

In this study, we have discovered the important role of host PRDX6 in blood stage growth of *P. falciparum*. This finding has opened up new questions which remain to be addressed in further studies. The following section discusses several approaches and methods to investigate these outstanding questions.

We have provided evidence that active transport of HcVs to the FV can be disrupted by treatment with Darapladib. However, the molecular mechanisms for this disruption are not understood. For example, it remains unclear whether PRDX6 inhibition leads to an increase of lipid oxidation and oxidative stress within HcVs and whether this could cause damage to the active transport machinery. To study the changes caused by Darapladib treatment, the oxidative environment in HcVs will be investigated using small molecular or fluorescent protein-based ROS sensors, such as roGFP, combined with super-resolution microscopy before and after treatment with Darapladib [320, 321]. Furthermore, oxidative damage of proteins involved in HcV transport will be investigated by redox proteomics, which allows to specifically assess oxidative modifications in the proteome of interest [322].

In this study, we used transgenic PRDX6^{-/-} mice in a rodent malaria model to confirm our inhibitor-based results. Unfortunately, this approach was found to give ambiguous results as the complete loss of PRDX6 causes compensatory expression of antioxidant enzymes in PRDX6^{-/-} mice [291]. As an alternative, transgenic mice expressing PRDX6 with the D140A mutation could be used. The PRDX6 D140A mutation selectively abolishes PLA₂ activity,

but does not affect the peroxidase activity of PRDX6 [153]. Mice expressing PRDX6 D140A have been generated in the lab of PROF. ARON B. FISHER, University of Pennsylvania [229]. The selective inactivation of the PLA₂ activity may not induce compensatory expression of antioxidant enzymes in PRDX6 D140A mice, as compared to PRDX6^{-/-} mice. Thus, PRDX6 D140A-expressing transgenic mice may serve as a better model to study the effect of abolished PLA₂ activity of PRDX6 on the growth of *P. berghei* and *P. yoelii*.

We identified Darapladib as a potent inhibitor of the PLA₂ activity of PRDX6. We demonstrated that Darapladib binds recombinant human PRDX6 in an ABPP assay and provided evidence that Darapladib inhibits the PLA₂ activity of PRDX6. Moreover, treatment of *P. falciparum* infected RBCs with Darapladib inhibits the progression of *P. falciparum* from ring to schizont stage and blocks blood stage parasite growth. However, the binding of Darapladib to PRDX6 in *P. falciparum* infected RBCs has not yet been directly demonstrated. We also do not know if Darapladib binds other targets. We will use mass spectrometry-based cellular thermal shift assay (CETSA) to confirm PRDX6 as a target for Darapladib in *P. falciparum* infected RBCs. In addition, with CETSA, we could also identify possible additional targets of Darapladib in the RBC or *P. falciparum*.

Despite our finding that Darapladib inhibits the PLA₂ activity of PRDX6 with an IC₅₀ in the sub-micromolar range, Darapladib has multiple shortcomings as a drug for the PLA₂ activity of PRDX6. Originally, Darapladib was developed as a selective inhibitor of *extracellular* human Lp-PLA₂ [160]. Thus, drug permeability and bioavailability were only of minor concern in the development of Darapladib. However, as human PRDX6 is an *intracellular* target, improved bioavailability, permeability and target affinity are crucial for pharmacologically active PRDX6 inhibitors. Therefore, the chemical scaffold of Darapladib does not serve as a good basis to develop improved inhibitors of the PRDX6-PLA₂ activity. Improved PRDX6 inhibitors are needed to further investigate the role of PRDX6 in *P. falciparum* blood stage growth. To develop such inhibitors, we will identify drug candidates using *in silico* identification of hits with novel scaffolds, which will be further investigated by high-throughput screening of small molecule libraries based on predicted hits and subsequent *in vitro* and *in vivo* validation of hits. Identified lead compounds will be further optimised using medicinal chemistry.

It was not possible to confirm the essentiality of host RBC PRDX6 for *P. berghei* and *P. yoelii* blood stage growth in PRDX6^{-/-} mice. The development of novel, specific, and highly active PRDX6 inhibitors with nanomolar IC₅₀ in parasite growth assays could help to validate PRDX6 as an essential enzyme for blood stage growth of *P. falciparum*. Furthermore, development of pharmacologically improved PRDX6 inhibitors could open up new approaches for development of antimalarials that target host enzymes, which would preclude the development of drug resistant parasites. Moreover, selective inhibition of host PRDX6 could also help overcome emerging drug resistance against Artemisinin-based therapies.

An efficient selective PRDX6 inhibitor may also find application for treatment of other diseases, such as cancer, where PRDX6 plays a role. Cancerous tumour cells show an increased production of ROS due to their elevated metabolism [217, 223]. As described earlier, PRDX6 plays a role in ROS detoxification and antioxidant protection and is therefore thought to play an important role in redox metabolism of cancer cells [138, 153]. Indeed, overexpression of PRDX6 promotes cancer cell proliferation and migration in various types of cancer, including cancer of the breast, lung, colorectal, gastric, ovarian, tongue, oesophagus, bladder, liver, gingiva, skin and mesothelium (cf. Section 3.6.4) [153, 217–222]. Accordingly, inhibition and knockdown of PRDX6 has been shown to be deleterious for carcinogenesis of multiple cancer types [217, 219, 220]. Thus, PRDX6 is a potential target for treatment of cancer. Treatment with novel selective PRDX6 inhibitors could reduce cancer cell proliferation and migration and serve as valuable tool in cancer treatment and chemotherapy.

7 Acknowledgements

Acknowledgements

First of all, I would like to thank Chetan Chitnis for his tremendous support and guidance since my first internship with him in 2016. I am very grateful for the excellent supervision during the last five years which helped me to grow both professionally and personally, encouraged me to follow my scientific instincts, and also provided me with focus and well-dosed reminders to not get lost during the journey. Thank you for your trust in me!

A special thanks goes to the whole BPV group for all the help and support since five years. Thanks for making the frustrating results less heartbreaking and for celebrating the good results so heartfully. Namely: Micheline, Dipto, Francisco, Christèle, Neele, Aditi, Pallavi, Kunal and Maryse.

I would like to thank Isabelle Tardieux, Caroline Demangel, Yves Colin-Aronovicz, Tim Gilberger and Kai Wengelnik for being part of my PhD jury.

I am grateful to the PPU program, especially Susanna Celli and Simonetta Gribaldo, for the assistance at every stage of the PhD. Furthermore, thanks to the Fondation pour la Recherche Médicale for financial support of the project.

I would like to thank Aron B. Fisher and Sheldon Feinstein for sending the PRDX6 KO mice and for their advice and help with the PRDX6 activity assays.

I would like to express my sincere gratitude to Pauline Formaglio and Rogerio Amino for the tremendous help with the mouse infection experiments.

I am very glad for the constant support of Lhousseine Touqui in numerous discussions about the complex field of PLA₂ enzymes and for the help with PLA₂ assays. Merci beaucoup!

I would like to offer my special thanks to Didier Ménard, Lucien Platon, Jean-Christophe Barale and Melissa Mairet-Khedim for the Artemisinin resistant parasite strains and help with the ring stage survival assays.

I would like to extend my sincere thanks to Olivier Gorgette, who performed the electron microscopy experiments and took the fascinating pictures of the PRDX6-filled vesicles, and to Olivier Sperandio and Luis Checa Ruano for the detailed and sophisticated *in silico* docking studies.

I am grateful to Gordon Langsley for many fruitful discussions and valuable advices.

A big thanks to H el ene Spangenberg for the valuable help with vesicular assays and the friendship since when we were tiny little biochemical students.

Dankesch on, Eva for proofreading my thesis and for the constant support from anywhere in the world.

Thanks to the Aunty/Uncle *x's y* club members Emilia, Lukas, Adriana, Marta and B er enice for going on this PhD-ride with me and supporting me during the whole journey!

Je voudrais exprimer mes remerciements de ouf   mon fellow Caramel Son and Jugaad Guruji Abhishek. This thesis will always be connected to the countless evenings we spent together jamming and recording our musical dreams.

A huge thanks goes to Alexandra for her invaluable support during the thesis: for her unconditional trust, for having my back in moments of despair and for her wholehearted honesty. Thank you for being the person you are and for helping me to become the person I want to be.

I am especially grateful to my parents for their unlimited support in all my decisions, their guidance, their trust in me finding my own way and for always being there for me. Danke, Mama und Papa!

8 Bibliography

Bibliography

- [1] J. S. Richards and J. G. Beeson. The future for blood-stage vaccines against malaria. *Immunol. Cell Biol.*, 87(5):377–390, Jul 2009. [Cited on page 13]
- [2] World Health Organization. World malaria report 2020. <https://www.who.int/publications/i/item/9789240015791>, 2020. [Online; Accessed 22.01.2021]. [Cited on page 13]
- [3] E. Worrall, S. Basu, and K. Hanson. Is malaria a disease of poverty? A review of the literature. *Trop. Med. Int. Health*, 10(10):1047–1059, Oct 2005. [Cited on page 13]
- [4] L. H. Miller, D. I. Baruch, K. Marsh, and O. K. Doumbo. The pathogenic basis of malaria. *Nature*, 415(6872):673–679, Feb 2002. [Cited on page 13]
- [5] S. Sinha, B. Medhi, and R. Sehgal. Challenges of drug-resistant malaria. *Parasite*, 21:61, 2014. [Cited on page 13]
- [6] F. Seeber and S. Steinfelder. Recent advances in understanding apicomplexan parasites. *F1000Res*, 5, 2016. [Cited on page 13]
- [7] N. Arisue and T. Hashimoto. Phylogeny and evolution of apicoplasts and apicomplexan parasites. *Parasitol. Int.*, 64(3):254–259, Jun 2015. [Cited on pages 13 and 34]
- [8] J. Liu, E. S. Istvan, I. Y. Gluzman, J. Gross, and D. E. Goldberg. Plasmodium falciparum ensures its amino acid supply with multiple acquisition pathways and redundant proteolytic enzyme systems. *Proc Natl Acad Sci U S A*, 103(23):8840–8845, Jun 2006. [Cited on pages 14 and 15]
- [9] W. H. Brown. Malarial Pigment so-called Melanin: Its nature and mode of production. *J. Exp. Med.*, 13(2):290–299, Feb 1911. [Cited on pages 14, 15, and 16]
- [10] E. Hempelmann and H. M. Marques. Analysis of malaria pigment from Plasmodium falciparum. *J Pharmacol Toxicol Methods*, 32(1):25–30, Sep 1994. [Cited on pages 14, 15, and 16]
- [11] E. Meibalan and M. Marti. Biology of Malaria Transmission. *Cold Spring Harb Perspect Med*, 7(3), Mar 2017. [Cited on pages 14 and 15]
- [12] R. Amino, S. Thiberge, S. Shorte, F. Frischknecht, and R. Menard. Quantitative imaging of Plasmodium sporozoites in the mammalian host. *C. R. Biol.*, 329(11):858–862, Nov 2006. [Cited on page 13]
- [13] U. Frevert, I. Uсынin, K. Baer, and C. Klotz. Nomadic or sessile: can Kupffer cells function as portals for malaria sporozoites to the liver? *Cell. Microbiol.*, 8(10):1537–1546, Oct 2006. [Cited on page 13]

- [14] M. M. Mota, J. C. Hafalla, and A. Rodriguez. Migration through host cells activates Plasmodium sporozoites for infection. *Nat. Med.*, 8(11):1318–1322, Nov 2002. [Cited on page 13]
- [15] A. F. Cowman, J. Healer, D. Marapana, and K. Marsh. Malaria: Biology and Disease. *Cell*, 167(3):610–624, Oct 2016. [Cited on pages 14 and 15]
- [16] A. Dawn, S. Singh, K. R. More, F. A. Siddiqui, N. Pachikara, G. Ramdani, G. Langsley, and C. E. Chitnis. The central role of cAMP in regulating Plasmodium falciparum merozoite invasion of human erythrocytes. *PLoS Pathog.*, 10(12):e1004520, Dec 2014. [Cited on page 14]
- [17] A. F. Cowman, D. Berry, and J. Baum. The cellular and molecular basis for malaria parasite invasion of the human red blood cell. *J. Cell Biol.*, 198(6):961–971, Sep 2012. [Cited on page 14]
- [18] A. R. Dluzewski, G. H. Mitchell, P. R. Fryer, S. Griffiths, R. J. Wilson, and W. B. Gratzer. Origins of the parasitophorous vacuole membrane of the malaria parasite, Plasmodium falciparum, in human red blood cells. *J. Cell. Sci.*, 102 (Pt 3):527–532, Jul 1992. [Cited on page 14]
- [19] F. C. Koyama, D. Chakrabarti, and C. R. Garcia. Molecular machinery of signal transduction and cell cycle regulation in Plasmodium. *Mol. Biochem. Parasitol.*, 165(1):1–7, May 2009. [Cited on page 15]
- [20] M. Ganter, J. M. Goldberg, J. D. Dvorin, J. A. Paulo, J. G. King, A. K. Tripathi, A. S. Paul, J. Yang, I. Coppens, R. H. Jiang, B. Elsworth, D. A. Baker, R. R. Dinglasan, S. P. Gygi, and M. T. Duraisingh. Plasmodium falciparum CRK4 directs continuous rounds of DNA replication during schizogony. *Nat Microbiol.*, 2:17017, Feb 2017. [Cited on page 15]
- [21] V. L. Hale, J. M. Watermeyer, F. Hackett, G. Vizcay-Barrena, C. van Ooij, J. A. Thomas, M. C. Spink, M. Harkiolaki, E. Duke, R. A. Fleck, M. J. Blackman, and H. R. Saibil. Parasitophorous vacuole poration precedes its rupture and rapid host erythrocyte cytoskeleton collapse in Plasmodium falciparum egress. *Proc. Natl. Acad. Sci. U.S.A.*, 114(13):3439–3444, Mar 2017. [Cited on page 15]
- [22] V. L. Lew. Malaria: endless fascination with merozoite release. *Curr. Biol.*, 15(18):R760–761, Sep 2005. [Cited on page 15]
- [23] V. L. Lew. Malaria: surprising mechanism of merozoite egress revealed. *Curr. Biol.*, 21(9):R314–316, May 2011. [Cited on page 15]
- [24] G. A. Josling and M. Llinas. Sexual development in Plasmodium parasites: knowing when it’s time to commit. *Nat. Rev. Microbiol.*, 13(9):573–587, Sep 2015. [Cited on page 15]
- [25] D. S. Guttery, M. Roques, A. A. Holder, and R. Tewari. Commit and Transmit: Molecular Players in Plasmodium Sexual Development and Zygote Differentiation. *Trends Parasitol.*, 31(12):676–685, Dec 2015. [Cited on page 15]
- [26] M. Singh, S. Kanika, G. Singh, A. Dubey, and R.K. Chaitanya. Plasmodium’s journey through the anopheles mosquito: A comprehensive review. *Biochimie*, 181:176–190, 2021. [Cited on page 15]

- [27] A. F. Cowman and B. S. Crabb. Invasion of red blood cells by malaria parasites. *Cell*, 124(4):755–766, Feb 2006. [Cited on page 15]
- [28] M. B. Markus. Malaria: origin of the term "hypnozoite". *J Hist Biol*, 44(4):781–786, 2011. [Cited on page 15]
- [29] B. Campo, O. Vandal, D. L. Wesche, and J. N. Burrows. Killing the hypnozoite—drug discovery approaches to prevent relapse in *Plasmodium vivax*. *Pathog Glob Health*, 109(3):107–122, May 2015. [Cited on page 15]
- [30] I. W. Sherman. Amino acid metabolism and protein synthesis in malarial parasites. *Bull World Health Organ*, 55(2-3):265–276, 1977. [Cited on page 15]
- [31] S. E. Francis, D. J. Sullivan, and D. E. Goldberg. Hemoglobin metabolism in the malaria parasite *Plasmodium falciparum*. *Annu Rev Microbiol*, 51:97–123, 1997. [Cited on pages 15, 18, and 19]
- [32] E. Hanssen, C. Knoechel, M. Dearnley, M. W. Dixon, M. Le Gros, C. Larabell, and L. Tilley. Soft X-ray microscopy analysis of cell volume and hemoglobin content in erythrocytes infected with asexual and sexual stages of *Plasmodium falciparum*. *J Struct Biol*, 177(2):224–232, Feb 2012. [Cited on page 15]
- [33] V. L. Lew, T. Tiffert, and H. Ginsburg. Excess hemoglobin digestion and the osmotic stability of *Plasmodium falciparum*-infected red blood cells. *Blood*, 101(10):4189–4194, May 2003. [Cited on pages 15 and 95]
- [34] V. L. Lew, L. Macdonald, H. Ginsburg, M. Krugliak, and T. Tiffert. Excess haemoglobin digestion by malaria parasites: a strategy to prevent premature host cell lysis. *Blood Cells Mol Dis*, 32(3):353–359, 2004. [Cited on pages 15 and 95]
- [35] B. Elsworth, C. D. Keroack, and M. T. Duraisingh. Elucidating Host Cell Uptake by Malaria Parasites. *Trends Parasitol*, 35(5):333–335, 05 2019. [Cited on pages 15, 16, and 18]
- [36] J. Wunderlich, P. Rohrbach, and J. P. Dalton. The malaria digestive vacuole. *Front Biosci (Schol Ed)*, 4:1424–1448, Jun 2012. [Cited on pages 16, 18, and 98]
- [37] M. Aikawa, C. G. Huff, and H. Spinz. Comparative feeding mechanisms of avian and primate malarial parasites. *Mil Med*, 131(9)::969–983, Sep 1966. [Cited on page 16]
- [38] R. Ladda, J. Arnold, and D. Martin. Electron microscopy of *Plasmodium falciparum* . 1. The structure of trophozoites in erythrocytes of human volunteers. *Trans R Soc Trop Med Hyg*, 60(3):369–375, 1966. [Cited on page 16]
- [39] S. Yamashita, J. Kikkawa, K. Yanagisawa, T. Nagai, K. Ishizuka, and K. Kimoto. Atomic number dependence of Z contrast in scanning transmission electron microscopy. *Sci Rep*, 8(1):12325, Aug 2018. [Cited on page 16]
- [40] O. L. Krivanek, M. F. Chisholm, V. Nicolosi, T. J. Pennycook, G. J. Corbin, N. Dellby, M. F. Murfitt, C. S. Own, Z. S. Szilagy, M. P. Oxley, S. T. Pantelides, and S. J. Pennycook. Atom-by-atom structural and chemical analysis by annular dark-field electron microscopy. *Nature*, 464(7288):571–574, Mar 2010. [Cited on page 16]

- [41] C. Slomianny. Three-dimensional reconstruction of the feeding process of the malaria parasite. *Blood Cells*, 16(2-3):369–378, 1990. [Cited on page 16]
- [42] T. Spielmann, S. Gras, R. Sabitzki, and M. Meissner. Endocytosis in Plasmodium and Toxoplasma Parasites. *Trends Parasitol*, 36(6):520–532, 06 2020. [Cited on pages 16, 17, 18, 20, and 36]
- [43] J. Birnbaum, S. Scharf, S. Schmidt, E. Jonscher, W. A. M. Hoeijmakers, S. Flemming, C. G. Toenhake, M. Schmitt, R. Sabitzki, B. Bergmann, U. Fröhlke, P. Mesén-Ramírez, A. Blancke Soares, H. Herrmann, R. Bártfai, and T. Spielmann. A Kelch13-defined endocytosis pathway mediates artemisinin resistance in malaria parasites. *Science*, 367(6473):51–59, 01 2020. [Cited on pages 16, 20, 21, and 99]
- [44] R. C. Henrici, R. L. Edwards, M. Zoltner, D. A. van Schalkwyk, M. N. Hart, F. Mohring, R. W. Moon, S. D. Nofal, A. Patel, C. Flueck, D. A. Baker, A. R. Odom John, M. C. Field, and C. J. Sutherland. The Plasmodium falciparum Artemisinin Susceptibility-Associated AP-2 Adaptin mu Subunit is Clathrin Independent and Essential for Schizont Maturation. *mBio*, 11(1), 02 2020. [Cited on pages 16, 20, and 21]
- [45] S. C. Xie, S. A. Ralph, and L. Tilley. K13, the Cytostome, and Artemisinin Resistance. *Trends Parasitol*, 36(6):533–544, 06 2020. [Cited on pages 16, 20, 21, and 98]
- [46] M. Kaksonen and A. Roux. Mechanisms of clathrin-mediated endocytosis. *Nat Rev Mol Cell Biol*, 19(5):313–326, 05 2018. [Cited on page 16]
- [47] C. C. Yap and B. Winckler. Adapting for endocytosis: roles for endocytic sorting adaptors in directing neural development. *Front Cell Neurosci*, 9:119, 2015. [Cited on page 16]
- [48] L. M. Traub. Sorting it out: AP-2 and alternate clathrin adaptors in endocytic cargo selection. *J Cell Biol*, 163(2):203–208, Oct 2003. [Cited on page 16]
- [49] K. J. Milani, T. G. Schneider, and T. F. Taraschi. Defining the morphology and mechanism of the hemoglobin transport pathway in Plasmodium falciparum-infected erythrocytes. *Eukaryot Cell*, 14(4):415–426, Apr 2015. [Cited on pages 17 and 18]
- [50] E. Jonscher, S. Flemming, M. Schmitt, R. Sabitzki, N. Reichard, J. Birnbaum, B. Bergmann, K. Höhn, and T. Spielmann. PfVPS45 Is Required for Host Cell Cytosol Uptake by Malaria Blood Stage Parasites. *Cell Host Microbe*, 25(1):166–173, 01 2019. [Cited on pages 17, 18, 52, and 96]
- [51] M. D. Lazarus, T. G. Schneider, and T. F. Taraschi. A new model for hemoglobin ingestion and transport by the human malaria parasite Plasmodium falciparum. *J Cell Sci*, 121(11):1937–1949, Jun 2008. [Cited on pages 17, 18, 76, 96, and 98]
- [52] W. A. Smythe, K. A. Joiner, and H. C. Hoppe. Actin is required for endocytic trafficking in the malaria parasite Plasmodium falciparum. *Cell Microbiol*, 10(2):452–464, Feb 2008. [Cited on pages 17 and 98]
- [53] A. Vaid, R. Ranjan, W. A. Smythe, H. C. Hoppe, and P. Sharma. PfPI3K, a phosphatidylinositol-3 kinase from Plasmodium falciparum, is exported to the host erythrocyte and is involved in hemoglobin trafficking. *Blood*, 115(12):2500–2507, Mar 2010. [Cited on pages 17 and 98]

- [54] R. Howe, M. Kelly, J. Jimah, D. Hodge, and A. R. Odom. Isoprenoid biosynthesis inhibition disrupts Rab5 localization and food vacuolar integrity in *Plasmodium falciparum*. *Eukaryot Cell*, 12(2):215–223, Feb 2013. [Cited on pages 17 and 98]
- [55] Y. Homma, S. Hiragi, and M. Fukuda. Rab family of small GTPases: an updated view on their regulation and functions. *FEBS J*, 288(1):36–55, Jan 2021. [Cited on page 17]
- [56] J. Birnbaum, S. Flemming, N. Reichard, A. B. Soares, P. Mesén-Ramírez, E. Jonscher, B. Bergmann, and T. Spielmann. A genetic system to study *Plasmodium falciparum* protein function. *Nat Methods*, 14(4):450–456, Apr 2017. [Cited on page 17]
- [57] K. Ebine, M. Hirai, M. Sakaguchi, K. Yahata, O. Kaneko, and Y. Saito-Nakano. *Plasmodium* Rab5b is secreted to the cytoplasmic face of the tubovesicular network in infected red blood cells together with N-acylated adenylate kinase 2. *Malar J*, 15:323, 06 2016. [Cited on page 18]
- [58] C. N. Ezougou, F. Ben-Rached, D. K. Moss, J. W. Lin, S. Black, E. Knuepfer, J. L. Green, S. M. Khan, A. Mukhopadhyay, C. J. Janse, I. Coppens, H. Yera, A. A. Holder, and G. Langsley. *Plasmodium falciparum* Rab5B is an N-terminally myristoylated Rab GTPase that is targeted to the parasite’s plasma and food vacuole membranes. *PLoS One*, 9(2):e87695, 2014. [Cited on page 18]
- [59] P. Krai, S. Dalal, and M. Klemba. Evidence for a Golgi-to-endosome protein sorting pathway in *Plasmodium falciparum*. *PLoS One*, 9(2):e89771, 2014. [Cited on page 18]
- [60] C. Slomianny and G. Prensier. A cytochemical ultrastructural study of the lysosomal system of different species of malaria parasites. *J Protozool*, 37(6):465–470, 1990. [Cited on page 18]
- [61] E. Hempelmann, C. Motta, R. Hughes, S. A. Ward, and P. G. Bray. *Plasmodium falciparum*: sacrificing membrane to grow crystals? *Trends Parasitol*, 19(1):23–26, Jan 2003. [Cited on page 18]
- [62] M. Klemba, W. Beatty, I. Gluzman, and D. E. Goldberg. Trafficking of plasmepsin II to the food vacuole of the malaria parasite *Plasmodium falciparum*. *J Cell Biol*, 164(1):47–56, Jan 2004. [Cited on page 18]
- [63] N. Abu Bakar, N. Klonis, E. Hanssen, C. Chan, and L. Tilley. Digestive-vacuole genesis and endocytic processes in the early intraerythrocytic stages of *Plasmodium falciparum*. *J Cell Sci*, 123(Pt 3):441–450, Feb 2010. [Cited on page 18]
- [64] R. Banerjee, J. Liu, W. Beatty, L. Pelosof, M. Klemba, and D. E. Goldberg. Four plasmepsins are active in the *Plasmodium falciparum* food vacuole, including a protease with an active-site histidine. *Proc Natl Acad Sci U S A*, 99(2):990–995, Jan 2002. [Cited on page 18]
- [65] D. A. Elliott, M. T. McIntosh, H. D. Hosgood, S. Chen, G. Zhang, P. Baevova, and K. A. Joiner. Four distinct pathways of hemoglobin uptake in the malaria parasite *Plasmodium falciparum*. *Proc Natl Acad Sci U S A*, 105(7):2463–2468, Feb 2008. [Cited on page 18]
- [66] H. Atamna and H. Ginsburg. Origin of reactive oxygen species in erythrocytes infected with *Plasmodium falciparum*. *Mol Biochem Parasitol*, 61(2):231–241, Oct 1993. [Cited on page 18]

- [67] P. Wardman and L. P. Candeias. Fenton chemistry: an introduction. *Radiat Res*, 145(5):523–531, May 1996. [Cited on page 18]
- [68] S. Pagola, P. W. Stephens, D. S. Bohle, A. D. Kosar, and S. K. Madsen. The structure of malaria pigment beta-haematin. *Nature*, 404(6775):307–310, Mar 2000. [Cited on page 19]
- [69] E. Hempelmann. Hemozoin biocrystallization in *Plasmodium falciparum* and the antimalarial activity of crystallization inhibitors. *Parasitol Res*, 100(4):671–676, Mar 2007. [Cited on page 19]
- [70] G. Kikuchi, T. Yoshida, and M. Noguchi. Heme oxygenase and heme degradation. *Biochem Biophys Res Commun*, 338(1):558–567, Dec 2005. [Cited on page 19]
- [71] D. Jani, R. Nagarkatti, W. Beatty, R. Angel, C. Slebodnick, J. Andersen, S. Kumar, and D. Rathore. HDP-a novel heme detoxification protein from the malaria parasite. *PLoS Pathog*, 4(4):e1000053, Apr 2008. [Cited on page 19]
- [72] P. Loria, S. Miller, M. Foley, and L. Tilley. Inhibition of the peroxidative degradation of haem as the basis of action of chloroquine and other quinoline antimalarials. *Biochem J*, 339 (Pt 2):363–370, Apr 1999. [Cited on page 19]
- [73] K. Becker, L. Tilley, J. L. Vennerstrom, D. Roberts, S. Rogerson, and H. Ginsburg. Oxidative stress in malaria parasite-infected erythrocytes: host-parasite interactions. *Int J Parasitol*, 34(2):163–189, Feb 2004. [Cited on pages 19, 22, 24, 25, 33, 34, and 36]
- [74] L. Tilley, P. Loria, and M. Foley. *Chloroquine and Other Quinoline Antimalarials*. Humana Press, Totowa, NJ, antimalarial chemotherapy. infectious disease. edition, 2001. [Cited on page 19]
- [75] A. U. Orjih, H. S. Banyal, R. Chevli, and C. D. Fitch. Hemin lyses malaria parasites. *Science*, 214(4521):667–669, Nov 1981. [Cited on page 19]
- [76] M. M. Stevenson and E. M. Riley. Innate immunity to malaria. *Nat Rev Immunol*, 4(3):169–180, Mar 2004. [Cited on page 19]
- [77] X. Chen, P. B. Comish, D. Tang, and R. Kang. Characteristics and Biomarkers of Ferroptosis. *Front Cell Dev Biol*, 9:637162, 2021. [Cited on pages 19, 24, and 25]
- [78] W. S. Yang and B. R. Stockwell. Ferroptosis: Death by Lipid Peroxidation. *Trends Cell Biol*, 26(3):165–176, Mar 2016. [Cited on page 19]
- [79] F. Kuang, J. Liu, D. Tang, and R. Kang. Oxidative Damage and Antioxidant Defense in Ferroptosis. *Front Cell Dev Biol*, 8:586578, 2020. [Cited on pages 19 and 22]
- [80] R. A. Kavishe, J. B. Koenderink, and M. Alifrangis. Oxidative stress in malaria and artemisinin combination therapy: Pros and Cons. *FEBS J*, 284(16):2579–2591, 08 2017. [Cited on pages 19 and 34]
- [81] N. Klonis, M. P. Crespo-Ortiz, I. Bottova, N. Abu-Bakar, S. Kenny, P. J. Rosenthal, and L. Tilley. Artemisinin activity against *Plasmodium falciparum* requires hemoglobin uptake and digestion. *Proc Natl Acad Sci U S A*, 108(28):11405–11410, Jul 2011. [Cited on pages 19 and 20]

- [82] Jigang Wang, Chengchao Xu, Yin Kwan Wong, Yujie Li, Fulong Liao, Tingliang Jiang, and Youyou Tu. Artemisinin, the magic drug discovered from traditional chinese medicine. *Engineering*, 5(1):32–39, 2019. [Cited on pages 19 and 20]
- [83] Y. Tu. The discovery of artemisinin (qinghaosu) and gifts from Chinese medicine. *Nat Med*, 17(10):1217–1220, Oct 2011. [Cited on page 19]
- [84] No authors listed. Antimalaria studies on Qinghaosu. *Chin Med J (Engl)*, 92(12):811–816, Dec 1979. [Cited on page 19]
- [85] Y. Suputtamongkol, P. N. Newton, B. Angus, P. Teja-Isavadharm, D. Keeratithakul, M. Rasameesoraj, S. Pukrittayakamee, and N. J. White. A comparison of oral artesunate and artemether antimalarial bioactivities in acute falciparum malaria. *Br J Clin Pharmacol*, 52(6):655–661, Dec 2001. [Cited on page 20]
- [86] L. Cui and X. Z. Su. Discovery, mechanisms of action and combination therapy of artemisinin. *Expert Rev Anti Infect Ther*, 7(8):999–1013, Oct 2009. [Cited on page 20]
- [87] P. M. O’Neill, V. E. Barton, and S. A. Ward. The molecular mechanism of action of artemisinin—the debate continues. *Molecules*, 15(3):1705–1721, Mar 2010. [Cited on page 20]
- [88] J. Wang, C. J. Zhang, W. N. Chia, C. C. Loh, Z. Li, Y. M. Lee, Y. He, L. X. Yuan, T. K. Lim, M. Liu, C. X. Liew, Y. Q. Lee, J. Zhang, N. Lu, C. T. Lim, Z. C. Hua, B. Liu, H. M. Shen, K. S. Tan, and Q. Lin. Haem-activated promiscuous targeting of artemisinin in *Plasmodium falciparum*. *Nat Commun*, 6:10111, Dec 2015. [Cited on page 20]
- [89] W. Li, W. Mo, D. Shen, L. Sun, J. Wang, S. Lu, J. M. Gitschier, and B. Zhou. Yeast model uncovers dual roles of mitochondria in action of artemisinin. *PLoS Genet*, 1(3):e36, Sep 2005. [Cited on page 20]
- [90] J. Wang, L. Huang, J. Li, Q. Fan, Y. Long, Y. Li, and B. Zhou. Artemisinin directly targets malarial mitochondria through its specific mitochondrial activation. *PLoS One*, 5(3):e9582, Mar 2010. [Cited on page 20]
- [91] U. Eckstein-Ludwig, R. J. Webb, I. D. Van Goethem, J. M. East, A. G. Lee, M. Kimura, P. M. O’Neill, P. G. Bray, S. A. Ward, and S. Krishna. Artemisinins target the SERCA of *Plasmodium falciparum*. *Nature*, 424(6951):957–961, Aug 2003. [Cited on page 20]
- [92] B. Arnou, C. Montigny, J. P. Morth, P. Nissen, C. Jaxel, J. V. Møller, and M. I. Maire. The *Plasmodium falciparum* Ca⁽²⁺⁾-ATPase PfATP6: insensitive to artemisinin, but a potential drug target. *Biochem Soc Trans*, 39(3):823–831, Jun 2011. [Cited on page 20]
- [93] H. M. Ismail, V. Barton, M. Phanchana, S. Charoensutthivarakul, M. H. Wong, J. Hemingway, G. A. Biagini, P. M. O’Neill, and S. A. Ward. Artemisinin activity-based probes identify multiple molecular targets within the asexual stage of the malaria parasites *Plasmodium falciparum* 3D7. *Proc Natl Acad Sci U S A*, 113(8):2080–2085, Feb 2016. [Cited on page 20]
- [94] B. Meunier and A. Robert. Heme as trigger and target for trioxane-containing antimalarial drugs. *Acc Chem Res*, 43(11):1444–1451, Nov 2010. [Cited on page 20]

- [95] J. L. Bridgford, S. C. Xie, S. A. Cobbold, C. F. A. Pasaje, S. Herrmann, T. Yang, D. L. Gillett, L. R. Dick, S. A. Ralph, C. Dogovski, N. J. Spillman, and L. Tilley. Artemisinin kills malaria parasites by damaging proteins and inhibiting the proteasome. *Nat Commun*, 9(1):3801, 09 2018. [Cited on page 20]
- [96] H. Noedl, Y. Se, K. Schaecher, B. L. Smith, D. Socheat, and M. M. Fukuda. Evidence of artemisinin-resistant malaria in western Cambodia. *N Engl J Med*, 359(24):2619–2620, Dec 2008. [Cited on page 20]
- [97] E. A. Ashley, M. Dhorda, R. M. Fairhurst, C. Amaratunga, P. Lim, S. Suon, S. Sreng, J. M. Anderson, S. Mao, B. Sam, C. Sopha, C. M. Chuor, C. Nguon, S. Sovannaroeth, S. Pukrittayakamee, P. Jittamala, K. Chotivanich, K. Chutasmit, C. Suchatsoonthorn, R. Runcharoen, T. T. Hien, N. T. Thuy-Nhien, N. V. Thanh, N. H. Phu, Y. Htut, K. T. Han, K. H. Aye, O. A. Mokuolu, R. R. Olaosebikan, O. O. Folaranmi, M. Mayxay, M. Khanthavong, B. Hongvanthong, P. N. Newton, M. A. Onyamboko, C. I. Fanello, A. K. Tshefu, N. Mishra, N. Valecha, A. P. Phyto, F. Nosten, P. Yi, R. Tripura, S. Borrmann, M. Bashraheil, J. Peshu, M. A. Faiz, A. Ghose, M. A. Hossain, R. Samad, M. R. Rahman, M. M. Hasan, A. Islam, O. Miotto, R. Amato, B. MacInnis, J. Stalker, D. P. Kwiatkowski, Z. Bozdech, A. Jeeyapant, P. Y. Cheah, T. Sakulthaew, J. Chalk, B. Intharabut, K. Silamut, S. J. Lee, B. Vihokhern, C. Kunasol, M. Imwong, J. Tarning, W. J. Taylor, S. Yeung, C. J. Woodrow, J. A. Flegg, D. Das, J. Smith, M. Venkatesan, C. V. Plowe, K. Stepniewska, P. J. Guerin, A. M. Dondorp, N. P. Day, and N. J. White. Spread of artemisinin resistance in *Plasmodium falciparum* malaria. *N Engl J Med*, 371(5):411–423, Jul 2014. [Cited on page 20]
- [98] F. Ariey, B. Witkowski, C. Amaratunga, J. Beghain, A. C. Langlois, N. Khim, S. Kim, V. Duru, C. Bouchier, L. Ma, P. Lim, R. Leang, S. Duong, S. Sreng, S. Suon, C. M. Chuor, D. M. Bout, S. Ménard, W. O. Rogers, B. Genton, T. Fandeur, O. Miotto, P. Ringwald, J. Le Bras, A. Berry, J. C. Barale, R. M. Fairhurst, F. Benoit-Vical, O. Mercereau-Puijalon, and D. Ménard. A molecular marker of artemisinin-resistant *Plasmodium falciparum* malaria. *Nature*, 505(7481):50–55, Jan 2014. [Cited on pages 20 and 99]
- [99] K. T. Batty, L. T. Thu, T. M. Davis, K. F. Ilett, T. X. Mai, N. C. Hung, N. P. Tien, S. M. Powell, H. V. Thien, T. Q. Binh, and N. V. Kim. A pharmacokinetic and pharmacodynamic study of intravenous vs oral artesunate in uncomplicated *falciparum* malaria. *Br J Clin Pharmacol*, 45(2):123–129, Feb 1998. [Cited on page 21]
- [100] D. B. Bethell, P. Teja-Isavadharm, X. T. Cao, T. T. Pham, T. T. Ta, T. N. Tran, T. T. Nguyen, T. P. Pham, D. Kyle, N. P. Day, and N. J. White. Pharmacokinetics of oral artesunate in children with moderately severe *Plasmodium falciparum* malaria. *Trans R Soc Trop Med Hyg*, 91(2):195–198, 1997. [Cited on page 21]
- [101] K. T. Batty, K. F. Ilett, T. Davis, and M. E. Davis. Chemical stability of artesunate injection and proposal for its administration by intravenous infusion. *J Pharm Pharmacol*, 48(1):22–26, Jan 1996. [Cited on page 21]
- [102] V. N. Bochkov, O. V. Oskolkova, K. G. Birukov, A. L. Levonen, C. J. Binder, and J. Stöckl. Generation and biological activities of oxidized phospholipids. *Antioxid Redox Signal*, 12(8):1009–1059, Apr 2010. [Cited on pages 21, 22, 23, 25, 26, 28, 36, 37, 84, and 87]

- [103] H. W. Gardner. Oxygen radical chemistry of polyunsaturated fatty acids. *Free Radic Biol Med*, 7(1):65–86, 1989. [Cited on pages 22 and 85]
- [104] X. Gu, M. Sun, B. Gugiu, S. Hazen, J. W. Crabb, and R. G. Salomon. Oxidatively truncated docosahexaenoate phospholipids: total synthesis, generation, and Peptide adduction chemistry. *J Org Chem*, 68(10):3749–3761, May 2003. [Cited on page 22]
- [105] T. M. McIntyre. Bioactive oxidatively truncated phospholipids in inflammation and apoptosis: formation, targets, and inactivation. *Biochim Biophys Acta*, 1818(10):2456–2464, Oct 2012. [Cited on pages 22 and 27]
- [106] L. L. Hsiao, R. J. Howard, M. Aikawa, and T. F. Taraschi. Modification of host cell membrane lipid composition by the intra-erythrocytic human malaria parasite *Plasmodium falciparum*. *Biochem J*, 274 (Pt 1):121–132, Feb 1991. [Cited on pages 22, 23, and 63]
- [107] A. B. Fisher, J. P. Vasquez-Medina, C. Dodia, E. M. Sorokina, J. Q. Tao, and S. I. Feinstein. Peroxiredoxin 6 phospholipid hydroperoxidase activity in the repair of peroxidized cell membranes. *Redox Biol*, 14:41–46, 04 2018. [Cited on pages 22, 25, 26, 29, 30, 31, 32, 34, 37, 84, and 87]
- [108] K. Sabatini, J. P. Mattila, F. M. Megli, and P. K. Kinnunen. Characterization of two oxidatively modified phospholipids in mixed monolayers with DPPC. *Biophys J*, 90(12):4488–4499, Jun 2006. [Cited on page 22]
- [109] J. W. Borst, N. V. Visser, O. Kouptsova, and A. J. Visser. Oxidation of unsaturated phospholipids in membrane bilayer mixtures is accompanied by membrane fluidity changes. *Biochim Biophys Acta*, 1487(1):61–73, Aug 2000. [Cited on page 22]
- [110] A. Bour, S. G. Kruglik, M. Chabanon, P. Rangamani, N. Puff, and S. Bonneau. Lipid Unsaturation Properties Govern the Sensitivity of Membranes to Photoinduced Oxidative Stress. *Biophys J*, 116(5):910–920, 03 2019. [Cited on page 22]
- [111] E. Agmon, J. Solon, P. Bassereau, and B. R. Stockwell. Modeling the effects of lipid peroxidation during ferroptosis on membrane properties. *Sci Rep*, 8(1):5155, 03 2018. [Cited on pages 22, 24, and 34]
- [112] K. A. Runas and N. Malmstadt. Low levels of lipid oxidation radically increase the passive permeability of lipid bilayers. *Soft Matter*, 11(3):499–505, Jan 2015. [Cited on page 22]
- [113] M. K. Chang, C. J. Binder, Y. I. Miller, G. Subbanagounder, G. J. Silverman, J. A. Berliner, and J. L. Witztum. Apoptotic cells with oxidation-specific epitopes are immunogenic and proinflammatory. *J Exp Med*, 200(11):1359–1370, Dec 2004. [Cited on page 22]
- [114] Y. Y. Tyurina, V. A. Tyurin, Q. Zhao, M. Djukic, P. J. Quinn, B. R. Pitt, and V. E. Kagan. Oxidation of phosphatidylserine: a mechanism for plasma membrane phospholipid scrambling during apoptosis? *Biochem Biophys Res Commun*, 324(3):1059–1064, Nov 2004. [Cited on page 22]
- [115] L. J. Su, J. H. Zhang, H. Gomez, R. Murugan, X. Hong, D. Xu, F. Jiang, and Z. Y. Peng. Reactive Oxygen Species-Induced Lipid Peroxidation in Apoptosis, Autophagy, and Ferroptosis. *Oxid Med Cell Longev*, 2019:5080843, 2019. [Cited on page 22]

- [116] J. Zhang, X. Wang, V. Vikash, Q. Ye, D. Wu, Y. Liu, and W. Dong. ROS and ROS-Mediated Cellular Signaling. *Oxid Med Cell Longev*, 2016:4350965, 2016. [Cited on page 22]
- [117] M. Dodson, R. Castro-Portuguez, and D. D. Zhang. NRF2 plays a critical role in mitigating lipid peroxidation and ferroptosis. *Redox Biol*, 23:101107, 05 2019. [Cited on page 22]
- [118] N. Androulakis, H. Durand, E. Ninio, and D. C. Tsoukatos. Molecular and mechanistic characterization of platelet-activating factor-like bioactivity produced upon LDL oxidation. *J Lipid Res*, 46(9):1923–1932, Sep 2005. [Cited on pages 22 and 87]
- [119] P. Singh, I. N. Singh, S. C. Mondal, L. Singh, and V. K. Garg. Platelet-activating factor (PAF)-antagonists of natural origin. *Fitoterapia*, 84:180–201, Jan 2013. [Cited on pages 22 and 87]
- [120] C. M. Spickett and A. R. Pitt. Oxidative lipidomics coming of age: advances in analysis of oxidized phospholipids in physiology and pathology. *Antioxid Redox Signal*, 22(18):1646–1666, Jun 2015. [Cited on page 23]
- [121] A. Ayala, M. F. Muñoz, and S. Argüelles. Lipid peroxidation: production, metabolism, and signaling mechanisms of malondialdehyde and 4-hydroxy-2-nonenal. *Oxid Med Cell Longev*, 2014:360438, 2014. [Cited on page 23]
- [122] H. Ohkawa, N. Ohishi, and K. Yagi. Reaction of linoleic acid hydroperoxide with thiobarbituric acid. *J Lipid Res*, 19(8):1053–1057, Nov 1978. [Cited on pages 23, 46, and 85]
- [123] D. R. Janero. Malondialdehyde and thiobarbituric acid-reactivity as diagnostic indices of lipid peroxidation and peroxidative tissue injury. *Free Radic Biol Med*, 9(6):515–540, 1990. [Cited on page 23]
- [124] G. M. Makrigiorgos. Detection of lipid peroxidation on erythrocytes using the excimer-forming property of a lipophilic BODIPY fluorescent dye. *J Biochem Biophys Methods*, 35(1):23–35, Aug 1997. [Cited on page 23]
- [125] M. L. MacDonald, I. V. Murray, and P. H. Axelsen. Mass spectrometric analysis demonstrates that BODIPY 581/591 C11 overestimates and inhibits oxidative lipid damage. *Free Radic Biol Med*, 42(9):1392–1397, May 2007. [Cited on pages 23 and 85]
- [126] Y. Fu, N. Klonis, C. Suarna, G. J. Maghzal, R. Stocker, and L. Tilley. A phosphatidylcholine-BODIPY 581/591 conjugate allows mapping of oxidative stress in *P. falciparum*-infected erythrocytes. *Cytometry A*, 75(5):390–404, May 2009. [Cited on pages 23, 24, 36, 46, 83, and 85]
- [127] M. R. Clemens and H. D. Waller. Lipid peroxidation in erythrocytes. *Chem Phys Lipids*, 45(2-4):251–268, 1987. [Cited on pages 23, 24, 33, 34, and 85]
- [128] J. P. Hale, C. P. Winlove, and P. G. Petrov. Effect of hydroperoxides on red blood cell membrane mechanical properties. *Biophys J*, 101(8):1921–1929, Oct 2011. [Cited on page 23]
- [129] A. Flammersfeld, C. Lang, A. Fliieger, and G. Pradel. Phospholipases during membrane dynamics in malaria parasites. *Int J Med Microbiol*, 308(1):129–141, Jan 2018. [Cited on pages 23, 35, 36, 37, 63, 65, 83, 84, and 86]
- [130] B. S. Das and N. K. Nanda. Evidence for erythrocyte lipid peroxidation in acute falciparum malaria. *Trans R Soc Trop Med Hyg*, 93(1):58–62, 1999. [Cited on pages 24 and 36]

- [131] C. Y. Botté, Y. Yamaryo-Botté, T. W. Rupasinghe, K. A. Mullin, J. I. MacRae, T. P. Spurck, M. Kalanon, M. J. Shears, R. L. Coppel, P. K. Crellin, E. Maréchal, M. J. McConville, and G. I. McFadden. Atypical lipid composition in the purified relict plastid (apicoplast) of malaria parasites. *Proc Natl Acad Sci U S A*, 110(18):7506–7511, Apr 2013. [Cited on page 24]
- [132] H. J. Vial, P. Eldin, A. G. Tielens, and J. J. van Hellemond. Phospholipids in parasitic protozoa. *Mol Biochem Parasitol*, 126(2):143–154, Feb 2003. [Cited on pages 24, 37, and 86]
- [133] R. Stocker, N. H. Hunt, G. D. Buffinton, M. J. Weidemann, P. H. Lewis-Hughes, and I. A. Clark. Oxidative stress and protective mechanisms in erythrocytes in relation to *Plasmodium vinckei* load. *Proc Natl Acad Sci U S A*, 82(2):548–551, Jan 1985. [Cited on pages 24 and 36]
- [134] A. P. Simões, J. J. van den Berg, B. Roelofsen, and J. A. Op den Kamp. Lipid peroxidation in *Plasmodium falciparum*-parasitized human erythrocytes. *Arch Biochem Biophys*, 298(2):651–657, Nov 1992. [Cited on pages 24 and 36]
- [135] F. Omodeo-Salè, A. Motti, N. Basilio, S. Parapini, P. Olliaro, and D. Taramelli. Accelerated senescence of human erythrocytes cultured with *Plasmodium falciparum*. *Blood*, 102(2):705–711, Jul 2003. [Cited on pages 24 and 36]
- [136] L. M. Kumaratilake, B. S. Robinson, A. Ferrante, and A. Poulos. Antimalarial properties of n-3 and n-6 polyunsaturated fatty acids: in vitro effects on *Plasmodium falciparum* and in vivo effects on *P. berghei*. *J Clin Invest*, 89(3):961–967, Mar 1992. [Cited on pages 24, 36, and 86]
- [137] H. S. Kain, E. K. K. Glennon, K. Vijayan, N. Arang, A. N. Douglass, C. L. Fortin, M. Zuck, A. J. Lewis, S. L. Whiteside, D. R. Dudgeon, J. S. Johnson, A. Aderem, K. R. Stevens, and A. Kaushansky. Liver stage malaria infection is controlled by host regulators of lipid peroxidation. *Cell Death Differ*, 27(1):44–54, 01 2020. [Cited on pages 24, 34, 36, 37, 83, and 87]
- [138] S. G. Rhee and I. S. Kil. Multiple Functions and Regulation of Mammalian Peroxiredoxins. *Annu Rev Biochem*, 86:749–775, 06 2017. [Cited on pages 24, 34, 36, 95, and 102]
- [139] Norma Francenia Santos-Sánchez, Raúl Salas-Coronado, Claudia Villanueva-Cañongo, and Beatriz Hernández-Carlos. Antioxidant compounds and their antioxidant mechanism. *Antioxidants*, Mar 2019. [Cited on page 24]
- [140] G. W. Burton, A. Joyce, and K. U. Ingold. Is vitamin E the only lipid-soluble, chain-breaking antioxidant in human blood plasma and erythrocyte membranes? *Arch Biochem Biophys*, 221(1):281–290, Feb 1983. [Cited on pages 24 and 33]
- [141] E. Niki. Role of vitamin E as a lipid-soluble peroxy radical scavenger: in vitro and in vivo evidence. *Free Radic Biol Med*, 66:3–12, Jan 2014. [Cited on pages 24, 33, 62, and 85]
- [142] O. Zilka, R. Shah, B. Li, J. P. Friedmann Angeli, M. Griesser, M. Conrad, and D. A. Pratt. On the Mechanism of Cytoprotection by Ferrostatin-1 and Lipoxstatin-1 and the Role of Lipid Peroxidation in Ferroptotic Cell Death. *ACS Cent Sci*, 3(3):232–243, Mar 2017. [Cited on pages 24 and 34]
- [143] Peter Spiteller and Gerhard Spiteller. 9-hydroxy-10,12-octadecadienoic acid (9-hode) and 13-hydroxy-9,11-octadecadienoic acid (13-hode): excellent markers for lipid peroxidation. *Chemistry and Physics of Lipids*, 89(2):131–139, 1997. [Cited on page 25]

- [144] S. Müller, T. W. Gilberger, Z. Krnajska, K. Lüersen, S. Meierjohann, and R. D. Walter. Thioredoxin and glutathione system of malaria parasite *Plasmodium falciparum*. *Protoplasma*, 217(1-3):43–49, 2001. [Cited on pages 25 and 34]
- [145] L. Luzzatto, C. Nannelli, and R. Notaro. Glucose-6-Phosphate Dehydrogenase Deficiency. *Hematol Oncol Clin North Am*, 30(2):373–393, Apr 2016. [Cited on pages 25 and 34]
- [146] Y. Yang, J. Z. Cheng, S. S. Singhal, M. Saini, U. Pandya, S. Awasthi, and Y. C. Awasthi. Role of glutathione S-transferases in protection against lipid peroxidation. Overexpression of hGSTA2-2 in K562 cells protects against hydrogen peroxide-induced apoptosis and inhibits JNK and caspase 3 activation. *J Biol Chem*, 276(22):19220–19230, Jun 2001. [Cited on page 25]
- [147] X. Kammerscheit, F. Chauvat, and C. Cassier-Chauvat. From Cyanobacteria to Human, MAPEG-Type Glutathione-S-Transferases Operate in Cell Tolerance to Heat, Cold, and Lipid Peroxidation. *Front Microbiol*, 10:2248, 2019. [Cited on page 25]
- [148] M. Björnstedt, M. Hamberg, S. Kumar, J. Xue, and A. Holmgren. Human thioredoxin reductase directly reduces lipid hydroperoxides by NADPH and selenocystine strongly stimulates the reaction via catalytically generated selenols. *J Biol Chem*, 270(20):11761–11764, May 1995. [Cited on page 25]
- [149] J. M. May, J. D. Morrow, and R. F. Burk. Thioredoxin reductase reduces lipid hydroperoxides and spares alpha-tocopherol. *Biochem Biophys Res Commun*, 292(1):45–49, Mar 2002. [Cited on page 25]
- [150] No authors listed. IUPAC-IUB joint commission on biochemical nomenclature (JCBN) nomenclature of glycolipids recommendations 1997. *J Mol Biol*, 286(3):963–970, Feb 1999. [Cited on page 26]
- [151] M. M. Manni, M. L. Tiberti, S. Pagnotta, H. Barelli, R. Gautier, and B. Antonny. Acyl chain asymmetry and polyunsaturation of brain phospholipids facilitate membrane vesiculation without leakage. *Elife*, 7, 03 2018. [Cited on pages 26, 37, and 86]
- [152] C. H. Huang. Mixed-chain phospholipids: structures and chain-melting behavior. *Lipids*, 36(10):1077–1097, Oct 2001. [Cited on pages 26 and 37]
- [153] A. B. Fisher. The phospholipase A2 activity of peroxiredoxin 6. *J Lipid Res*, 59(7):1132–1147, 07 2018. [Cited on pages 26, 29, 30, 31, 32, 33, 37, 66, 67, 74, 83, 87, 101, and 102]
- [154] A. B. Fisher, C. Dodia, E. M. Sorokina, H. Li, S. Zhou, T. Raabe, and S. I. Feinstein. A novel lysophosphatidylcholine acyl transferase activity is expressed by peroxiredoxin 6. *J Lipid Res*, 57(4):587–596, Apr 2016. [Cited on pages 26, 29, 30, and 31]
- [155] G. Subbanagounder, N. Leitinger, D. C. Schwenke, J. W. Wong, H. Lee, C. Rizza, A. D. Watson, K. F. Faull, A. M. Fogelman, and J. A. Berliner. Determinants of bioactivity of oxidized phospholipids. Specific oxidized fatty acyl groups at the sn-2 position. *Arterioscler Thromb Vasc Biol*, 20(10):2248–2254, Oct 2000. [Cited on page 26]
- [156] E. A. Dennis, J. Cao, Y. H. Hsu, V. Magrioti, and G. Kokotos. Phospholipase A2 enzymes: physical structure, biological function, disease implication, chemical inhibition, and therapeutic intervention. *Chem Rev*, 111(10):6130–6185, Oct 2011. [Cited on pages 27, 28, 29, 30, 37, and 87]

- [157] F. Huang, H. Hu, K. Wang, C. Peng, W. Xu, Y. Zhang, J. Gao, Y. Liu, H. Zhou, R. Huang, M. Li, J. Shen, and Y. Xu. Identification of Highly Selective Lipoprotein-Associated Phospholipase A2 (Lp-PLA2) Inhibitors by a Covalent Fragment-Based Approach. *J Med Chem*, 63(13):7052–7065, 07 2020. [Cited on page 27]
- [158] K. E. Stremmler, D. M. Stafforini, S. M. Prescott, and T. M. McIntyre. Human plasma platelet-activating factor acetylhydrolase. Oxidatively fragmented phospholipids as substrates. *J Biol Chem*, 266(17):11095–11103, Jun 1991. [Cited on page 27]
- [159] D. M. Stafforini and G. A. Zimmerman. Unraveling the PAF-AH/Lp-PLA2 controversy. *J Lipid Res*, 55(9):1811–1814, Sep 2014. [Cited on pages 27 and 65]
- [160] J. A. Blackie, J. C. Bloomer, M. J. Brown, H. Y. Cheng, B. Hammond, D. M. Hickey, R. J. Ife, C. A. Leach, V. A. Lewis, C. H. Macphee, K. J. Milliner, K. E. Moores, I. L. Pinto, S. A. Smith, I. G. Stansfield, S. J. Stanway, M. A. Taylor, and C. J. Theobald. The identification of clinical candidate SB-480848: a potent inhibitor of lipoprotein-associated phospholipase A2. *Bioorg Med Chem Lett*, 13(6):1067–1070, Mar 2003. [Cited on pages 27, 63, 86, and 101]
- [161] A. Mullard. GSK’s darapladib failures dim hopes for anti-inflammatory heart drugs. *Nat Rev Drug Discov*, 13(7):481–482, Jul 2014. [Cited on page 27]
- [162] M. Dave, M. Nash, G. C. Young, H. Ellens, M. H. Magee, A. D. Roberts, M. A. Taylor, R. W. Greenhill, and G. W. Boyle. Disposition and metabolism of darapladib, a lipoprotein-associated phospholipase A2 inhibitor, in humans. *Drug Metab Dispos*, 42(3):415–430, Mar 2014. [Cited on pages 28, 72, and 94]
- [163] P. J. Kell, M. H. Creer, K. N. Crown, K. Wirsig, and J. McHowat. Inhibition of platelet-activating factor (PAF) acetylhydrolase by methyl arachidonyl fluorophosphonate potentiates PAF synthesis in thrombin-stimulated human coronary artery endothelial cells. *J Pharmacol Exp Ther*, 307(3):1163–1170, Dec 2003. [Cited on pages 28 and 63]
- [164] J. Chen, L. Yang, J. M. Foulks, A. S. Weyrich, G. K. Marathe, and T. M. McIntyre. Intracellular PAF catabolism by PAF acetylhydrolase counteracts continual PAF synthesis. *J Lipid Res*, 48(11):2365–2376, Nov 2007. [Cited on pages 28 and 63]
- [165] K. Hattori, H. Adachi, A. Matsuzawa, K. Yamamoto, M. Tsujimoto, J. Aoki, M. Hattori, H. Arai, and K. Inoue. cDNA cloning and expression of intracellular platelet-activating factor (PAF) acetylhydrolase II. Its homology with plasma PAF acetylhydrolase. *J Biol Chem*, 271(51):33032–33038, Dec 1996. [Cited on page 28]
- [166] S. Q. Rice, C. Southan, H. F. Boyd, J. A. Terrett, C. H. MacPhee, K. Moores, I. S. Gloger, and D. G. Tew. Expression, purification and characterization of a human serine-dependent phospholipase A2 with high specificity for oxidized phospholipids and platelet activating factor. *Biochem J*, 330 (Pt 3):1309–1315, Mar 1998. [Cited on page 28]
- [167] D. K. Nomura and J. E. Casida. Lipases and their inhibitors in health and disease. *Chem Biol Interact*, 259(Pt B):211–222, Nov 2016. [Cited on page 28]

- [168] J. W. Chang, A. M. Zuhl, A. E. Speers, S. Niessen, S. J. Brown, M. M. Mulvihill, Y. C. Fan, T. P. Spicer, M. Southern, L. Scampavia, V. Fernandez-Vega, M. M. Dix, M. D. Cameron, P. S. Hodder, H. Rosen, D. K. Nomura, O. Kwon, K. L. Hsu, and B. F. Cravatt. Selective inhibitor of platelet-activating factor acetylhydrolases 1b2 and 1b3 that impairs cancer cell survival. *ACS Chem Biol*, 10(4):925–932, Apr 2015. [Cited on pages 28, 35, and 87]
- [169] K. Karasawa, M. Shirakura, A. Harada, N. Satoh, K. Yokoyama, M. Setaka, and K. Inoue. Red blood cells highly express type I platelet-activating factor-acetylhydrolase (PAF-AH) which consists of the alpha1/alpha2 complex. *J Biochem*, 138(4):509–517, Oct 2005. [Cited on page 28]
- [170] G. Zhou, G. K. Marathe, B. Willard, and T. M. McIntyre. Intracellular erythrocyte platelet-activating factor acetylhydrolase I inactivates aspirin in blood. *J Biol Chem*, 286(40):34820–34829, Oct 2011. [Cited on pages 28 and 35]
- [171] M. Hattori, H. Arai, and K. Inoue. Purification and characterization of bovine brain platelet-activating factor acetylhydrolase. *J Biol Chem*, 268(25):18748–18753, Sep 1993. [Cited on page 28]
- [172] K. Hattori, M. Hattori, H. Adachi, M. Tsujimoto, H. Arai, and K. Inoue. Purification and characterization of platelet-activating factor acetylhydrolase II from bovine liver cytosol. *J Biol Chem*, 270(38):22308–22313, Sep 1995. [Cited on page 28]
- [173] M. V. Winstead, J. Balsinde, and E. A. Dennis. Calcium-independent phospholipase A(2): structure and function. *Biochim Biophys Acta*, 1488(1-2):28–39, Oct 2000. [Cited on page 28]
- [174] Y. H. Hsu, J. E. Burke, D. L. Stephens, R. A. Deems, S. Li, K. M. Asmus, V. L. Woods, and E. A. Dennis. Calcium binding rigidifies the C2 domain and the intradomain interaction of GIVA phospholipase A2 as revealed by hydrogen/deuterium exchange mass spectrometry. *J Biol Chem*, 283(15):9820–9827, Apr 2008. [Cited on page 28]
- [175] J. Huber, A. Fürnkranz, V. N. Bochkov, M. K. Patricia, H. Lee, C. C. Hedrick, J. A. Berliner, B. R. Binder, and N. Leitinger. Specific monocyte adhesion to endothelial cells induced by oxidized phospholipids involves activation of cPLA2 and lipoxygenase. *J Lipid Res*, 47(5):1054–1062, May 2006. [Cited on page 28]
- [176] L. A. Trimble, I. P. Street, H. Perrier, N. M. Tremblay, P. K. Weech, and M. A. Bernstein. NMR structural studies of the tight complex between a trifluoromethyl ketone inhibitor and the 85-kDa human phospholipase A2. *Biochemistry*, 32(47):12560–12565, Nov 1993. [Cited on page 28]
- [177] I. P. Street, H. K. Lin, F. Laliberté, F. Ghomashchi, Z. Wang, H. Perrier, N. M. Tremblay, Z. Huang, P. K. Weech, and M. H. Gelb. Slow- and tight-binding inhibitors of the 85-kDa human phospholipase A2. *Biochemistry*, 32(23):5935–5940, Jun 1993. [Cited on page 28]
- [178] I. Walters, C. Bennion, S. Connolly, P. J. Croshaw, K. Hardy, P. Hartopp, C. G. Jackson, S. J. King, L. Lawrence, A. Mete, D. Murray, D. H. Robinson, L. Stein, E. Wells, and W. John Withnall. Synthesis and evaluation of substrate-mimicking cytosolic phospholipase A2 inhibitors—reducing the lipophilicity of the arachidonyl chain isostere. *Bioorg Med Chem Lett*, 14(14):3645–3649, Jul 2004. [Cited on page 28]

- [179] H. S. Hoover, J. L. Blankman, S. Niessen, and B. F. Cravatt. Selectivity of inhibitors of endocannabinoid biosynthesis evaluated by activity-based protein profiling. *Bioorg Med Chem Lett*, 18(22):5838–5841, Nov 2008. [Cited on pages 28 and 30]
- [180] R. H. Schaloske and E. A. Dennis. The phospholipase A2 superfamily and its group numbering system. *Biochim Biophys Acta*, 1761(11):1246–1259, Nov 2006. [Cited on pages 28 and 29]
- [181] S. K. Wilson and L. J. Knoll. Patatin-like phospholipases in microbial infections with emerging roles in fatty acid metabolism and immune regulation by Apicomplexa. *Mol Microbiol*, 107(1):34–46, Jan 2018. [Cited on pages 28, 35, 65, and 86]
- [182] Y. C. Lio, L. J. Reynolds, J. Balsinde, and E. A. Dennis. Irreversible inhibition of Ca(2+)-independent phospholipase A2 by methyl arachidonyl fluorophosphonate. *Biochim Biophys Acta*, 1302(1):55–60, Jul 1996. [Cited on page 28]
- [183] P. Sartipy, G. Camejo, L. Svensson, and E. Hurt-Camejo. Phospholipase A2 modification of lipoproteins: potential effects on atherogenesis. *Adv Exp Med Biol*, 507:3–7, 2002. [Cited on page 29]
- [184] No authors listed. Varespladib. *Am J Cardiovasc Drugs*, 11(2):137–143, 2011. [Cited on page 29]
- [185] J. A. Shayman and J. J. G. Tesmer. Lysosomal phospholipase A2. *Biochim Biophys Acta Mol Cell Biol Lipids*, 1864(6):932–940, 06 2019. [Cited on pages 29 and 31]
- [186] A. Abe, M. Hiraoka, H. Ohguro, J. J. Tesmer, and J. A. Shayman. Preferential hydrolysis of truncated oxidized glycerophospholipids by lysosomal phospholipase A2. *J Lipid Res*, 58(2):339–349, 02 2017. [Cited on pages 29 and 31]
- [187] A. Glukhova, V. Hinkovska-Galcheva, R. Kelly, A. Abe, J. A. Shayman, and J. J. Tesmer. Structure and function of lysosomal phospholipase A2 and lecithin:cholesterol acyltransferase. *Nat Commun*, 6:6250, Mar 2015. [Cited on page 29]
- [188] Y. Nagata, Y. Yamamoto, and E. Niki. Reaction of phosphatidylcholine hydroperoxide in human plasma: the role of peroxidase and lecithin:cholesterol acyltransferase. *Arch Biochem Biophys*, 329(1):24–30, May 1996. [Cited on page 29]
- [189] D. E. Piper, W. G. Romanow, R. N. Gunawardane, P. Fordstrom, S. Masterman, O. Pan, S. T. Thibault, R. Zhang, D. Meininger, M. Schwarz, Z. Wang, C. King, M. Zhou, and N. P. Walker. The high-resolution crystal structure of human LCAT. *J Lipid Res*, 56(9):1711–1719, Sep 2015. [Cited on page 29]
- [190] J. Goyal, K. Wang, M. Liu, and P. V. Subbaiah. Novel function of lecithin-cholesterol acyltransferase. Hydrolysis of oxidized polar phospholipids generated during lipoprotein oxidation. *J Biol Chem*, 272(26):16231–16239, Jun 1997. [Cited on page 29]
- [191] V. S. Subramanian, J. Goyal, M. Miwa, J. Sugatami, M. Akiyama, M. Liu, and P. V. Subbaiah. Role of lecithin-cholesterol acyltransferase in the metabolism of oxidized phospholipids in plasma: studies with platelet-activating factor-acetyl hydrolase-deficient plasma. *Biochim Biophys Acta*, 1439(1):95–109, Jul 1999. [Cited on page 29]

- [192] J. W. Chen, C. Dodia, S. I. Feinstein, M. K. Jain, and A. B. Fisher. 1-Cys peroxiredoxin, a bifunctional enzyme with glutathione peroxidase and phospholipase A2 activities. *J Biol Chem*, 275(37):28421–28427, Sep 2000. [Cited on pages 29 and 31]
- [193] P. J. Leavey, C. Gonzalez-Aller, G. Thurman, M. Kleinberg, L. Rinckel, D. W. Ambruso, S. Freeman, F. A. Kuypers, and D. R. Ambruso. A 29-kDa protein associated with p67phox expresses both peroxiredoxin and phospholipase A2 activity and enhances superoxide anion production by a cell-free system of NADPH oxidase activity. *J Biol Chem*, 277(47):45181–45187, Nov 2002. [Cited on pages 29 and 30]
- [194] H. Li, B. Benipal, S. Zhou, C. Dodia, S. Chatterjee, J. Q. Tao, E. M. Sorokina, T. Raabe, S. I. Feinstein, and A. B. Fisher. Critical role of peroxiredoxin 6 in the repair of peroxidized cell membranes following oxidative stress. *Free Radic Biol Med*, 87:356–365, Oct 2015. [Cited on pages 29, 30, 31, and 32]
- [195] Y. C. Lien, S. I. Feinstein, C. Dodia, and A. B. Fisher. The roles of peroxidase and phospholipase A2 activities of peroxiredoxin 6 in protecting pulmonary microvascular endothelial cells against peroxidative stress. *Antioxid Redox Signal*, 16(5):440–451, Mar 2012. [Cited on pages 30 and 31]
- [196] Y. Manevich, K. S. Reddy, T. Shuvaeva, S. I. Feinstein, and A. B. Fisher. Structure and phospholipase function of peroxiredoxin 6: identification of the catalytic triad and its role in phospholipid substrate binding. *J Lipid Res*, 48(10):2306–2318, Oct 2007. [Cited on page 30]
- [197] S. Akiba, C. Dodia, X. Chen, and A. B. Fisher. Characterization of acidic Ca(2+)-independent phospholipase A2 of bovine lung. *Comp Biochem Physiol B Biochem Mol Biol*, 120(2):393–404, Jun 1998. [Cited on page 30]
- [198] Y. Wu, S. I. Feinstein, Y. Manevich, I. Chowdhury, J. H. Pak, A. Kazi, C. Dodia, D. W. Speicher, and A. B. Fisher. Mitogen-activated protein kinase-mediated phosphorylation of peroxiredoxin 6 regulates its phospholipase A(2) activity. *Biochem J*, 419(3):669–679, May 2009. [Cited on pages 30, 31, 48, and 67]
- [199] B. F. Cravatt, A. T. Wright, and J. W. Kozarich. Activity-based protein profiling: from enzyme chemistry to proteomic chemistry. *Annu Rev Biochem*, 77:383–414, 2008. [Cited on pages 30 and 67]
- [200] K. H. Kim, W. Lee, and E. E. Kim. Crystal structures of human peroxiredoxin 6 in different oxidation states. *Biochem Biophys Res Commun*, 477(4):717–722, 09 2016. [Cited on pages 30, 47, and 90]
- [201] A. B. Fisher, C. Dodia, Y. Manevich, J. W. Chen, and S. I. Feinstein. Phospholipid hydroperoxides are substrates for non-selenium glutathione peroxidase. *J Biol Chem*, 274(30):21326–21334, Jul 1999. [Cited on page 31]
- [202] S. Y. Kim, H. Y. Jo, M. H. Kim, Y. Y. Cha, S. W. Choi, J. H. Shim, T. J. Kim, and K. Y. Lee. H₂O₂-dependent hyperoxidation of peroxiredoxin 6 (Prdx6) plays a role in cellular toxicity via up-regulation of iPLA2 activity. *J Biol Chem*, 283(48):33563–33568, Nov 2008. [Cited on page 31]

- [203] S. Shahnaj, R. K. Chowhan, P. A. Meetei, P. Kakchingtabam, K. Herojit Singh, L. Rajendrakumar Singh, P. Nongdam, A. B. Fisher, and H. Rahaman. Hyperoxidation of Peroxiredoxin 6 Induces Alteration from Dimeric to Oligomeric State. *Antioxidants (Basel)*, 8(2), Feb 2019. [Cited on page 31]
- [204] H. Rahaman, S. Zhou, C. Dodia, S. I. Feinstein, S. Huang, D. Speicher, and A. B. Fisher. Increased phospholipase A2 activity with phosphorylation of peroxiredoxin 6 requires a conformational change in the protein. *Biochemistry*, 51(27):5521–5530, Jul 2012. [Cited on page 31]
- [205] S. Zhou, E. M. Sorokina, S. Harper, H. Li, L. Ralat, C. Dodia, D. W. Speicher, S. I. Feinstein, and A. B. Fisher. Peroxiredoxin 6 homodimerization and heterodimerization with glutathione S-transferase pi are required for its peroxidase but not phospholipase A2 activity. *Free Radic Biol Med*, 94:145–156, 05 2016. [Cited on page 31]
- [206] A. B. Fisher, C. Dodia, A. Chander, and M. Jain. A competitive inhibitor of phospholipase A2 decreases surfactant phosphatidylcholine degradation by the rat lung. *Biochem J*, 288 (Pt 2):407–411, Dec 1992. [Cited on page 31]
- [207] M. K. Jain, W. J. Tao, J. Rogers, C. Arenson, H. Eibl, and B. Z. Yu. Active-site-directed specific competitive inhibitors of phospholipase A2: novel transition-state analogues. *Biochemistry*, 30(42):10256–10268, Oct 1991. [Cited on page 31]
- [208] A. B. Fisher, C. Dodia, and A. Chander. Inhibition of lung calcium-independent phospholipase A2 by surfactant protein A. *Am J Physiol*, 267(3 Pt 1):L335–341, Sep 1994. [Cited on pages 31 and 48]
- [209] S. W. Kang, I. C. Baines, and S. G. Rhee. Characterization of a mammalian peroxiredoxin that contains one conserved cysteine. *J Biol Chem*, 273(11):6303–6311, Mar 1998. [Cited on page 31]
- [210] S. Chatterjee, S. I. Feinstein, C. Dodia, E. Sorokina, Y. C. Lien, S. Nguyen, K. Debolt, D. Speicher, and A. B. Fisher. Peroxiredoxin 6 phosphorylation and subsequent phospholipase A2 activity are required for agonist-mediated activation of NADPH oxidase in mouse pulmonary microvascular endothelium and alveolar macrophages. *J Biol Chem*, 286(13):11696–11706, Apr 2011. [Cited on page 32]
- [211] D. R. Ambruso, M. A. Ellison, G. W. Thurman, and T. L. Leto. Peroxiredoxin 6 translocates to the plasma membrane during neutrophil activation and is required for optimal NADPH oxidase activity. *Biochim Biophys Acta*, 1823(2):306–315, Feb 2012. [Cited on page 32]
- [212] K. M. Holmström and T. Finkel. Cellular mechanisms and physiological consequences of redox-dependent signalling. *Nat Rev Mol Cell Biol*, 15(6):411–421, Jun 2014. [Cited on page 32]
- [213] A. R. Moawad, M. C. Fernandez, E. Scarlata, C. Dodia, S. I. Feinstein, A. B. Fisher, and C. O’Flaherty. Deficiency of peroxiredoxin 6 or inhibition of its phospholipase A2 activity impair the in vitro sperm fertilizing competence in mice. *Sci Rep*, 7(1):12994, 10 2017. [Cited on page 32]

- [214] S. Gong, M. C. San Gabriel, A. Zini, P. Chan, and C. O’Flaherty. Low amounts and high thiol oxidation of peroxiredoxins in spermatozoa from infertile men. *J Androl*, 33(6):1342–1351, 2012. [Cited on page 32]
- [215] F. Pacifici, R. Arriga, G. P. Sorice, B. Capuani, M. G. Scioli, D. Pastore, G. Donadel, A. Bellia, S. Caratelli, A. Coppola, F. Ferrelli, M. Federici, G. Sconocchia, M. Tesauero, P. Sbraccia, D. Della-Morte, A. Giaccari, A. Orlandi, and D. Lauro. Peroxiredoxin 6, a novel player in the pathogenesis of diabetes. *Diabetes*, 63(10):3210–3220, Oct 2014. [Cited on page 32]
- [216] E. G. Novoselova, O. V. Glushkova, S. M. Lunin, M. O. Khrenov, S. B. Parfenyuk, T. V. Novoselova, M. G. Sharapov, A. E. Gordeeva, V. I. Novoselov, and E. E. Fesenko. Thymulin and peroxiredoxin 6 have protective effects against streptozotocin-induced type 1 diabetes in mice. *Int J Immunopathol Pharmacol*, 35:20587384211005645, 2021. [Cited on page 32]
- [217] A. Nicolussi, S. D’Inzeo, C. Capalbo, G. Giannini, and A. Coppa. The role of peroxiredoxins in cancer. *Mol Clin Oncol*, 6(2):139–153, Feb 2017. [Cited on pages 32, 33, and 102]
- [218] W. S. Huang, C. Y. Huang, M. C. Hsieh, Y. H. Kuo, S. Y. Tung, C. H. Shen, Y. Y. Hsieh, C. C. Teng, K. C. Lee, K. F. Lee, and H. C. Kuo. Expression of PRDX6 Correlates with Migration and Invasiveness of Colorectal Cancer Cells. *Cell Physiol Biochem*, 51(6):2616–2630, 2018. [Cited on pages 32 and 102]
- [219] G. Wang, W. C. Zhong, Y. H. Bi, S. Y. Tao, H. Zhu, H. X. Zhu, and A. M. Xu. The Prognosis Of Peroxiredoxin Family In Breast Cancer. *Cancer Manag Res*, 11:9685–9699, 2019. [Cited on pages 32 and 102]
- [220] M. J. López-Grueso, D. J. Lagal, Á. F. García-Jiménez, R. M. Tarradas, B. Carmona-Hidalgo, J. Peinado, R. Requejo-Aguilar, J. A. Bárcena, and C. A. Padilla. Knockout of PRDX6 induces mitochondrial dysfunction and cell cycle arrest at G2/M in HepG2 hepatocarcinoma cells. *Redox Biol*, 37:101737, 10 2020. [Cited on pages 32 and 102]
- [221] S. Li, X. Hu, M. Ye, and X. Zhu. The prognostic values of the peroxiredoxins family in ovarian cancer. *Biosci Rep*, 38(5), 10 2018. [Cited on pages 32 and 102]
- [222] M. Jo, H. M. Yun, K. R. Park, M. Hee Park, T. Myoung Kim, J. Ho Pak, S. Jae Lee, D. C. Moon, C. W. Park, S. Song, C. K. Lee, S. Bae Han, and J. Tae Hong. Lung tumor growth-promoting function of peroxiredoxin 6. *Free Radic Biol Med*, 61:453–463, Aug 2013. [Cited on pages 32 and 102]
- [223] G. Y. Liou and P. Storz. Reactive oxygen species in cancer. *Free Radic Res*, 44(5):479–496, May 2010. [Cited on pages 32 and 102]
- [224] J. S. Clerkin, R. Naughton, C. Quiney, and T. G. Cotter. Mechanisms of ROS modulated cell survival during carcinogenesis. *Cancer Lett*, 266(1):30–36, Jul 2008. [Cited on page 32]
- [225] F. Rolfs, M. Huber, F. Gruber, F. Böhm, H. J. Pfister, V. N. Bochkov, E. Tschachler, R. Dummer, D. Hohl, M. Schäfer, and S. Werner. Dual role of the antioxidant enzyme peroxiredoxin 6 in skin carcinogenesis. *Cancer Res*, 73(11):3460–3469, Jun 2013. [Cited on page 33]

- [226] Y. Mo, S. I. Feinstein, Y. Manevich, Q. Zhang, L. Lu, Y. S. Ho, and A. B. Fisher. 1-Cys peroxiredoxin knock-out mice express mRNA but not protein for a highly related intronless gene. *FEBS Lett*, 555(2):192–198, Dec 2003. [Cited on pages 33, 40, and 92]
- [227] E. Scarlata, M. C. Fernandez, and C. O’Flaherty. A Novel Combination of gamma-Tocopherol-Rich Mixture of Tocopherols and Ascorbic Acid Restores Fertility in Cases of Tyrosine Nitration-Associated Male Infertility in Mice. *Antioxidants (Basel)*, 9(7), Jul 2020. [Cited on page 33]
- [228] J. P. Vázquez-Medina, J. Q. Tao, P. Patel, R. Bannitz-Fernandes, C. Dodia, E. M. Sorokina, S. I. Feinstein, S. Chatterjee, and A. B. Fisher. Genetic inactivation of the phospholipase A2 activity of peroxiredoxin 6 in mice protects against LPS-induced acute lung injury. *Am J Physiol Lung Cell Mol Physiol*, 316(4):L656–L668, 04 2019. [Cited on page 33]
- [229] S. I. Feinstein. Mouse Models of Genetically Altered Peroxiredoxin 6. *Antioxidants (Basel)*, 8(4), Mar 2019. [Cited on pages 33, 92, and 101]
- [230] M. Rushefski, R. Aplenc, N. Meyer, M. Li, R. Feng, P. N. Lancken, R. Gallop, S. Bellamy, A. R. Localio, S. I. Feinstein, A. B. Fisher, S. M. Albelda, and J. D. Christie. Novel variants in the PRDX6 Gene and the risk of Acute Lung Injury following major trauma. *BMC Med Genet*, 12:77, May 2011. [Cited on page 33]
- [231] R. A. C. Sussmann, W. L. Fotoran, E. A. Kimura, and A. M. Katzin. Plasmodium falciparum uses vitamin E to avoid oxidative stress. *Parasit Vectors*, 10(1):461, Oct 2017. [Cited on pages 33 and 34]
- [232] S. Fritsche, X. Wang, and C. Jung. Recent Advances in our Understanding of Tocopherol Biosynthesis in Plants: An Overview of Key Genes, Functions, and Breeding of Vitamin E Improved Crops. *Antioxidants (Basel)*, 6(4), Dec 2017. [Cited on page 33]
- [233] R. A. Sussmann, C. B. Angeli, V. J. Peres, E. A. Kimura, and A. M. Katzin. Intraerythrocytic stages of Plasmodium falciparum biosynthesize vitamin E. *FEBS Lett*, 585(24):3985–3991, Dec 2011. [Cited on page 33]
- [234] A. Mellors and A. L. Tappel. Quinones and quinols as inhibitors of lipid peroxidation. *Lipids*, 1(4):282–284, Jul 1966. [Cited on page 34]
- [235] P. Niklowitz, A. Sonnenschein, B. Janetzky, W. Andler, and T. Menke. Enrichment of coenzyme Q10 in plasma and blood cells: defense against oxidative damage. *Int J Biol Sci*, 3(4):257–262, Apr 2007. [Cited on page 34]
- [236] G. P. Littarru, M. Battino, M. Tomasetti, A. Mordente, S. Santini, A. Oradei, A. Manto, and G. Ghirlanda. Metabolic implications of coenzyme Q10 in red blood cells and plasma lipoproteins. *Mol Aspects Med*, 15 Suppl:67–72, 1994. [Cited on page 34]
- [237] R. Skouta, S. J. Dixon, J. Wang, D. E. Dunn, M. Orman, K. Shimada, P. A. Rosenberg, D. C. Lo, J. M. Weinberg, A. Linkermann, and B. R. Stockwell. Ferrostatins inhibit oxidative lipid damage and cell death in diverse disease models. *J Am Chem Soc*, 136(12):4551–4556, Mar 2014. [Cited on page 34]

- [238] E. F. Gautier, M. Leduc, S. Cochet, K. Bailly, C. Lacombe, N. Mohandas, F. Guillonnet, W. El Nemer, and P. Mayeux. Absolute proteome quantification of highly purified populations of circulating reticulocytes and mature erythrocytes. *Blood Adv*, 2(20):2646–2657, Oct 2018. [Cited on pages 34, 35, 63, 66, and 87]
- [239] S. G. Rhee, H. Z. Chae, and K. Kim. Peroxiredoxins: a historical overview and speculative preview of novel mechanisms and emerging concepts in cell signaling. *Free Radic Biol Med*, 38(12):1543–1552, Jun 2005. [Cited on page 34]
- [240] A. Perkins, K. J. Nelson, D. Parsonage, L. B. Poole, and P. A. Karplus. Peroxiredoxins: guardians against oxidative stress and modulators of peroxide signaling. *Trends Biochem Sci*, 40(8):435–445, Aug 2015. [Cited on page 34]
- [241] Qitao Ran and Hanyu Liang. *The Use of Gpx4 Knockout Mice and Transgenic Mice to Study the Roles of Lipid Peroxidation in Diseases and Aging*, pages 265–278. Humana Press, Totowa, NJ, 2011. [Cited on pages 34, 66, and 87]
- [242] S. Tiwari, N. Sharma, G. P. Sharma, and N. Mishra. Redox interactome in malaria parasite *Plasmodium falciparum*. *Parasitol Res*, 120(2):423–434, Feb 2021. [Cited on pages 34 and 36]
- [243] K. Becker, S. M. Kanzok, R. Iozef, M. Fischer, R. H. Schirmer, and S. Rahlfs. Plasmoredoxin, a novel redox-active protein unique for malarial parasites. *Eur J Biochem*, 270(6):1057–1064, Mar 2003. [Cited on page 34]
- [244] E. Jortzik and K. Becker. Thioredoxin and glutathione systems in *Plasmodium falciparum*. *Int J Med Microbiol*, 302(4-5):187–194, Oct 2012. [Cited on page 34]
- [245] S. Müller. Role and Regulation of Glutathione Metabolism in *Plasmodium falciparum*. *Molecules*, 20(6):10511–10534, Jun 2015. [Cited on page 34]
- [246] R. Chaudhari, S. Sharma, and S. Patankar. Glutathione and thioredoxin systems of the malaria parasite *Plasmodium falciparum*: Partners in crime? *Biochem Biophys Res Commun*, 488(1):95–100, 06 2017. [Cited on page 34]
- [247] S. Rahlfs, M. Fischer, and K. Becker. *Plasmodium falciparum* possesses a classical glutaredoxin and a second, glutaredoxin-like protein with a PICOT homology domain. *J Biol Chem*, 276(40):37133–37140, Oct 2001. [Cited on page 34]
- [248] S. Kawazu, N. Tsuji, T. Hatabu, S. Kawai, Y. Matsumoto, and S. Kano. Molecular cloning and characterization of a peroxiredoxin from the human malaria parasite *Plasmodium falciparum*. *Mol Biochem Parasitol*, 109(2):165–169, Jul 2000. [Cited on page 34]
- [249] R. J. Richardson, N. D. Hein, S. J. Wijeyesakere, J. K. Fink, and G. F. Makhaeva. Neuropathy target esterase (NTE): overview and future. *Chem Biol Interact*, 203(1):238–244, Mar 2013. [Cited on pages 35 and 87]
- [250] P. Singh, A. Alaganan, K. R. More, A. Lorthiois, S. Thiberge, O. Gorgette, M. Guillotte Blisnick, J. Guglielmini, S. S. Aguilera, L. Touqui, S. Singh, and C. E. Chitnis. Role of a patatin-like phospholipase in *Plasmodium falciparum* gametogenesis and malaria transmission. *Proc Natl Acad Sci U S A*, 116(35):17498–17508, 08 2019. [Cited on pages 35, 36, and 84]

- [251] P. C. Burda, M. A. Roelli, M. Schaffner, S. M. Khan, C. J. Janse, and V. T. Heussler. A Plasmodium phospholipase is involved in disruption of the liver stage parasitophorous vacuole membrane. *PLoS Pathog*, 11(3):e1004760, Mar 2015. [Cited on page 35]
- [252] L. D. Saffer and J. D. Schwartzman. A soluble phospholipase of *Toxoplasma gondii* associated with host cell penetration. *J Protozool*, 38(5):454–460, 1991. [Cited on page 35]
- [253] S. Cassaing, J. Fauvel, M. H. Bessières, S. Guy, J. P. Séguéla, and H. Chap. *Toxoplasma gondii* secretes a calcium-independent phospholipase A(2). *Int J Parasitol*, 30(11):1137–1142, Oct 2000. [Cited on page 35]
- [254] M. F. Lévêque, L. Berry, Y. Yamaryo-Botté, H. M. Nguyen, M. Galera, C. Y. Botté, and S. Besteiro. TgPL2, a patatin-like phospholipase domain-containing protein, is involved in the maintenance of apicoplast lipids homeostasis in *Toxoplasma*. *Mol Microbiol*, 105(1):158–174, 07 2017. [Cited on page 35]
- [255] S. K. Wilson, J. Heckendorn, B. Martorelli Di Genova, L. L. Koch, P. J. Rooney, N. Morrisette, M. Lebrun, and L. J. Knoll. A *Toxoplasma gondii* patatin-like phospholipase contributes to host cell invasion. *PLoS Pathog*, 16(7):e1008650, 07 2020. [Cited on page 35]
- [256] R. C. Pollok, V. McDonald, P. Kelly, and M. J. Farthing. The role of *Cryptosporidium parvum*-derived phospholipase in intestinal epithelial cell invasion. *Parasitol Res*, 90(3):181–186, Jun 2003. [Cited on page 35]
- [257] M. C. Pawlowic and K. Zhang. *Leishmania* parasites possess a platelet-activating factor acetylhydrolase important for virulence. *Mol Biochem Parasitol*, 186(1):11–20, Nov 2012. [Cited on page 35]
- [258] M. L. A. C. Bordon, M. D. Laurenti, S. P. Ribeiro, M. H. Toyama, D. O. Toyama, and L. F. D. Passero. Effect of phospholipase A2 inhibitors during infection caused by *Leishmania (Leishmania) amazonensis*. *J Venom Anim Toxins Incl Trop Dis*, 24:21, 2018. [Cited on page 35]
- [259] A. C. S. Fernandes, D. C. Soares, R. F. C. Neves, C. M. Koeller, N. Heise, C. M. Adade, S. Frases, J. R. Meyer-Fernandes, E. M. Saraiva, and T. Souto-Pradrón. Endocytosis and Exocytosis in *Leishmania amazonensis* Are Modulated by Bromoenol Lactone. *Front Cell Infect Microbiol*, 10:39, 2020. [Cited on page 35]
- [260] M. L. Belaunzarán, E. M. Lammel, and E. L. de Isola. Phospholipases a in trypanosomatids. *Enzyme Res*, 2011:392082, 2011. [Cited on page 35]
- [261] H. Atamna and H. Ginsburg. The malaria parasite supplies glutathione to its host cell—investigation of glutathione transport and metabolism in human erythrocytes infected with *Plasmodium falciparum*. *Eur J Biochem*, 250(3):670–679, Dec 1997. [Cited on page 36]
- [262] S. Koncarevic, P. Rohrbach, M. Deponte, G. Krohne, J. H. Prieto, J. Yates, S. Rahlfs, and K. Becker. The malarial parasite *Plasmodium falciparum* imports the human protein peroxiredoxin 2 for peroxide detoxification. *Proc Natl Acad Sci U S A*, 106(32):13323–13328, Aug 2009. [Cited on pages 36, 37, 72, 83, and 95]

- [263] F. Mi-Ichi, S. Kano, and T. Mitamura. Oleic acid is indispensable for intraerythrocytic proliferation of *Plasmodium falciparum*. *Parasitology*, 134(Pt 12):1671–1677, Nov 2007. [Cited on pages 36, 63, and 86]
- [264] S. Gulati, E. H. Ekland, K. V. Ruggles, R. B. Chan, B. Jayabalasingham, B. Zhou, P. Y. Mantel, M. C. Lee, N. Spottiswoode, O. Coburn-Flynn, D. Hjelmqvist, T. S. Worgall, M. Marti, G. Di Paolo, and D. A. Fidock. Profiling the Essential Nature of Lipid Metabolism in Asexual Blood and Gametocyte Stages of *Plasmodium falciparum*. *Cell Host Microbe*, 18(3):371–381, Sep 2015. [Cited on pages 36, 37, 83, and 86]
- [265] Y. P. van der Meer-Janssen, J. van Galen, J. J. Batenburg, and J. B. Helms. Lipids in host-pathogen interactions: pathogens exploit the complexity of the host cell lipodome. *Prog Lipid Res*, 49(1):1–26, Jan 2010. [Cited on pages 36 and 37]
- [266] N. M. B. Brancucci, J. P. Gerdt, C. Wang, M. De Niz, N. Philip, S. R. Adapa, M. Zhang, E. Hitz, I. Niederwieser, S. D. Boltryk, M. C. Laffitte, M. A. Clark, C. Grüring, D. Ravel, A. Blancke Soares, A. Demas, S. Bopp, B. Rubio-Ruiz, A. Conejo-Garcia, D. F. Wirth, E. Gendaszewska-Darmach, M. T. Duraisingh, J. H. Adams, T. S. Voss, A. P. Waters, R. H. Y. Jiang, J. Clardy, and M. Marti. Lysophosphatidylcholine Regulates Sexual Stage Differentiation in the Human Malaria Parasite *Plasmodium falciparum*. *Cell*, 171(7):1532–1544, Dec 2017. [Cited on pages 37, 83, and 92]
- [267] C. Ben Mamoun, S. T. Prigge, and H. Vial. Targeting the Lipid Metabolic Pathways for the Treatment of Malaria. *Drug Dev Res*, 71(1):44–55, Feb 2010. [Cited on pages 37 and 83]
- [268] T. Ishino, Y. Orito, Y. Chinzei, and M. Yuda. A calcium-dependent protein kinase regulates *Plasmodium* ookinete access to the midgut epithelial cell. *Mol Microbiol*, 59(4):1175–1184, Feb 2006. [Cited on pages 39 and 50]
- [269] Y. C. Peng, Y. Qi, C. Zhang, X. Yao, J. Wu, S. Pattaradilokrat, L. Xia, K. C. Tumas, X. He, T. Ishizaki, C. F. Qi, A. A. Holder, T. G. Myers, C. A. Long, O. Kaneko, J. Li, and X. Z. Su. *Plasmodium yoelii* Erythrocyte-Binding-like Protein Modulates Host Cell Membrane Structure, Immunity, and Disease Severity. *mBio*, 11(1), 01 2020. [Cited on pages 39 and 50]
- [270] W. Trager and J. B. Jensen. Human malaria parasites in continuous culture. *Science*, 193(4254):673–675, Aug 1976. [Cited on page 41]
- [271] C. Lambros and J. P. Vanderberg. Synchronization of *Plasmodium falciparum* erythrocytic stages in culture. *J. Parasitol.*, 65(3):418–420, Jun 1979. [Cited on page 42]
- [272] A. R. Dluzewski, I. T. Ling, K. Rangachari, P. A. Bates, and R. J. Wilson. A simple method for isolating viable mature parasites of *Plasmodium falciparum* from cultures. *Trans. R. Soc. Trop. Med. Hyg.*, 78(5):622–624, 1984. [Cited on page 42]
- [273] B. T. Grimberg. Methodology and application of flow cytometry for investigation of human malaria parasites. *J. Immunol. Methods*, 367(1-2):1–16, Mar 2011. [Cited on pages 43 and 83]
- [274] S. Izumiyama, M. Omura, T. Takasaki, H. Ohmae, and H. Asahi. *Plasmodium falciparum*: development and validation of a measure of intraerythrocytic growth using SYBR Green I in a flow cytometer. *Exp. Parasitol.*, 121(2):144–150, Feb 2009. [Cited on page 43]

- [275] B. Witkowski, C. Amaratunga, N. Khim, S. Sreng, P. Chim, S. Kim, P. Lim, S. Mao, C. Sopha, B. Sam, J. M. Anderson, S. Duong, C. M. Chuor, W. R. Taylor, S. Suon, O. Mercereau-Puijalon, R. M. Fairhurst, and D. Menard. Novel phenotypic assays for the detection of artemisinin-resistant *Plasmodium falciparum* malaria in Cambodia: in-vitro and ex-vivo drug-response studies. *Lancet Infect Dis*, 13(12):1043–1049, Dec 2013. [Cited on page 45]
- [276] M. Jemaà, M. Fezai, R. Bissinger, and F. Lang. Methods Employed in Cytofluorometric Assessment of Eryptosis, the Suicidal Erythrocyte Death. *Cell Physiol Biochem*, 43(2):431–444, 2017. [Cited on page 46]
- [277] J. Pikul and D. E. Leszczynski. Butylated hydroxytoluene addition improves the thiobarbituric acid assay for malonaldehyde from chicken plasma fat. *Nahrung*, 30(7):673–678, 1986. [Cited on page 46]
- [278] C. Aurrecochea, J. Brestelli, B. P. Brunk, J. Dommer, S. Fischer, B. Gajria, X. Gao, A. Gingle, G. Grant, O. S. Harb, M. Heiges, F. Innamorato, J. Iodice, J. C. Kissinger, E. Kraemer, W. Li, J. A. Miller, V. Nayak, C. Pennington, D. F. Pinney, D. S. Roos, C. Ross, C. J. Stoeckert, C. Treatman, and H. Wang. PlasmoDB: a functional genomic database for malaria parasites. *Nucleic Acids Res*, 37(Database issue):D539–543, Jan 2009. [Cited on page 47]
- [279] M. T. Makler and D. J. Hinrichs. Measurement of the lactate dehydrogenase activity of *Plasmodium falciparum* as an assessment of parasitemia. *Am J Trop Med Hyg*, 48(2):205–210, Feb 1993. [Cited on page 48]
- [280] M. M. Nachlas, S. I. Margulies, J. D. Goldberg, and A. M. Seligman. The determination of lactic dehydrogenase with a tetrazolium salt. *Anal Biochem*, 1:317–326, Dec 1960. [Cited on page 48]
- [281] M. Katsumata, C. Gupta, and A. S. Goldman. A rapid assay for activity of phospholipase A2 using radioactive substrate. *Anal Biochem*, 154(2):676–681, May 1986. [Cited on page 48]
- [282] L. J. Tong, L. W. Dong, and M. S. Liu. GTP-binding protein mediated phospholipase A2 activation in rat liver during the progression of sepsis. *Mol Cell Biochem*, 189(1-2):55–61, Dec 1998. [Cited on page 49]
- [283] J. M. Nagano, K. L. Hsu, L. R. Whitby, M. J. Niphakis, A. E. Speers, S. J. Brown, T. Spicer, V. Fernandez-Vega, J. Ferguson, P. Hodder, P. Srinivasan, T. D. Gonzalez, H. Rosen, B. J. Bahnon, and B. F. Cravatt. Selective inhibitors and tailored activity probes for lipoprotein-associated phospholipase A(2). *Bioorg Med Chem Lett*, 23(3):839–843, Feb 2013. [Cited on page 49]
- [284] R. Quiroga and M. A. Villarreal. Vinardo: A Scoring Function Based on Autodock Vina Improves Scoring, Docking, and Virtual Screening. *PLoS One*, 11(5):e0155183, 2016. [Cited on page 49]
- [285] Z. W. Chang, B. Malleret, B. Russell, L. Rénia, and C. Claser. Ex Vivo Maturation Assay for Testing Antimalarial Sensitivity of Rodent Malaria Parasites. *Antimicrob Agents Chemother*, 60(11):6859–6866, 11 2016. [Cited on pages 50 and 94]

- [286] C. J. Tonkin, G. G. van Dooren, T. P. Spurck, N. S. Struck, R. T. Good, E. Handman, A. F. Cowman, and G. I. McFadden. Localization of organellar proteins in *Plasmodium falciparum* using a novel set of transfection vectors and a new immunofluorescence fixation method. *Mol Biochem Parasitol*, 137(1):13–21, Sep 2004. [Cited on page 51]
- [287] Y. Z. Wu, M. Abolhassani, M. Ollero, F. Dif, N. Uozumi, M. Lagranderie, T. Shimizu, M. Chignard, and L. Touqui. Cytosolic phospholipase A2alpha mediates *Pseudomonas aeruginosa* LPS-induced airway constriction of CFTR $-/-$ mice. *Respir Res*, 11:49, Apr 2010. [Cited on page 63]
- [288] T. Tougan, J. R. Edula, M. Morita, E. Takashima, H. Honma, T. Tsuboi, and T. Horii. The malaria parasite *Plasmodium falciparum* in red blood cells selectively takes up serum proteins that affect host pathogenicity. *Malar J*, 19(1):155, Apr 2020. [Cited on pages 63 and 87]
- [289] Y. Sun, S. Yin, Y. Feng, J. Li, J. Zhou, C. Liu, G. Zhu, and Z. Guo. Molecular basis of the general base catalysis of an alpha/beta-hydrolase catalytic triad. *J Biol Chem*, 289(22):15867–15879, May 2014. [Cited on page 67]
- [290] Q. Liu, X. Chen, W. Chen, X. Yuan, H. Su, J. Shen, and Y. Xu. Structural and Thermodynamic Characterization of Protein-Ligand Interactions Formed between Lipoprotein-Associated Phospholipase A2 and Inhibitors. *J Med Chem*, 59(10):5115–5120, 05 2016. [Cited on pages 70 and 90]
- [291] H. Melhem, M. R. Spalinger, J. Cosin-Roger, K. Atrott, S. Lang, K. A. Wojtal, S. R. Vavricka, G. Rogler, and I. Frey-Wagner. Prdx6 Deficiency Ameliorates DSS Colitis: Relevance of Compensatory Antioxidant Mechanisms. *J Crohns Colitis*, 11(7):871–884, Jul 2017. [Cited on pages 72, 92, 93, 94, and 100]
- [292] S. Izumiyama, M. Omura, T. Takasaki, H. Ohmae, and H. Asahi. *Plasmodium falciparum*: development and validation of a measure of intraerythrocytic growth using SYBR Green I in a flow cytometer. *Exp Parasitol*, 121(2):144–150, Feb 2009. [Cited on page 83]
- [293] J. K. Eaton, L. Furst, L. L. Cai, V. S. Viswanathan, and S. L. Schreiber. Structure-activity relationships of GPX4 inhibitor warheads. *Bioorg Med Chem Lett*, 30(23):127538, 12 2020. [Cited on page 88]
- [294] M. Koch, J. Cegla, B. Jones, Y. Lu, Z. Mallat, A. M. Blagborough, F. Angrisano, and J. Baum. The effects of dyslipidaemia and cholesterol modulation on erythrocyte susceptibility to malaria parasite infection. *Malar J*, 18(1):381, Nov 2019. [Cited on page 89]
- [295] X. An, V. P. Schulz, N. Mohandas, and P. G. Gallagher. Human and murine erythropoiesis. *Curr Opin Hematol*, 22(3):206–211, May 2015. [Cited on pages 91 and 92]
- [296] U. Kanjee, C. Grüring, M. Chaand, K. M. Lin, E. Egan, J. Manzo, P. L. Jones, T. Yu, R. Barker, M. P. Weekes, and M. T. Duraisingh. CRISPR/Cas9 knockouts reveal genetic interaction between strain-transcendent erythrocyte determinants of *Plasmodium falciparum* invasion. *Proc Natl Acad Sci U S A*, 114(44):E9356–E9365, 10 2017. [Cited on page 91]

- [297] E. J. Scully, E. Shabani, G. W. Rangel, C. Grüring, U. Kanjee, M. A. Clark, M. Chaand, R. Kurita, Y. Nakamura, M. U. Ferreira, and M. T. Duraisingh. Generation of an immortalized erythroid progenitor cell line from peripheral blood: A model system for the functional analysis of *Plasmodium* spp. invasion. *Am J Hematol*, 94(9):963–974, 09 2019. [Cited on page 91]
- [298] R. Killick-Kendrick. Parasitic protozoa of the blood of rodents: a revision of *Plasmodium berghei*. *Parasitology*, 69(2):225–237, Oct 1974. [Cited on page 92]
- [299] D. Chen and D. K. Kaul. Rheologic and hemodynamic characteristics of red cells of mouse, rat and human. *Biorheology*, 31(1):103–113, 1994. [Cited on page 92]
- [300] M. Nishikimi, R. Fukuyama, S. Minoshima, N. Shimizu, and K. Yagi. Cloning and chromosomal mapping of the human nonfunctional gene for L-gulonono-gamma-lactone oxidase, the enzyme for L-ascorbic acid biosynthesis missing in man. *J Biol Chem*, 269(18):13685–13688, May 1994. [Cited on page 92]
- [301] A. Montel-Hagen, S. Kinet, N. Manel, C. Mongellaz, R. Prohaska, J. L. Battini, J. Delaunay, M. Sitbon, and N. Taylor. Erythrocyte Glut1 triggers dehydroascorbic acid uptake in mammals unable to synthesize vitamin C. *Cell*, 132(6):1039–1048, Mar 2008. [Cited on page 92]
- [302] J. M. Sage and A. Carruthers. Human erythrocytes transport dehydroascorbic acid and sugars using the same transporter complex. *Am J Physiol Cell Physiol*, 306(10):C910–917, May 2014. [Cited on page 92]
- [303] E. Delpire and D. B. Mount. Human and murine phenotypes associated with defects in cation-chloride cotransport. *Annu Rev Physiol*, 64:803–843, 2002. [Cited on page 92]
- [304] A. Varki and S. Kornfeld. An autosomal dominant gene regulates the extent of 9-O-acetylation of murine erythrocyte sialic acids. A probable explanation for the variation in capacity to activate the human alternate complement pathway. *J Exp Med*, 152(3):532–544, Sep 1980. [Cited on page 92]
- [305] N. Pishesha, P. Thiru, J. Shi, J. C. Eng, V. G. Sankaran, and H. F. Lodish. Transcriptional divergence and conservation of human and mouse erythropoiesis. *Proc Natl Acad Sci U S A*, 111(11):4103–4108, Mar 2014. [Cited on page 92]
- [306] E. F. Gautier, M. Leduc, M. Ladli, V. P. Schulz, C. Lefèvre, I. Boussaid, M. Fontenay, C. Lacombe, F. Verdier, F. Guillonneau, C. D. Hillyer, N. Mohandas, P. G. Gallagher, and P. Mayeux. Comprehensive proteomic analysis of murine terminal erythroid differentiation. *Blood Adv*, 4(7):1464–1477, Apr 2020. [Cited on page 92]
- [307] L. A. Kirkman and K. W. Deitsch. Vive la Différence: Exploiting the Differences between Rodent and Human Malarias. *Trends Parasitol*, 36(6):504–511, 06 2020. [Cited on page 92]
- [308] J. Langhorne, P. Buffet, M. Galinski, M. Good, J. Harty, D. Leroy, M. M. Mota, E. Pasini, L. Renia, E. Riley, M. Stins, and P. Duffy. The relevance of non-human primate and rodent malaria models for humans. *Malar J*, 10:23, Feb 2011. [Cited on page 92]
- [309] L. A. Sanni, L. F. Fonseca, and J. Langhorne. Mouse models for erythrocytic-stage malaria. *Methods Mol Med*, 72:57–76, 2002. [Cited on page 92]

- [310] M. N. Wykes and M. F. Good. What have we learnt from mouse models for the study of malaria? *Eur J Immunol*, 39(8):2004–2007, Aug 2009. [Cited on page 92]
- [311] I. Landau and Y. Boulard. 2 - Life Cycles and Morphology. In R. Killick-Kendrick and W. Peters, editors, *Rodent Malaria*, pages 53–84. Academic Press, 1978. [Cited on page 92]
- [312] T. Eismann, N. Huber, T. Shin, S. Kuboki, E. Galloway, M. Wyder, M. J. Edwards, K. D. Greis, H. G. Shertzer, A. B. Fisher, and A. B. Lentsch. Peroxiredoxin-6 protects against mitochondrial dysfunction and liver injury during ischemia-reperfusion in mice. *Am J Physiol Gastrointest Liver Physiol*, 296(2):G266–274, Feb 2009. [Cited on page 93]
- [313] I. K. Sundar, S. Chung, J. W. Hwang, G. Arunachalam, S. Cook, H. Yao, W. Mazur, V. L. Kinnula, A. B. Fisher, and I. Rahman. Peroxiredoxin 6 differentially regulates acute and chronic cigarette smoke-mediated lung inflammatory response and injury. *Exp Lung Res*, 36(8):451–462, Oct 2010. [Cited on page 93]
- [314] A. U. Orjih. Requirements for maximal enrichment of viable intraerythrocytic *Plasmodium falciparum* rings by saponin hemolysis. *Exp Biol Med (Maywood)*, 233(11):1359–1367, Nov 2008. [Cited on page 95]
- [315] D. E. Goldberg and P. A. Sigala. *Plasmodium* heme biosynthesis: To be or not to be essential? *PLoS Pathog*, 13(9):e1006511, 09 2017. [Cited on page 95]
- [316] V. A. Nagaraj and G. Padmanaban. Insights on Heme Synthesis in the Malaria Parasite. *Trends Parasitol*, 33(8):583–586, 08 2017. [Cited on page 95]
- [317] M. Dzieciatkowska, C. C. Silliman, E. E. Moore, M. R. Kelher, A. Banerjee, K. J. Land, M. Ellison, F. B. West, D. R. Ambruso, and K. C. Hansen. Proteomic analysis of the supernatant of red blood cell units: the effects of storage and leucoreduction. *Vox Sang*, 105(3):210–218, Oct 2013. [Cited on page 95]
- [318] T. C. Chou and P. Talalay. Quantitative analysis of dose-effect relationships: the combined effects of multiple drugs or enzyme inhibitors. *Adv Enzyme Regul*, 22:27–55, 1984. [Cited on page 99]
- [319] J. Straimer, N. F. Gnädig, B. Witkowski, C. Amaratunga, V. Duru, A. P. Ramadani, M. Dacheux, N. Khim, L. Zhang, S. Lam, P. D. Gregory, F. D. Urnov, O. Mercereau-Puijalon, F. Benoit-Vical, R. M. Fairhurst, D. Ménard, and D. A. Fidock. Drug resistance. K13-propeller mutations confer artemisinin resistance in *Plasmodium falciparum* clinical isolates. *Science*, 347(6220):428–431, Jan 2015. [Cited on page 99]
- [320] G. T. Hanson, R. Aggeler, D. Oglesbee, M. Cannon, R. A. Capaldi, R. Y. Tsien, and S. J. Remington. Investigating mitochondrial redox potential with redox-sensitive green fluorescent protein indicators. *J Biol Chem*, 279(13):13044–13053, Mar 2004. [Cited on page 100]
- [321] L. Wu, A. C. Sedgwick, X. Sun, S. D. Bull, X. P. He, and T. D. James. Reaction-Based Fluorescent Probes for the Detection and Imaging of Reactive Oxygen, Nitrogen, and Sulfur Species. *Acc Chem Res*, 52(9):2582–2597, 09 2019. [Cited on page 100]

-
- [322] D. A. Butterfield and M. Perluigi. Redox Proteomics: A Key Tool for New Insights into Protein Modification with Relevance to Disease. *Antioxid Redox Signal*, 26(7):277–279, 03 2017. [Cited on page [100](#)]

9 Appendix

I List of figures

3.1	The life cycle of <i>Plasmodium falciparum</i>	14
3.2	Current model for host cell cytosol uptake in <i>P. falciparum</i>	17
3.3	Artemisinin and its clinically relevant derivatives	19
3.4	Molecular mechanism of the lipid oxidation radical chain reaction	21
3.5	Control and repair of lipid oxidation	25
3.6	Repair of OxPLs by PLA ₂	26
3.7	Inhibitors of PLA ₂	27
3.8	Model for OxPL detoxification by PRDX6	30
4.1	Gating strategy for flow cytometric measurement of different <i>P. falciparum</i> blood stages	44
5.1	Screening of fluorescent nucleic acid dyes	56
5.2	Establishment of the optimal SYBR Green concentration	57
5.3	Validation of gating strategy and separation of life stages	58
5.4	Effect of PLA ₂ inhibitors on progression and growth	59
5.5	Darapladib increases lipid oxidation	61
5.6	α -Tocopherol and DOPC restore <i>P. falciparum</i> blood stage progression inhibited by Darapladib	62
5.7	Lp-PLA ₂ activity was absent in <i>Pf</i> schizont lysates. PAF-signalling is not essential for parasite development	64
5.8	Pre-treatment of uninfected RBCs with MAFP allowed <i>P. falciparum</i> invasion, but inhibited ring to schizont progression	66
5.9	Recombinant expression and validation of human PRDX6	67
5.10	Darapladib, MAFP and ATK, but not Varespladib bind to human PRDX6	68
5.11	Darapladib inhibits the PLA ₂ activity of PRDX6	69
5.12	<i>In silico</i> docking of Darapladib to hPRDX6	70
5.13	Growth of rodent malaria strains <i>P. berghei</i> ANKA and <i>P. yoelii</i> YM in PRDX6 ^{-/-} mice	71
5.14	hPRDX6 is internalised by the parasite and shows vesicular co-localisation with the parasite	73
5.15	Human PRDX6 is internalised by <i>P. falciparum</i> and localises to HcVs migrating towards the FV	74
5.16	Darapladib treatment disrupts HcV transport	76
5.17	Darapladib inhibits delivery of host cell cytosol to the FV	78

5.18 Treatment with Darapladib decreases hemozoin crystal size	79
5.19 Co-treatment of ART-resistant parasites with DHA and Darapladib synergistically reduces parasite survival	80
6.1 Model for Darapladib-inhibited host cell cytosol uptake in <i>P. falciparum</i>	97
IV.1 Vector map of human PRDX6 in pET28a plasmid.	vi

II List of tables

4.1 Media and buffers	39
4.2 Antibodies	40
4.3 Drugs and Inhibitors	40
4.4 Enzymes	41
4.5 Fluorophores and fluorescent probes	41
4.6 Lipids	41
4.7 Screening of nuclear acid dyes	43
4.8 Lasers and Filters for BODIPY ^{581/591} C11 and Hoechst 33342 measurement	46
4.9 Lasers and Filters for LysoSensor Blue/Yellow and SYTO61 measurement	52
5.1 Co-treatment with Darapladib and Artemisinin shows synergism	81
6.1 Host cell tropism of different human and rodent malaria species and strains	92

III Abbreviations

AP2 μ	Adaptor protein complex 2 μ
ART	Artemisinin
ATK	Arachidonyl trifluoromethyl ketone
BSA	Bovine serum albumin
BODIPY	Boron-dipyrromethene, 4,4-difluoro-4-bora-3a,4a-diaza-s-indacene
CD71	Cluster of Differentiation 71 (Transferrin receptor protein 1)
(μ)Ci	(Micro)Curie (Unit)
cPLA ₂	cytosolic Phospholipase A ₂
cRPMI	complete RPMI-1640
DHA	Dihydroartemisinin
DIC	Differential interference contrast
DLPC	Dilinoleoyl phosphatidylcholine (18:2 PC)
DMSO	Dimethyl sulfoxide
DNA	Desoxyribonucleic acid
DOPC	Dioleoyl phosphatidylcholine (18:1 PC)
DPPC	Dipalmitoyl phosphatidylcholine (16:0 PC)
DSPC	Distearoyl phosphatidylcholine (18:0 PC)
DTT	Dithithreitol
EDTA	Ethylenediaminetetraacetic acid
EPS15	Epidermal growth factor receptor substrate 15
ER	Endoplasmatic reticulum
EtBr	Ethidium bromide
FA	Fatty acid
Fe	Iron
FSC-A/H	Forward scatter-Area/Height
FV	Food vacuole
G6PD	glucose-6-phosphate dehydrogenase
GFP	Green Fluorescent Protein
GPx	Glutathion peroxidase
GR	Glutathion reductase
GSH	Glutathion
GST	Glutathion S-transferase
<i>h</i>	human
Hb	Hemoglobin
HCCU	Host cell cytosol uptake
HcV	Host cell cytosol-containing vesicles

hpi/hpe	Hours post invasion/egress
HRP	Horse Radish Peroxidase
iPLA ₂	Ca ²⁺ -independent Phospholipase A ₂
iRPMI	incomplete RPMI-1640
K13	Kelch13
KIC	Kelch13 interaction candidates
LDH	Lactate dehydrogenase
LPLA ₂	Lysosomal Phospholipase A ₂
Lp-PLA ₂	Lipoprotein-associated Phospholipase A ₂
mRBC	mature Red blood cells
mRNA	messenger-RNA
MAFP	Methoxy arachidonyl fluorophosphonate
MAPK	Mitogen-activated protein kinase
MFI	Mean fluorescence intensity
MUFA	mono-unsaturated fatty acid
NRF2	Nuclear factor erythroid 2-related factor 2
NF- κ B	nuclear factor- κ B
<i>P.</i> *	<i>Plasmodium</i> *
OxPL	Oxidised phospholipid
PAF	Platelet-activating factor
PAF-AH	Platelet-activating factor acetylhydrolase
PAFR	Platelet-activating factor receptor
<i>Pb</i>	<i>Plasmodium berghei</i>
PC	Phosphatidylcholine
<i>Pf</i>	<i>Plasmodium falciparum</i>
PG	Phosphatidylglycerol
PL	Phospholipid
PLA _{1,2}	Phospholipase A _{1,2}
PLB	Phospholipase B
PRDX	Peroxioredoxin
PUFA	poly-unsaturated fatty acid
PV	Parasitophorous vacuole
PVM	Parasitophorous vacuole membrane
PS	Phosphatidylserine
<i>Py</i>	<i>Plasmodium yoelii</i>
Rab	Ras-associated binding (protein)
(i)RBC	(infected) Red blood cell
RBCM	RBC membrane

ROS	Reactive oxygen species
RT	Room temperature
SERCA	sarco/endoplasmic reticulum Ca ²⁺ -ATPase
sPLA ₂	secreted Phospholipase A ₂
SSC-A/H	Sideward scatter-Area/Height
<i>sn</i>	stereospecifically numbered
<i>T. gondii</i>	<i>Toxoplasma gondii</i>
TPx	Thioredoxin peroxidase
TR	Thioredoxin reductase
Trx	Thioredoxin
UBP1	Ubiquitin carboxyl-terminal hydrolase 1
VPS45	Vacuolar protein sorting-associated protein 45
WHO	World Health Organization

IV Gen sequences

IV.i Human PRDX6 6x-His tagged

```

1 ATGCATCAGC ACCACCATCA CCCCGGAGGG TTGTTGCTGG GCGACGTTGC CCCCAACTTT
61 GAAGCTAATA CCACGGTTGG TCGTATTCGT TTTCACGATT TCCTGGGCGA CTCTTGGGGT
121 ATTCTGTTCA GCCATCCGCG TGACTTTACC CCGGTATGTA CCACGGAACT GGGCAGAGCG
181 GCAAAGTTGG CGCCAGAATT TGCGAAACGT AATGTTAAAC TTATCGCCCT GTCGATCGAC
241 TCCGTGGAAG ATCACCTGGC GTGGAGCAAA GACATCAACG CATATAACTG CGAAGAGCCG
301 ACCGAGAAGT TACCGTTTCC GATTATCGAT GATCGTAATC GTGAACTGGC GATTTTGCTG
361 GGCATGCTGG ATCCGGCGGA GAAGGACGAG AAGGGTATGC CGGTCACCGC GCGTGTGGTG
421 TTCGTGTTTG GTCCGGATAA AAAACTTAAAG TTGTCCATTC TGTACCCGGC TACCACGGGT
481 CGCAACTTCG ACGAGATCCT CCGCGTCGTG ATCAGCCTGC AACTGACCGC AGAGAAGCGC
541 GTGGTACTC CGGTTGATTG GAAAGACGGT GACAGCGTTA TGGTTCTGCC TACAATTCCG
601 GAAGAGGAGG CGAAAAAGTT GTTCCCGAAA GCGGTTTTCA CCAAGGAAC TCCGAGCGGT
661 AAAAAGTATC TGCCTACAC CCCACAGCCG TAA

```

6× His-Tag

IV.ii hPRDX6-His in pET28a

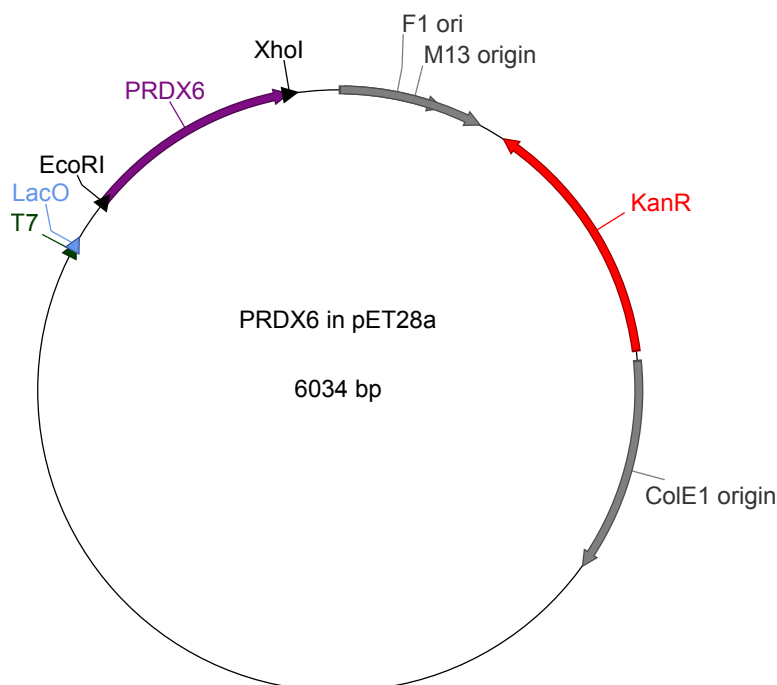


Figure IV.1: Vector map of human PRDX6 in pET28a plasmid.